



Hydrogen production from ethanol over ceria supported iridium and rhodium catalysts

Weijie Cai

► To cite this version:

Weijie Cai. Hydrogen production from ethanol over ceria supported iridium and rhodium catalysts. Tissues and Organs [q-bio.TO]. Université Claude Bernard - Lyon I, 2008. English. NNT: . tel-00430733

HAL Id: tel-00430733

<https://theses.hal.science/tel-00430733>

Submitted on 9 Nov 2009

HAL is a multi-disciplinary open access archive for the deposit and dissemination of scientific research documents, whether they are published or not. The documents may come from teaching and research institutions in France or abroad, or from public or private research centers.

L'archive ouverte pluridisciplinaire **HAL**, est destinée au dépôt et à la diffusion de documents scientifiques de niveau recherche, publiés ou non, émanant des établissements d'enseignement et de recherche français ou étrangers, des laboratoires publics ou privés.

THESE

présentée devant

l'UNIVERSITE CLAUDE BERNARD-LYON1

Spécialité : Chimie-Catalyse

pour l'obtention du

DIPLOME DE DOCTORAT EN CO-TUTELLE

(Arrêté du 01 septembre 2006)
avec l'Institut de Chimie Physique de Dalian
Académie Chinoise des Sciences

Présentée et soutenue publiquement le 18 Décembre 2008

par

Weijie CAI

TITRE

**Production d'hydrogène par reformage de l'éthanol
sur catalyseurs à base d'iridium et rhodium supportés sur cérine**

Directeurs de thèse:
Claude MIRODATOS et Wenjie SHEN

JURY :

M. Daniel DUPREZ (Rapporteur)
M. Philippe MIELE
M. Claude MIRODATOS
M. Wenjie SHEN
M. André C. VAN VEEN
M. Jianguo WANG (Rapporteur)

Invitée: Mme. Hélène PROVENDIER

Chapter I Introduction and literature survey.....	1
I.1. Advantages and challenges for hydrogen production from bio-ethanol.....	1
I.1.1. Steam reforming.....	2
I.1.2. Partial oxidation.....	3
I.1.3. Oxidative steam reforming	3
I.2. Catalysts for hydrogen production from bio-ethanol.....	4
I.2.1. Catalysts for ethanol steam reforming.....	4
I.2.2. Catalysts for ethanol partial oxidation	8
I.2.3. Catalysts for ethanol oxidative steam reforming	9
I.2.4. Concluding remarks on catalyst formulations.....	11
I.3. Mechanisms of hydrogen production from ethanol.....	11
I.3.1. Thermodynamics	11
I.3.2. Reaction pathways networks	14
I.3.3. Kinetics	18
I.4. Reaction engineering features.....	20
I.4.1. Short contact time reactors.....	20
I.4.2. Monolith reactors.....	21
I.4.3. Micro-structured reactors.....	22
I.4.4. Concluding remarks on engineering features	24
I.5. Objectives of the present PhD thesis.....	24
Chapter II Catalysts preparation, characterization techniques and experimental procedures.....	29
II.1. Catalysts preparation.....	29
II.1.1. Preparation of the 2% Ir/CeO ₂ catalyst	29
II.1.2. Preparation of the 1% Rh/CeO ₂ catalyst	29
II.2. Catalytic measurements under steady-state conditions.....	30
II.3. Catalyst characterization.....	32
II.3.1. Chemical analysis using ICP	32
II.3.2. Specific surface area (BET).....	32
II.3.3. X-ray diffraction (XRD)	32
II.3.4. Fourier transform infrared spectroscopy (FT-IR)	33
II.3.5. Temperature programmed reduction (TPR)	33
II.3.6. Temperature-programmed desorption (TPD) and surface reaction (TPSR).....	33
II.3.7. Oxygen storage capacity (OSC)	34
II.3.8. Carbon deposits (TPO).....	34
II.3.9. Transmission electron microscopy (TEM)	35
Chapter III Characterization of fresh Ir/CeO₂ catalysts.....	37
III.1. Physical and chemical characteristics of Ir/Ce₄₀₀ catalyst.....	37
III.2. Effect of ceria particle sizes	42
III.3. Conclusion	46
Chapter IV Comparison between SR, POX and OSR over Ir/CeO₂ catalyst in fixed bed reactor.....	49
IV.1. Homogeneous reaction	49

IV.2. Steam reforming of ethanol over Ir/Ce400 catalyst.....	51
IV.2.1. Effect of reaction temperature on activity	51
IV.2.2. Long term stability test	52
IV.3. Partial oxidation of ethanol over Ir/Ce400 catalyst	54
IV.3.1. Effect of reaction temperature on activity	54
IV.3.2. Long term stability test	55
IV.4. Oxidative steam reforming of ethanol over Ir/Ce400 catalyst	56
IV.4.1. Effect of reaction temperature on activity	56
IV.4.2. Long term stability test	58
IV.5. Comparison between SR, POX and OSR over Ir/Ce400 catalyst.....	59
IV.6. Influence of ceria particle size for OSR over Ir/CeO ₂ catalysts.....	60
IV.6.1. Effect of reaction temperature on product distributions.....	61
IV.6.2. Effect of ceria particle size on long term stability tests.....	63
IV.7. Catalyst characterization after aging tests.....	65
IV.7.1. Characterization of SR, POX and OSR aged Ir/Ce400 catalyst	65
IV.7.2. Characterization of OSR aged Ir/CeO ₂ with different ceria sizes	69
IV.8. Conclusion	71
Chapter V Effects of noble metal nature: comparison between Rh/Ce400 and Ir/Ce400 catalysts	75
V.1. Catalytic performance	75
V.2. Characterization of Rh/Ce400 catalyst before and after testing	77
V.3. Conclusion	79
Chapter VI. Investigation of ethanol conversion mechanism over Ir/CeO ₂ catalyst and comparison with other systems	81
VI.1. FTIR of ethanol activation under temperature programmed conditions.....	82
VI.1.1. Ethanol adsorption over Ce400	82
VI.1.2. Ethanol adsorption over Ir/Ce400.....	84
VI.2. TPD and TPSR over Ir/Ce400 catalyst	86
VI.2.1. TPD of ethanol over Ir/Ce400 catalyst.....	86
VI.2.2. TPSR over Ir/Ce400 catalyst.....	88
VI.3. Comparison of OSR over Ni-Cu/SiO ₂ , Rh/Al ₂ O ₃ , Rh/Ce400 and Ir/Ce400.....	92
VI.3.1. Catalytic performances under OSR conditions	92
VI.3.2. Overall comparison of DRIFT-TPD analysis for three catalysts.....	94
VI.4. Preliminary kinetic analysis on Ir/Ce400 catalyst	98
VI.5. Conclusion	100
Chapter VII. Hydrogen production from ethanol over Ir/Ce400 catalyst in micro-reactors.....	103
VII.1. Micro-reactors used in this study.....	104
VII.1.1. Micro-reactor housings	104
VII.1.2. Micro-structured platelets	105
VII.2. Wash-coating of Ir/Ce400 catalyst onto micro-structured platelets	106
VII.2.1. Platelets pre-treatment.....	106
VII.2.2. Preparation of wash-coating slurry	106
VII.2.3. Platelet coating.....	107

VII.3. OSR over Ir/Ce400 in low temperature micro-structured reactor	107
VII.3.1. Influence of reaction temperature	107
VII.3.2. Influence of contact time.....	110
VII.3.3. Long term stability test	111
VII.3.4. Characterization of used catalyst after long term testing	113
VII.3.5. Discussion on catalyst stability in micro-structured reactor.....	114
VII.3.6. Comparison between fixed bed and micro-structured reactor	115
VII.4. Comparison between SR over Ir/Ce400 in micro-structured and fixed bed reactors	117
VII.5. Conclusion.....	119
Chapter VIII General discussion and conclusion.....	121
References	129
List of Publications.....	139
Acknowledgement	141

Chapter I Introduction and literature survey

I.1. Advantages and challenges for hydrogen production from bio-ethanol

Energy is one of the major cornerstones in our everyday lives. Most of the energy we use nowadays comes from the combustion of fossil fuels--a non-renewable energy source with large CO₂ footprint. In turn, our dependence on fossil energy sources has caused serious environmental problems, i.e. the hazardous impact of air pollutants and global warming caused by greenhouse gas emission, and is strongly non sustainable given the natural resources depletion. The need for renewable alternatives is becoming ever more urgent. Solar, wind, and biomass are promising renewable resources but are generally site-specific, intermittent, and thus, not steadily available as needed to sustain an entire economy.

Hydrogen, when produced from renewable sources, has been identified as an ideal energy carrier to support sustainable energy development [1-4]. Hydrogen can be used in a fuel cell to generate electricity with high efficiency only water as by-product. In order to support sustainable hydrogen economy, it is therefore crucial to produce it cleanly and renewably.

At present, steam reforming of hydrocarbons, and essentially natural gas, is the most commonly used and generally neglecting the follow-up costs of the environmental impact also the most economically competitive method for hydrogen production [1-3]. However, natural gas is a fossil fuel, and its use as hydrogen source produces huge amounts of carbon dioxide emission during the reforming processes. The same statement holds indeed also for the coal or mineral oil use. As a result, there is a growing interest for effective alternatives to produce hydrogen from renewable sources.

Among the various renewable feedstock alternatives, ethanol is very attractive because of its relatively high hydrogen content, availability, non-toxicity, and storage and handling ease and safety. Ethanol can be produced by fermentation of biomass resources, such as

sugar, starch or cellulose containing energy plants, agro-industrial wastes, forestry residue materials, and the organic fraction of municipal solid waste. The ethanol produced in this way is called bio-ethanol, which is a mixture of ethanol and water and can be further distilled to fuel quality, i.e., including traces of higher alcohols, methanol, inorganic compounds (Cu, P, S, chlorines) etc [5-7].

As growing biomass takes in carbon dioxide from the atmosphere, reforming of biomass-derived ethanol has a close to zero net CO₂ emission and does not contribute to the global warming [8]. Indeed biomass can also be gasified (to syngas) and/or liquefied (to bio-oils), which makes other renewable routes for hydrogen production. One might note here a strong open debate about the interest or irrelevancy to consider biomass routes competing with the food chains. In that sense, ethanol reforming for producing hydrogen might be less relevant when using grown resources like sugar canes or beetroot than starting from agro-industrial wastes, forestry residue materials, and organic fraction of municipal solid waste. However, the purity of the feedstock might become an issue to consider for the latter cases, which is far beyond the scope of the present thesis.

The ethanol reforming process for hydrogen production can be generally classified into three groups: (1) steam reforming (SR) (2) partial oxidation (POX) and (3) oxidative steam reforming (OSR).

I.1.1. Steam reforming

SR is by far the most studied route since it produces the highest hydrogen yield [9-12]. Its chemical reaction equation can be written by considering arbitrarily the highest possible hydrogen, assuming a full conversion of CO into CO₂.



The highest production of syngas also can be considered as well for evaluating the highest possible H₂/CO ratio:



Thus, SR can generate a H₂/CO ratio of 2 but it has the disadvantage of being an

endothermic process and therefore it requires a large energy input to drive the reactions. In addition, coke formation may be favoured under SR conditions.

I.1.2. Partial oxidation

Alternatively, hydrogen can be obtained by partial oxidation of ethanol according to the following reactions [13-15]



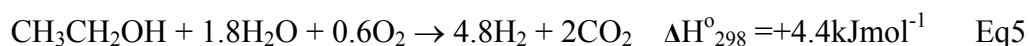
or



leading to a maximum H_2/CO of 3/2. Due to their exothermic character, POX systems allow a fast start up and have short response time, which make them attractive for applications involving frequently transient operations with rapidly varying loads. Moreover, a POX reactor is more compact than a steam reformer, since it does not need the indirect supply of heat via heat exchangers. However, the hydrogen yield for the POX of ethanol remains indeed relatively low. In contrast, coke formation is by far less favored under this oxidizing environment.

I.1.3. Oxidative steam reforming

The OSR of ethanol is a combination of the SR and the POX reactions, aiming at a more energy efficient process. Ideally, the exothermic partial oxidation of ethanol would supply the heat necessary for the endothermic steam reforming of ethanol. Thus, by feeding $\text{CH}_3\text{CH}_2\text{OH}$, H_2O , and O_2 in a proper ratio, the overall reaction is operated in a close to thermally neutral state (ATR), meanwhile H_2 and CO_2 could be obtained as the end products



These equations indicate that the OSR does not only support a thermally sustained operation, but it leads also to a still reasonably high hydrogen production. In addition, OSR seems to present a good alternative for reducing rate of carbon deposition and more favorable thermal equilibrium between heat generation and heat loss in the process can be

established as a function of the oxygen feed [16].

Though carbon dioxide produced from bio-ethanol would not contribute to increase its concentration in the atmosphere, it might be relevant to consider the ethanol reforming with CO₂ for possible recycling of CO₂ produced from fossil sources. Ethanol dry reforming with CO₂ can generate a H₂/CO ratio of 1 [17].



Ethanol dry reforming was only scarcely investigated. Tsiakaras et al. [18] studied the thermodynamics of ethanol dry reforming, but did not perform any experimental work.

I.2. Catalysts for hydrogen production from bio-ethanol

In the above-mentioned reactions, catalysts play a crucial role both for driving ethanol conversion towards the thermodynamic limits (i.e., complete conversion) but also for achieving an maximum hydrogen production with the highest possible yields (i.e., corresponding to an equilibrated WGS reaction).

In more details, ethanol reforming reactions include several steps involving the need for catalytic surface able to: (i) dehydrogenate and/or dehydrate ethanol into intermediates leading eventually to acetaldehyde and ethylene products (ii) cleave the carbon-carbon bond of C₂ surface intermediates to produce CO_x and CH₄ and (iii) reform these C₁ products to generate hydrogen. The choice of the catalyst and its engineering environment (shaping, type of reactor, operating conditions) are key factors for fulfilling the above requirements.

I.2.1. Catalysts for ethanol steam reforming

Considering the main results reported in literature, noble and non-noble metals are generally considered as the required active phases for performing the formulation of catalysts in SR.

I.2.1.1. Noble metal based systems.

Noble metal catalysts are well known for their high catalytic activity in any type of reactions involving hydrocarbon activation, especially when a formation of coke by

over-cracking has to be avoided. For ethanol SR, Rh, Ru, Pd, and Pt have been extensively investigated, in combination with conventional non reducible supports like alumina or redox materials able to store/release oxygen like ceria-based systems.

The group of Duprez [19] has investigated the influence of the noble metal (Rh, Pt) and the role of the support (Al_2O_3 , $\text{Al}_2\text{O}_3\text{-CeO}_2$, CeO_2 , $\text{Ce}_{0.63}\text{Zr}_{0.37}\text{O}_2$) for the ethanol steam reforming. It was found that the activity of the catalyst in the SR increased with increasing OH group mobility at the catalyst surface and that the selectivity of the catalyst towards CO_2 decreased with increasing efficiency of the catalyst in the reverse WGS (RWGS) reaction. They also investigated another original formula, $\text{Rh/Mg}_x\text{Ni}_{1-x}\text{Al}_2\text{O}_3$ spinel oxide [20], in order to combine various functions of noble and non noble metals together with a well adjusted support basicity. The performances obtained for SR at 700°C from 1 to 11 atm ($\text{H}_2\text{O}/\text{ethanol}$ molar ratio of 4, space velocity 24000h^{-1}) demonstrated well that acid and base properties of the materials are crucial parameters inasmuch as they impact on the control of the primary selectivity to ethylene or acetaldehyde.

In a recent study, Breen et al. [21] investigated support effect for ethanol steam reforming on Rh, Pt and Pd supported on Al_2O_3 and CeO_2 systems. Alumina-supported catalysts were found very active at relatively low temperatures (400°C) for the dehydration of ethanol to ethylene which was converted into H_2 , CO and CO_2 as major products and CH_4 as a minor one at higher temperatures (above 600°C). The order of activity was $\text{Rh} > \text{Pd} > \text{Pt}$. With ceria supported catalyst, the formation of ethylene was not observed and the order of activity at high temperatures (above 600°C) was $\text{Pt} > \text{Rh} > \text{Pd}$. The nature of the support was also shown to play an important role in long-term operation of catalysts. Acidic supports, i.e. Al_2O_3 , induced ethanol dehydration producing ethylene, which was a source of coke formation.

Frusteri et al. [22] evaluated the catalytic performance of MgO supported Pd, Rh, Ni and Co for hydrogen production by ethanol steam reforming. Rh/MgO showed the best performance in terms of ethanol conversion and stability. Coke formation rate on Rh/MgO was very low as MgO was basic. It was also found that the deactivation was mainly due to metal sintering.

Liguras et al.[23] compared the catalytic performance of Rh, Ru, Pt and Pd catalysts in the temperature range of 600-850°C with a metal loading of 0-5wt%; Rh was found to give the highest ethanol conversion and hydrogen yield. Although inactive at low loadings, Ru showed a catalytic activity comparable to Rh at high loading (5wt%). The 5%Ru/Al₂O₃ could completely convert ethanol into syngas with hydrogen selectivity above 95%.

I.2.1.2. Non noble metal based catalysts

Catalysts using non-noble metals have been also widely investigated for ethanol steam reforming, essentially for their lower cost as compared to noble metals containing ones.

Ni is widely used in industry as a low-cost non-noble metal catalyst for a number of chemical reaction processes. For ethanol reforming, Ni also works well as it favors C-C rupture. Fatsikostas et al. [24] compared the catalytic activity of Ni catalysts supported on La₂O₃, Al₂O₃, YSZ and MgO. The higher activity and stability of Ni/La₂O₃ was attributed to the formation of lanthanum oxycarbonate species (La₂O₂CO₃) able to react with surface carbon deposited during the reaction and thus preventing Ni deactivation. Sun et al. [25] also compared the catalytic activity of Ni/Y₂O₃ and Ni/La₂O₃, and Ni/Al₂O₃ for hydrogen production by ethanol steam reforming. The catalysts were prepared using nickel oxalate as precursor and in an impregnation – decomposition - reduction method. Operating at ambient pressure and at 320°C, the conversion of ethanol using Ni/Y₂O₃ and Ni/La₂O₃ was 93.1% and 99.5%, respectively, while the selectivity of hydrogen was 53.2% and 48.5%, respectively. For comparison, the selectivity of hydrogen for a Ni/Al₂O₃ catalyst reached a maximum of 47.7% at 300°C. The reported selectivity to hydrogen was relatively low, probably due to the low water/ethanol molar ratio used (3:1). It was demonstrated that increasing water/ethanol molar ratio could significantly increase the selectivity to hydrogen [26].

Besides La₂O₃ and Al₂O₃, other oxides have also been studied as alternative supports for Ni catalyst. Yang et al. [27] showed that at 650°C and with Ni loading of 10wt%, almost 100% conversion of ethanol was attained with a selectivity to hydrogen ranked as: Ni/ZnO=Ni/La₂O₃ > Ni/MgO > Ni/Al₂O₃.

Frusteri et al. [28] investigated the effect of alkali addition (e.g. Li, Na, K) on the behavior of a Ni/MgO catalyst in the bio-ethanol steam reforming. Li and Na were found to promote the NiO reduction but worsen the dispersion of the Ni phase, whereas K did not significantly affect either Ni morphology or dispersion. Li and K enhanced the stability of Ni/MgO mainly by inhibiting long term Ni sintering.

Cobalt, having properties close to Ni, was indeed also deeply investigated [29]. In a recent work, Cavallaro et al. [30] investigated the support influence on the catalytic stability of several supported catalysts. They observed that Co/Al₂O₃ catalysts were deactivated after 2-3h in the ethanol SR (650°C), and MgO represented a more suitable support for Co catalyst because of its lower acidity compared to Al₂O₃. As generally assumed, the deactivation was attributed to cobalt oxidation and coke formation.

Apart from the nature of the metal and the support, the synthesis conditions are also considered as important parameters determining the activity and stability of Co-based catalyst [31]. Prepared by the incipient wetness technique or impregnation (IMP), the sol-gel (SG) method, and the combination of the two methods (ISG), Co/SiO₂ and Co/Al₂O₃ exhibited various surface areas, surface compositions, and mean dispersions, resulting in an apparent difference in catalytic activities. With 8wt% Co loading, a maximum hydrogen selectivity of 62% and 67% was obtained with Co/SiO₂ prepared by ISG and Co/Al₂O₃ prepared by IMP [8]. Differences in metal phase dispersion related to different interactions with the support might explain these preparation effects [32].

I.2.1.3. Bi(multi)metallic alloys based catalysts

As a general trend observed in catalyst formulation screening, in addition to monometallic formulas, bi or multi-metallic compositions were also investigated in this ethanol reforming reaction [33].

Marino et al. [34] studied the catalytic activity of Cu-Ni-K/Al₂O₃ catalysts. From the comparison with monometallic systems, ethanol dehydrogenation and C-C bond rupture were easily over Cu and Ni, respectively. In addition, K reduced the possibility of coke formation by neutralized acidic sites of Al₂O₃.

Baltaciogiu et al. [35] studied the effect of Pt and Ni contents on the SR reaction characteristics of the bimetallic catalyst. The best performance was achieved over 0.3wt%Pt-15wt%Ni/Al₂O₃ probably due to better dispersion of Pt and Ni and abundance of Ni sites promoting the reforming reaction. The apparent activation energy of the SR reaction over 0.3wt%Pt-15wt%Ni/Al₂O₃ was calculated as $59.3 \pm 2.3 \text{ kJ mol}^{-1}$.

To summarize, SR has been extensively investigated in the recent years. Rh and Ni are so far the best active phased for the SR reaction targeting on the hydrogen production. The selection of a proper support and the method of catalyst preparation affect also significantly the catalytic performances. So far, the development of a catalyst for ethanol reforming is basically a trial-and-error approach. The main challenge is the deactivation caused by coke formation. Stable, active, selective and low cost catalytic systems for the SR are still required for practical applications.

I.2.2. Catalysts for ethanol partial oxidation

Like for ethanol SR, a variety of metals were investigated for POX, also focusing on the role of the support, but with a specific trend to also consider redox systems like ceria based supports which are supposed to play a major role in oxygen management [36-39].

I.2.2.1. Non noble metal based systems.

Wang et al. [40] evaluated the effect of Ni/Fe ratio on the performance of Ni and Fe-based catalysts (Ni₉₀Fe₁₀, Ni₇₀Fe₃₀, Ni₅₀Fe₅₀, Ni₃₀Fe₇₀, Ni₁₀Fe₉₀) at 300°C and O₂/ethanol=1.5. All catalysts presented a good performance in the partial oxidation of ethanol. However, Ni₅₀Fe₅₀ showed the highest ethanol conversion (86.91%) and H₂ selectivity (50.66%). The good performance of Ni-Fe catalysts was related to the presence of the spinel-structured (Ni,Fe) Fe₂O₄ and FeNi₃ alloys, which were considered as the active species for the partial oxidation of ethanol.

I.2.2.2. Noble metal based systems

Salge et al. [41] studied the partial oxidation of ethanol over noble metals (Rh, Ru, Pd,

Pt) supported on ceria-coated alumina foams at 700°C and C/O=0.7. Rh-Ce/Al₂O₃ catalysts performed more stable than those with the noble metals alone. Concerning the H₂ selectivity, Rh-Ce/Al₂O₃ presented the best performance. Among noble metals, Pt and Pd showed the lowest catalytic activity. The by-products were CH₄, C₂H₄ and acetaldehyde for all catalysts. However, Pt, Pd and Rh supported on Al₂O₃ exhibited a higher selectivity to CH₄ and C₂H₄ than Rh-Ce/Al₂O₃. The better performance of Rh-Ce/Al₂O₃ was assigned to redox properties of Ceria.

Noronha et al. [42] studied the effect of the metal nature on the performance of ceria-supported catalysts in the partial oxidation of ethanol at 300°C and an O₂/ethanol molar ratio of 0.5. The results revealed that the Pt/CeO₂ catalyst had a higher initial activity (conversion level of 80%) and the product distribution was strongly affected by the nature of the metal. Acetaldehyde was practically the only product formed on Co/CeO₂ catalyst while there was also methane formation on Pt/CeO₂ and Pd/CeO₂ catalysts.

To summarize, it comes clear that one metallic active phase (noble or non noble) cannot be considered intrinsically better but that exhibited performances strongly related to the nature of its support, especially for the ceria based systems. The latter tends to limit coke formation due to its ability to generate active oxygen species. However, further research should focus on the active metal stability due to the strong thermal effects (hot spots) occurring under POX conditions.

1.2.3. Catalysts for ethanol oxidative steam reforming

In recent years, ethanol OSR has attracted more and more attention, for the obvious energy management benefits underlined in the beginning of this review [43-44]. Several catalysts screening studies have been reported for this reaction, which tended logically to integrate formulations related both to steam reforming and to partial oxidation. Some experimental conditions and results are summarized for comparison in Table 1.

Kugai et al. [45] investigated ethanol OSR over Ni-Rh/CeO₂ catalysts at temperatures below 400°C. The Rh dispersion was found to increase while the Ni one decreased upon decreasing crystallite sizes of CeO₂. Both ethanol conversion and H₂ selectivity increased

and the selectivity for undesirable byproducts decreased with increasing Rh metal dispersion. These observations tend to strongly link metal and support dispersion for this particular case. For achieving a more general overview the latter observation will be carefully investigated for other catalysts during this work.

Active phase	Support	Temp(°C)	O ₂ /H ₂ O/C ₂ H ₅ OH molar ratio	C ₂ H ₅ OH Conv.(%)	S _{H2}	Ref
Ni ₅ Rh ₁	CeO ₂	600	0.4/4/1	100	55	45
Pd	ZnO	450	0.5/13/1	100	61	46
Pd	SiO ₂	450	0.5/13/1	48.7	35	
CuNiZnAl	Al ₂ O ₃	300	0.4/3/1	85-95	50	47
Pt	Al ₂ O ₃	400	0.36/2.28/1	73.3	32	48
Pt	Al ₂ O ₃ -La	400	0.36/2.28/1	69.1	48	
Pt	Al ₂ O ₃ -Ce	400	0.36/2.28/1	94.8	56	
Pt	Al ₂ O ₃ -La-Ce	400	0.36/2.28/1	87.2	38	
Ni(11wt%)	Al ₂ O ₃	1000	0.68/1.6/1	100	45	49
(20wt%)	Al ₂ O ₃	1000	0.68/1.6/1	100	95	
Ni	CeO ₂	550	0.5/8/1	100	85	50

Table 1 Review of catalysts tested for the oxidative steam reforming of ethanol. Ref [8]

Velu et al. [47] tested the OSR reaction using a series of CuNiZnAl multi-component mixed metal catalysts with various Cu/Ni ratios. They observed that Cu rich catalyst favored ethanol to acetaldehyde dehydrogenation reaction whereas an addition of Ni promoted the C-C bond rupture, as already mentioned for POX studies.

In the previous works performed by Fierro et al. in our group [51,52], ethanol OSR has been studied over Ni/Al₂O₃, Ni-Cu/SiO₂ and Rh/Al₂O₃ catalysts. A wide range of catalyst with different metal loading was investigated in order to identify optimal formulas. Ni_{16.7}-Cu_{2.1}/SiO₂ and 5wt%Rh/Al₂O₃ were found to exhibit the best catalytic performance in term of hydrogen yield and catalyst stability.

Thus, it can be observed in Table 1 as well as in the above quoted works that ethanol conversion and hydrogen selectivity for OSR vary greatly with the type of catalyst, support and oxygen/steam/ethanol molar ratios. One should note that such a statement makes a strict

comparison between these works quite uncertain, and would therefore reinforce the strategy developed in this thesis to test simultaneously the various reforming reactions for the same or for different catalysts under as close conditions as possible.

Furthermore, as expected for investigations in the presence of gaseous oxygen, OSR studies show that coke formation is greatly inhibited by oxidation, ensuring long-term stable operation. In turn, the presence of water maintains a reasonable yield in hydrogen as compared to pure steam reforming.

I.2.4. Concluding remarks on catalyst formulations

From a comprehensive literature survey, it can be seen that among the two main categories of active phases, Rh and Ni exhibited respectively the best performances in terms of bio-ethanol conversion and hydrogen yield. In order to maximize the hydrogen production, a proper preparation of the catalyst and suitable supports are required. The challenge of bio-ethanol reforming is avoiding or at least limiting the carbon deposition on the catalyst, as coke can cause further catalyst deactivation. Suitable supports, like MgO, ZnO, CeO₂ and La₂O₃ or mixed oxides, can inhibit carbon deposition to some extent. The preparation method is also important for determining catalyst electronic structure. A development of bi-metallic catalyst appears also promising to optimize hydrogen production and minimize carbon deposition.

I.3. Mechanisms of hydrogen production from ethanol

I.3.1. Thermodynamics

Thermodynamics studies have shown the feasibility of hydrogen production from ethanol for fuel cell applications [53-55]. We used HSC software version 4 (based on Gibbs energy minimization) to calculate the equilibrium compositions of the SR, POX and OSR reactions under our selected operating conditions. The species considered are hydrogen, carbon monoxide, carbon dioxide, methane, water, ethanol ethylene, ethane, acetaldehyde and acetic acid as well as solid carbon.

I.3.1.1. Ethanol steam reforming

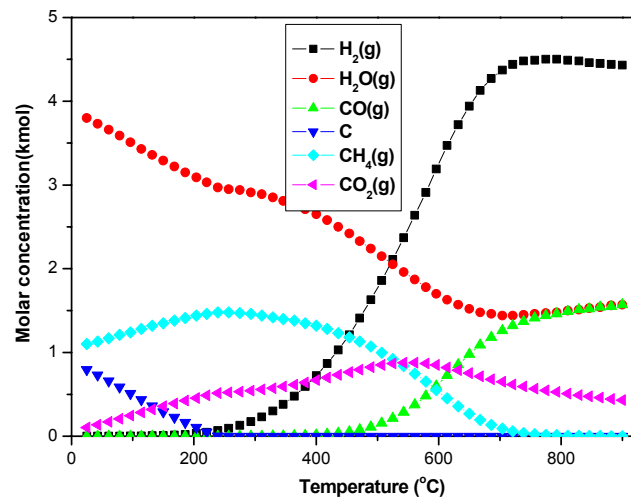


Figure 1 Effect of temperature on equilibrium concentrations for the ethanol steam reforming ($\text{H}_2\text{O}/\text{EtOH}=3$, pressure: 1atm)

Fig 1 shows the molar product concentration and coke formation in ethanol steam reforming. The temperature has a significant effect on the equilibrium concentrations of the products. Ethanol may be completely converted over the whole temperature range. As the temperature increases, the H_2 concentration increases and reaches a maximum at 750°C , which coincides with the total disappearance of methane. CH_4 and CO_2 concentrations have a maximum at around 250 and 525°C respectively and decrease steadily at higher temperature while CO increases. There is no formation of C_2 products predicted since they are not thermodynamically stable. The coke formation in the SR reaction at low temperature may still be considerable. However, above 200°C , coke formation becomes unfavorable.

I.3.1.2. Ethanol partial oxidation and oxidative steam reforming

The results of the thermodynamic calculation for the POX and OSR case are shown in Fig 2 and Fig 3, respectively. As expected, the maximum hydrogen concentration in the POX case is much lower than expectable for the SR reaction. In the case of the POX reaction there is still much coke formation possible below 800°C . Probably this relates to the low oxygen content chosen as operating conditions in order to avoid in an experimental study a catalyst over heating (the molar ratio $\text{O}_2/\text{ethanol}=0.6$). Above 800°C , a higher

CO/CO₂ ratio is obtained in POX than in SR, again attributed to the assumed low oxygen content and indeed much lower water content.

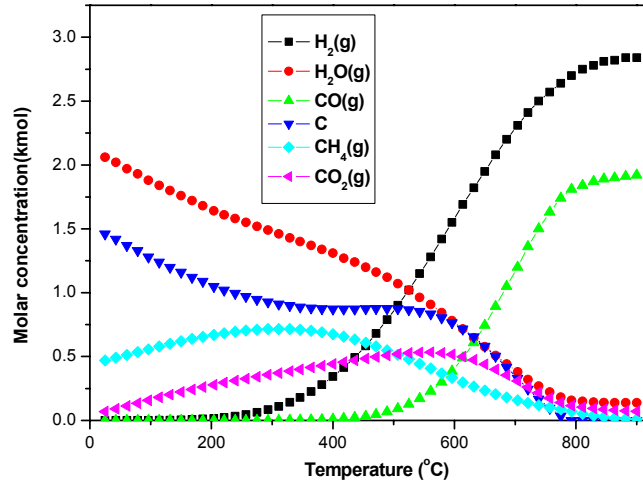


Figure 2 Effect of reactor temperature on equilibrium concentrations for the ethanol partial oxidation ($O_2/EtOH=0.6$, pressure: 1atm)

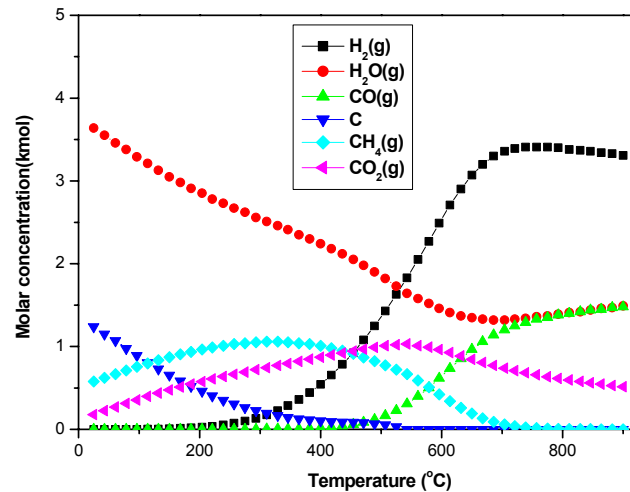


Figure 3 Effect of reactor temperature on equilibrium concentrations for the ethanol oxidative steam reforming ($EtOH/H_2O/O_2=1/1.8/0.6$, pressure: 1atm)

OSR operation is combination of SR and POX operation. It is interesting to notice that the OSR reaction reduces the coke-formation rate, as compared to POX, due to the beneficial effect of carbon removal with the added water.

Therefore, it can be deduced from these thermodynamics calculations, that i) maximizing hydrogen production requires high temperature for all reactions, ii) ethanol and any oxyginate or C₂ intermediates are fully converted at equilibrium, iii) carbon deposits (though much care has to be taken since thermodynamics data depends actually highly on

the real nature of coke formed) are strongly inhibited at high temperature. Finally, there is a much more pronounced tendency to avoid carbon deposits in the presence of water than in the presence of low concentrations of oxygen.

Nevertheless, the catalytic reforming of ethanol is a very complex reaction where many reaction pathways are possible. Many mechanistic studies aimed at identifying actual network of reaction pathways, either as lumped or as elementary steps, either as homogeneous (gas phase) or catalytic (gas/surface and surface/surface) steps. This mechanistic approach is analyzed below.

I.3.2. Reaction pathways networks

A detailed analysis of reactant species, intermediate product species, and final product species is required to investigate reaction mechanisms, as well as transient investigations like TPD, TPR, SSITKA, often combined with operando spectroscopy (Raman, DRIFT, neutron scattering etc).

I.3.2.1. Mechanism for steam reforming

Yates and co-workers [56,57] have shown that the energy for bond breaking in an ethanol molecule ranks in the following increasing order: O-H, -CH₂-, C-C and -CH₃. Therefore, it can be foreseen in a first approximation that a sequence of elementary processes for activating ethanol occurs at increasing temperature, whatever be the catalyst.

The easiest step is the formation of surface adsorbed ethoxy species, CH₃CH₂O_{ads}, from the OH group dehydrogenation. Then the ethoxy intermediates further dehydrogenate to produce acetaldehyde. Both steps can be lumped as:



Then, acetaldehyde decomposition leads to methane and carbon monoxide formation via C-C bond cleavage, also written according to a step lumped as:



Methane can finally be reformed with steam in the next reaction step via CH activation

in methyl groups, to obtain hydrogen and carbon monoxide



The last expected process is the water gas shift reaction that converts in the presence of water part of the carbon monoxide to hydrogen and carbon dioxide.



Several side reactions, catalytic or not, might be considered as well, like ethanol dehydration to ethylene, which might be favored on acidic supports:



Coke formation from ethylene oligomerization/condensation:



Methane coupling to ethane



On the basis of works based on ethanol decomposition, several overall mechanistic schemes, more or less detailed, have been reported in the literature, depending on the type of catalytic materials [58-62]. The scheme in Fig 4 tentatively describes a general network of the main lumped reactions occurring during the conversion of ethanol to hydrogen.

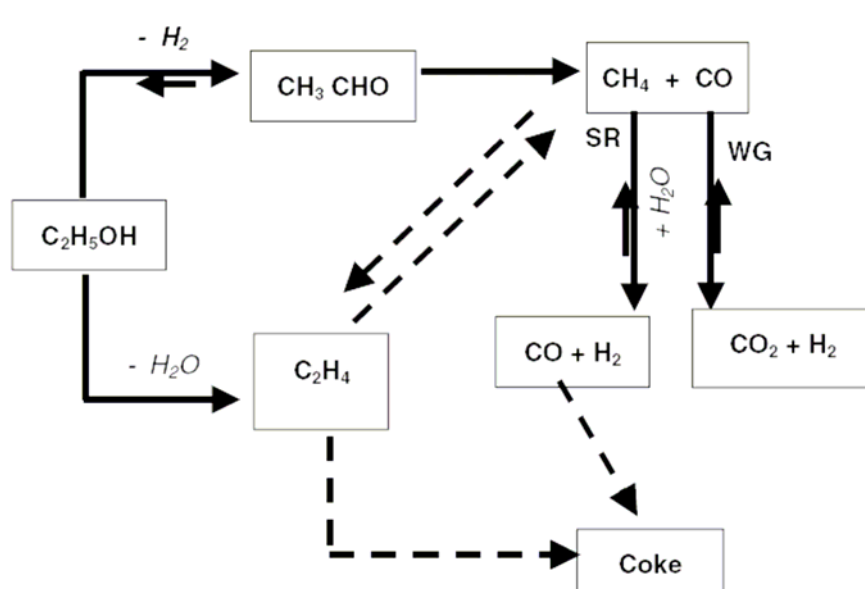


Figure 4 Reaction network of ethanol steam reforming (Ref22)

Both, the dehydrogenation to the acetaldehyde and dehydration to ethylene occur depending on the nature of the support. Acidic supports induced ethanol dehydration to produce ethylene, which was a precursor of coke formation.



In general, a high surface basicity will favor dehydrogenation rather than dehydration.

Other secondary products mostly resulting from acetaldehyde conversion, were also observed for the reaction of ethanol over catalysts. These include: crotonaldehyde (formed by aldolisation of acetaldehyde) [63], ethyl acetate (formed by dimerisation of two acetaldehyde molecules), acetates (formed by direct oxidation of acetaldehyde), and butenes (formed by reductive coupling of two molecules of acetaldehyde over defected sites [64].

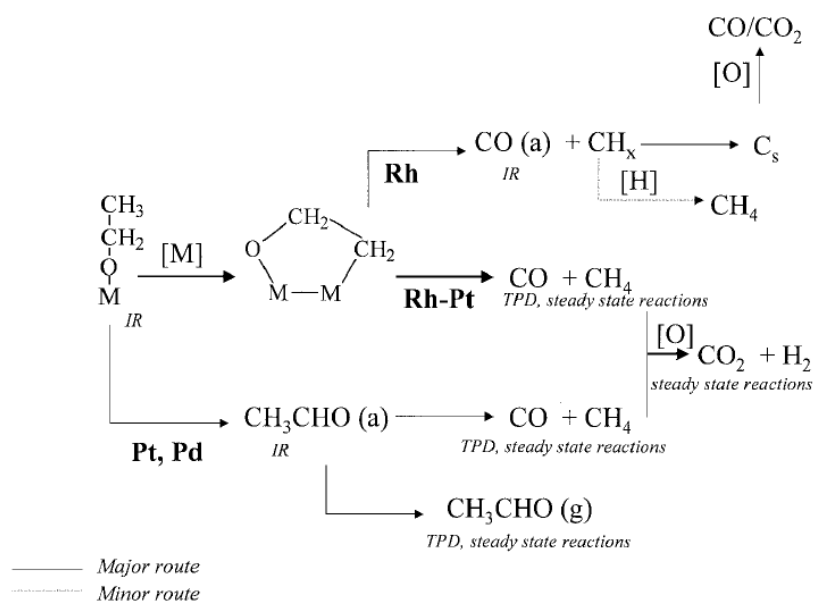


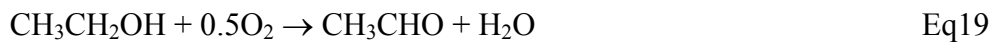
Figure 5 Reaction pathways of ethanol over Rh supported catalyst (Ref 65)

A mechanistic approach was proposed in a recent study over Rh supported catalysts by Idriss et al. [65,66]. There were some differences by comparing SR on Rh and on other metals. On Pt, Pd or Ni, ethanol first dissociates to ethoxide further on oxidized to acetaldehyde. For the case of Rh, ethoxide species would dehydrogenate to give an oxametallacycle (a)-OCH₂CH₂-(a) intermediate, where (a) is an adsorption site. This

intermediate latter would decompose to CO upon further annealing.

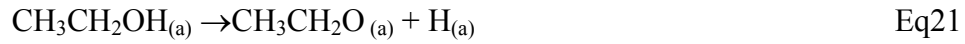
I.3.2.2. Mechanisms in POX and OSR

In the case of the partial oxidation and the oxidative steam reforming of ethanol, several additional reactions are proposed to account for the presence of oxygen [67].



By considering elementary steps, Bi et al [68] proposed the following pathways in ethanol OSR over a Pt-Ru/ZrO₂ catalyst, as depicted in

(1) Sequential abstraction of hydrogen



(2) Cleavage of C-C bond



(3) Products formation



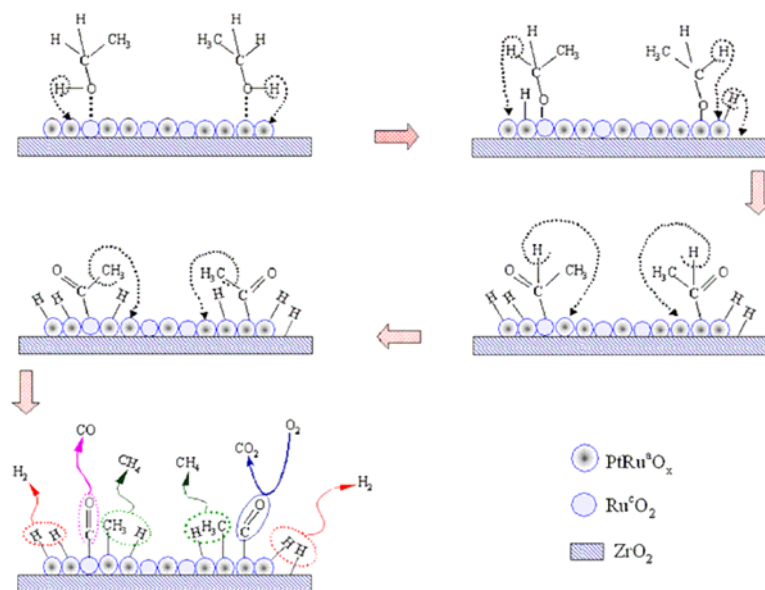


Figure 6 The reaction scheme for ethanol oxidative steam reforming over Pt-Ru/ZrO₂ catalyst [Ref 68]

In our group, Akdim [69] investigated the reaction mechanism of the oxidative steam reforming of ethanol over Ni-Cu/SiO₂ and Rh/Al₂O₃ catalysts. It was found that the reaction proceeded via different routes depending on the nature of the active phase. Essentially, only the metal alloy phase Ni-Cu, which can easily undergo redox cycles with oxide and/or hydroxide state plays a catalytic role for the Ni_{16.7}-Cu_{2.1}/SiO₂ catalyst. The contribution of complex nickel hydroxy-silicate sites for producing ethylene at low temperature is also likely. In contrast, for the noble metal based systems (Rh/Al₂O₃), the metal phase remains essentially in a metallic state, while the support plays a key catalytic role to store intermediates from ethanol decomposition and water activation.

To sum up this review on proposed mechanistic schemes, it appears that a number of steps are more or less agreed on by most authors (like step one for ethoxy formation), but the entire scheme remains quite variable according the nature of both metals and supports. In addition, a large part of the proposals are rather speculative due in general to a lack of detailed analysis of reactant species, intermediate product species, and final product species.

I.3.3. Kinetics

In contrast to the large number of mechanistic studies, studies on kinetic analysis and modeling for the ethanol reforming reaction and especially for the POX and OSR operation

remained rather scarce. Sun et al. [70] reported a power law rate equation for ethanol conversion with a first order in respect to ethanol and the reaction order for water need to be determined later, for a temperature range of 250-350°C when using nickel-supported catalysts.

$$r = k[\text{ethanol}][\text{H}_2\text{O}]^n \quad \text{Eq29}$$

For different catalysts the rate of conversion decreased in the following order: Ni/La₂O₃ > Ni/Y₂O₃ > Ni/Al₂O₃, while the activation energy increased from 1.87 kJ/mol to 7.04 kJ/mol to 16.88 kJ/mol, respectively. These astonishingly low values indicate with a high likeliness a limitation of the reaction by mass transfer.

The most relevant study in the domain was reported in [71] where a kinetic model describes crude ethanol SR over a 15%-Ni/Al₂O₃ catalyst. The kinetic experiments were carried out at atmospheric pressure in a packed bed tubular reactor in the temperature range of 320–520°C. Eley Rideal assumptions (where the surface reaction involved an adsorbed species and a free gaseous species) were used to construct variants of the reaction mechanism and four models were proposed based on these mechanisms. From this there was a new kinetic model based on the dissociation of adsorbed crude ethanol as the rate-determining step developed for this novel catalytic process. The proposed rate equation was of the form: $-r_A = (2.08 \times 10^3 e^{-4430/RT} N_A) / [1 + 3.83 \times 10^7 N_A]^2$. The average absolute deviation between experimental rates and the model predicted ones was about 6%.

Since the development of a robust kinetic model is required for any further engineering study, it must be stated that a much larger effort should be dedicated to kinetic modelling, despite the difficulty to run the reaction in a proper catalytic regime, with a minimized impact of heat and mass transfer limitations.

Finally, it could be mentioned that to our knowledge no mathematical relationship has been established between kinetic parameters (rate of conversion or selectivity, rate constants, orders, activation energies etc) and the intrinsic parameters of the different materials constituting the catalyst (in other word a so called QSAR, for quantitative structure activity relationship) is completely missing, which might be a challenge for the

future.

I.4. Reaction engineering features

As already stressed in the introduction, the perspective of an hydrogen based economy has induced a massive effort in terms of process intensification for miniaturizing and enhancing safety of chemical processes for producing hydrogen when its storage is considered as a major issue [72,73]. Typical mass or niche potential applications are on-board hydrogen generation for i) electrical vehicles (main or auxiliary power units), ii) for improving fuel combustion in conventional engine, iii) domestic small scale power generators and iv) scattered and remote industrial uses where hydrogen distribution via networking is economically or technically not possible. Most of these medium-to-small scale applications would involve in addition frequent transient regimes arising from changes in the power demand. Within this frame, conventional multi-tubular reactors with randomly packed catalytic beds which generally exhibit strong limitations in heat and mass transfer are badly adapted to fulfill the dynamics of these new systems. In addition, their scaling-up or down-sizing depending on the targeted application is not straightforward and alternative engineering strategies have to be considered.

New generations of reactors are presently heavily studied for meeting these challenges, which can be denominated as "structured reactors", since a major characteristic will be to limit pressure drops while maximizing surface contact between the reactants and the catalytic phase.

I.4.1. Short contact time reactors

In recent years, a millisecond-contact time auto-thermal reactor for efficient oxidative reforming of hydrocarbons has been developed by the University of Minnesota [74-77]. The benefit of short contact time is that homogeneous reactions producing carbon, acetaldehyde, ethylene, and total combustion products can be minimized, as rapid vaporization and mixing are performed at sufficiently low temperature and sufficiently short time. A scheme of the millisecond auto-thermal reactor is shown in Fig.7.

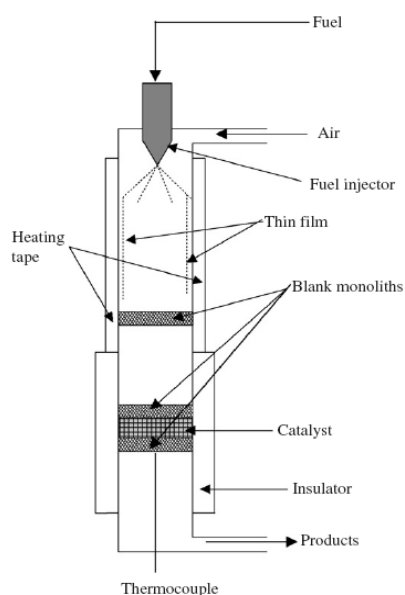


Figure 7 Schematic view of a millisecond auto-thermal reforming reactor [ref 75].

An automotive fuel injector is used and placed at the top of the reactor to facilitate vaporization and mixing of reactants before reaching the catalyst bed. During operation, the ethanol fuel is delivered at the top of the reactor by the injector. The conical dispersion of fuel droplets creates a thin film of liquid fuel on the inner wall of the reactor, which is heated to about 140°C. The thin film absorbs heat and vaporizes near the wall, where there is little oxygen due to the formation of fuel vapor boundary layer. Through this fast vaporization and mixing, occurrence of flames and pyrolysis of the fuel vapor before reaching the catalyst can be greatly avoided. The flow rate can be accurately controlled by the pressure in the fuel supply tank as well as the duty cycle. Thus, the short residence time of ethanol on Rh-Ce/Al₂O₃ catalyst below 10ms can be achieved [8].

I.4.2. Monolith reactors

Monoliths are mainly used in structured reactors, for applications where pressure drop needs to be minimized (like for car exhaust de-pollution) (Fig 8). Usually the expression monolith refers to blocks of parallel straight channels coated with catalysts [78]. Main characteristics of monolith reactors include: i) a low-pressure drop; ii) the elimination of external mass transfer and internal diffusion limitations; iii) a low axial dispersion and back-mixing, and therefore high product selectivity; iv) a large external surface; v) an easy

scaling-up etc [79]. As drawbacks, they are more expensive than particle/pellet catalysts. Of extreme importance is that the inlet well-distribution should be ensured. Casanovas et al [80] investigated the ethanol steam reforming over a cordierite monolith coated with Co/ZnO catalyst. $5.6\text{molH}_2/\text{molC}_2\text{H}_5\text{OH}$ was obtained from a $\text{C}_2\text{H}_5\text{OH}/\text{H}_2\text{O}=1/6$ gaseous mixture at 350°C and 0.33ml/min of liquid $\text{C}_2\text{H}_5\text{OH}$.

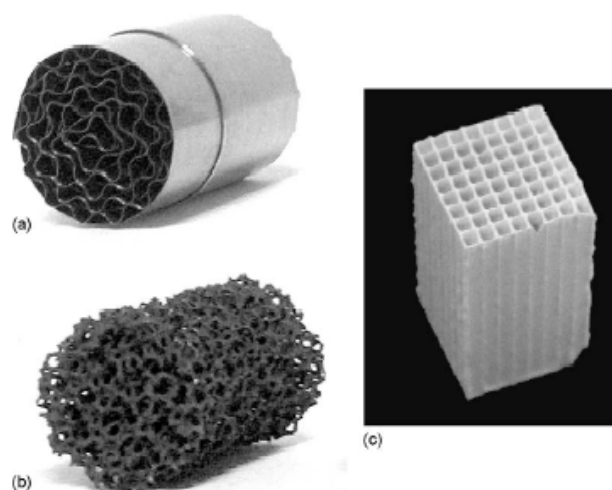


Figure 8 Various types of monoliths

I.4.3. Micro-structured reactors

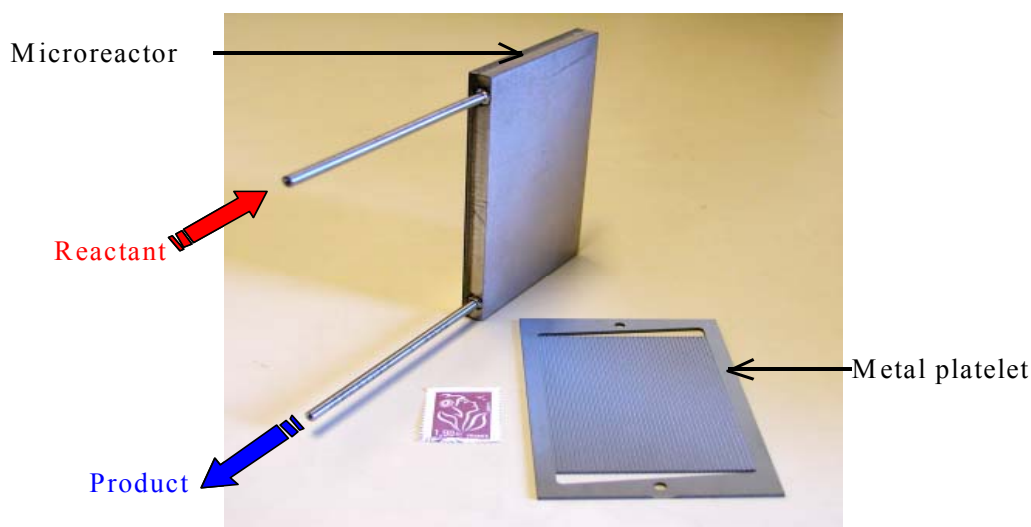


Figure 9 Example of micro-structured reactors

For fulfilling compactness requirements, a new kind of structured reactor is developed. Their characteristic dimensions in the reacting zones are on the micro- or meso-scale, which

make them referred as to "micro-structured reactors", often abbreviated as "microreactors" (Fig 9).

Micro-structured reactors are characterized by three dimensional structures in the sub-millimeter range. Mainly multi-channel reactors are currently used with channel diameters with hundred to several hundred micrometers depth and width. Therefore, one of the main features of microreactors is their high surface-to-volume ratio, which is several orders of magnitude higher compared to traditional chemical reactors. These characteristics lead to strongly improved heat and mass transfer properties, as required for process intensification [81,82]. Within channels having these dimensions, micro-structured multi-channel reactors work under laminar flow conditions and low-pressure drop as compared to turbulent fixed-bed reactor. Their small radial dimension and in turn short times required for bulk wall diffusion lead to narrow residence time distributions of the traversing gases. This allows optimizing the contact time of the reactants and therefore avoiding the formation of unwanted by-products. Moreover, the short residence time ($<0.1\text{s}$) and channels volume are quite favorable for a fast response to dynamic changes in the inlet conditions [83,84]. Since the small channel dimensions often lie below the quenching distance, explosive gas mixtures can be handled safely [85]. These micro-structured reactors are most generally made of metallic substrates like corrugated foils or channeled platelets, stacked and soldered together. This feature is essential for ensuring the highest thermal conductivity and avoiding hot-spot, especially when combining exothermic and endothermic reactions aiming at auto-thermal systems [86]. These substrates are, before or after assembly, coated with various layers (base layers like alumina or silica) further impregnated with various dopants and active phases to constitute the so called "structured" catalytic layer. In order to maximize the surface contact between the reactants and the active species, while minimizing the amount of costly active phase (if noble metal based), coating techniques are adapted for optimizing the catalyst dispersion within the porous structure of the layers [87].

Specificities of the micro-structured reactors in term of coating requirements and use as kinetic devices for hydrogen production and purification are analyzed by Dupont et al. in

our laboratory [88,89]. As far as reforming reactions are concerned, most of the reported studies were mainly focused on methanol or methane reforming [90-92]. Hessel research team [93,94] studied the propane partial oxidation and steam reforming with the aim of syngas production. Rhodium, platinum, nickel and palladium catalysts were tested. Rhodium was identified as the best candidate concerning activity.

Men et al. [95] investigated the ethanol steam reforming over supported catalysts in a micro-channel reactor. The metal nature, metal loading and type of the carriers were found to influence markedly the catalytic activity and selectivity of the catalysts. Rh-based catalysts exhibited the highest catalytic activity, as compared to Co and Ni-based catalysts

I.4.4. Concluding remarks on engineering features

Micro-structured systems are the most promising development for process intensification, but still numerous engineering aspects need to be solved (from reactor assembly, catalysts stability, cost, corrosion issues etc). Until now, the mainstream of studies available in open literature presents only the microreactor's catalytic performance without explicit details about the catalyst development or characteristics. There are only rare publications where the coatings on micro-channel metallic platelets were discussed [96,97]. One might stress the importance of understanding mechanisms for a correct rational design of the micro-structured reactor, which is also scarcely implemented. The other aspect is that there are only very few works on ethanol reforming in microreactors. Great attention should be focused on this field due to the advantages of the microreactors.

I.5. Objectives of the present PhD thesis

From the above literature analysis and considering the main targets to be met for any industrial application, the following questions/requirements have to be addressed:

i) Stability: two main factors were identified as monitoring catalysts stability under ethanol reforming conditions: a) coke formation and deposition over or around the catalyst, b) both the support and/or active metal sintering. Specific studies on these subjects remain

still scarce and the processes involved (and possibly interconnected) are still not clearly understood.

ii) Activity: one obvious challenge is to screen formulations for reactions (SR, POX or OSR) which are easily limited by thermodynamics, i.e., leading to full conversion of ethanol. Working at partial conversion may involve lower temperature where undesired side reaction like ethanol conversion to oxygenates or to coke might be favored. Preferentially, shorter contact times should be explored, which might also have hydrodynamic impacts, but they might lift mass and heat transfer drawbacks.

iii) Selectivity: hydrogen selectivity cannot be considered independently since it is strongly related to the adjustment of the WGS equilibrium, also frequently achieved from thermodynamics calculations. The challenge is to maximize its yield but keeping the CO production as low as possible for minimizing bulky and costly downstream hydrogen purification steps.

iv) Mechanism: many mechanistic approaches have been reported, which are generally specific to the tested materials, operating conditions and possibly from the used techniques and methodologies. It can be inferred that any new type of catalysts deserves to be studied also from a mechanistic point of view, which might be used for further kinetic modeling.

iv) Engineering aspects: between highly endothermic SR and highly exothermic POX, a key challenge is to reach an auto-thermal process, which might offer an efficient heat management. Avoiding detrimental hot spots (metal/support sintering) or cold spots (carbon deposition and undesired sub-products formation) is another major task.

By considering the above statements, a general target should be to identify a well performing catalyst (in terms of stability and hydrogen yield) and to investigate the specific features of the ethanol conversion mechanism (from low to high temperature, in the absence and in the presence of co-reactants like water and oxygen). In parallel, engineering developments should be carried out aiming on improving the heat management.

From a catalyst formulation and mechanistic point of view, a "performing catalyst" should favor the C-C bond rupture rather than promoting mainly the C-O bond activation. Since Ni based materials tend to promote easily this C-C bond cleavage but also the carbon

deposition, noble metals remain the most promising candidates, though a comparison between various elements deserves to be carefully undertaken.

As generally outlined, the nature of the support also plays a major role in the catalyst performance:

(i) It should ensure metal phase stability and dispersion avoiding sintering but prevent also deactivation via strong metal-support interaction.

(ii) To complement the metal specific activity mostly dedicated to syngas management, it should promote water and oxygen activation and possess very mobile OH groups or O species to favor the reaction with the CH_x fragments formed on the metal particles.

(iii) It should favor ethanol dehydrogenation to acetaldehyde instead of alcohol dehydration to ethylene, to prevent coke formation.

In previous studies carried out in both French and Chinese laboratories involved in this co-tutelle program [51,52,98,99], many formulations have been tested either under ethanol SR or OSR conditions.

Among other performing systems, Ir/CeO₂ catalysts showed rather high activity and stability for ethanol steam reforming, while Rh/Al₂O₃ was found quite adapted to the OSR conditions.

In this work, it was decided to focus on the ceria support as the most promising and probably versatile material for investigating the various reactions aiming at producing hydrogen from ethanol in a systematic way. Ir and Rh noble metals were considered preferentially as the active phase of the catalysts, focusing on the conditions required for ensuring a strong metal-support interaction and therefore a high stability under reforming conditions. From a methodological point of view, the decomposition of ethanol in the absence or in the presence of co-reactants was investigated via a combination of in situ DRIFTS spectroscopy and temperature programmed desorption (TPD) techniques

The potential of using this type of catalyst in micro-structured reactors was considered as well, with preliminary results aiming at identifying the advantages and drawbacks of this engineering approach.

As such, this PhD manuscript was structured as follows, including this introduction

chapter:

- (i) Chapter II: Catalysts preparation, characterization techniques and experimental procedures.
- (ii) Chapter III: Characterization of the fresh Ir/CeO₂ catalysts
- (iii) Chapter IV: Comparison between SR, POX and OSR over Ir/CeO₂ catalyst in fixed bed reactor.
- (iv) Chapter V: Effect of noble metal nature: comparison between Rh/Ce400 and Ir/Ce400 catalysts
- (v) Chapter VI: Investigation of ethanol conversion mechanism over Ir/CeO₂ catalyst and comparison with other systems
- (vi) Chapter VII: Hydrogen production from ethanol over Ir/CeO₂ catalyst in the micro-structured reactor.
- (vii) Chapter VIII General discussion and conclusion.

Chapter II Catalysts preparation, characterization techniques and experimental procedures

This chapter presents the main techniques used for i) preparing the catalysts and ii) characterizing them and the way that the respective procedures are implemented.

II.1. Catalysts preparation

II.1.1. Preparation of the 2% Ir/CeO₂ catalyst

The CeO₂ support was prepared by precipitation of ammonia cerium nitrate with urea in aqueous solution. 60 g of (NH₄)₂Ce(NO₃)₆ and 200 g of urea were dissolved into 2000 ml of water and the mixture was heated gradually to 90°C under stirring and kept at this temperature for 27 h. After filtration and thorough washing with water, the precipitate was dried at 100°C for 12 h, and finally calcined at 400, 550, 700 or 850°C separately for 5 h in air. These CeO₂ samples were designed as Ce400, Ce550, Ce700 and Ce850 respectively.

The Ir/CeO₂ catalyst with an Ir nominal loading of 2wt% was prepared by a deposition-precipitation method. CeO₂ powders obtained at different calcination temperatures were suspended in aqueous solution containing appropriate amounts of Ir precursor (H₂IrCl₆·6H₂O), and the mixture was heated to 75°C under stirring. A 0.1 M Na₂CO₃ aqueous solution was gradually added gradually until the pH value of the mixture reached 9.0, followed by further aging at 75°C for 1 h, during which the precipitate was exclusively deposited on the surface of ceria. After filtration and washing with water, the solid obtained was dried at 100°C overnight and finally calcined at 400°C for 5 h in air. The obtained catalyst was designed as Ir/Ce400, Ir/Ce550, Ir/Ce700 and Ir/Ce850 respectively.

II.1.2. Preparation of the 1% Rh/CeO₂ catalyst

1% Rh/CeO₂ catalyst was also prepared by the deposition-precipitation method. The CeO₂ support was first suspended into the aqueous solution containing certain rhodium

precursor ($\text{RhCl}_3 \cdot n\text{H}_2\text{O}$) and heated to 75°C under stirring. A 0.1mol/L Na_2CO_3 aqueous solution was then gradually added until the pH value of the mixture reached 9.0 and further aged for 1h. After filtration and washing with hot water, the obtained solid was dried at 100°C overnight and calcined at 400°C for 5h in air. The obtained catalyst was designed as 1%Rh/Ce400.

II.2. Catalytic measurements under steady-state conditions

Catalytic bench

Catalytic reactions were conducted at atmospheric pressure with a continuous-flow fixed-bed quartz reactor (8 mm of internal diameter) equipped with GC for gas analysis (Fig.1).

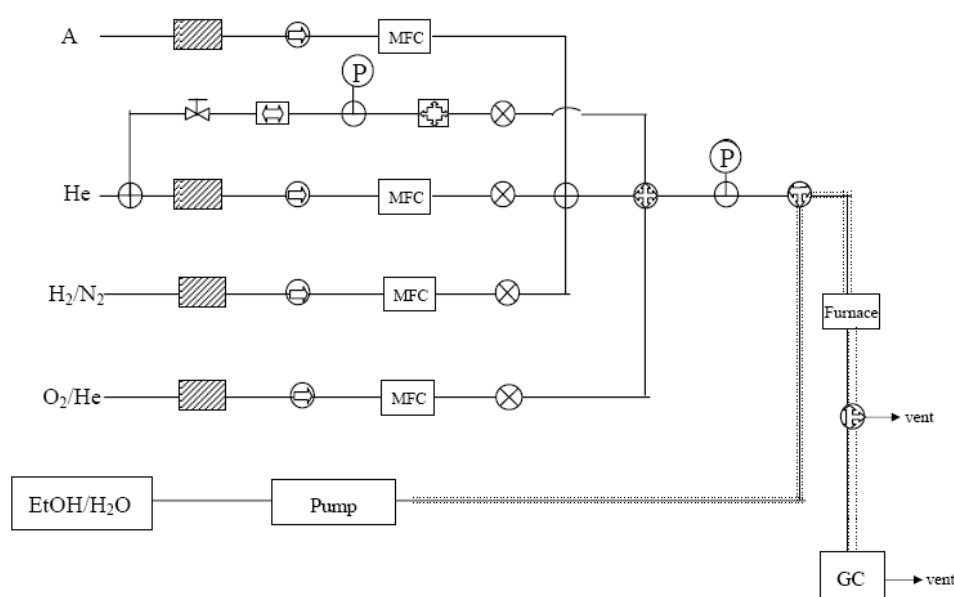


Figure 1 set up for the catalytic testing with fixed-bed reactor.

Testing conditions

300 mg of catalyst (40-60 mesh) were loaded in this reactor and sandwiched by two layers of quartz wool. Before the reaction, the catalyst was reduced with 5vol% H_2/He (30 mL/min) at 400°C for 1 h. SR and OSR reactions were carried out with stoichiometric feed compositions of ethanol/water (1:3 molar ratio) and ethanol/water/ O_2 (1:1.8:0.6 molar

ratio), respectively. For comparison, POX was carried out using a feed composition of ethanol/O₂ (1:0.6 molar ratio). Pure ethanol or aqueous ethanol solutions were fed by a micro-pump to a vaporizer heated to 200°C and the vapors were mixed with the oxygen stream coming from a mass-flow controller.

The effluent from the reactor was analyzed on-line by gas chromatography. H₂, CO and CO₂ were separated by a packed column (HayeSep D) and analyzed by a thermal conductivity detector (TCD) using He as carrier gas. Hydrocarbons and oxygenates were separated with a capillary column (INNOWAX) and analyzed with a flame ionization detector (FID).

Calculation of performance

To compare the rate of the 3 reactions, turn-over frequencies (TOF) were evaluated by considering a mean Ir particle size of 2nm (as deduced from TEM pictures on aged samples), i.e. a metal dispersion of around 50%.

The ethanol conversion is calculated according to:

$$X_{\text{EtOH}} = \{[\sum n^*(C_i)_{\text{outlet}}] - [2^*(C_{\text{EtOH}})_{\text{outlet}}]\} / [\sum n^*(C_i)_{\text{outlet}}] \quad \text{Eq1}$$

with (C_i)_{outlet}: molar concentration of carbon containing species (labeled as i) in the outlet gas.

n=1 for CO, CO₂ and CH₄; n=2 for C₂H₆, C₂H₄, CH₃CH₂OH and CH₃CHO; n=3 for CH₃COCH₃.

The molar concentration of hydrogen in the outlet dry gas (except water) is calculated according to:

$$C_{\text{H}_2}^* = (C_{\text{H}_2})_{\text{outlet}} / [(C_{\text{H}_2})_{\text{outlet}} + \sum n^*(C_i)_{\text{outlet}}] \quad \text{Eq2}$$

Molar concentrations of carbon containing species (labeled as i) in the outlet dry gas (except water) are calculated according to:

$$C_i^* = (C_i)_{\text{outlet}} / [(C_{\text{H}_2})_{\text{outlet}} + \sum n^*(C_i)_{\text{outlet}}] \quad \text{Eq3}$$

with (C_{H₂})_{outlet}: molar concentration of hydrogen in the outlet gas.

The kinetic experiments were carried out in the temperature range of 150-250°C and at

a total pressure of 1atm. The weight of the catalyst was varied in the range of 25-100mg. The flow rate of ethanol was in the range of 7.5-30cm³/min, while the flow rate of water was varied in the range of 7.5-90cm³/min. For Arrhenius plots, the ethanol conversion was kept below 10%.

II.3. Catalyst characterization

II.3.1. Chemical analysis using ICP

The actual metal content in Ir/CeO₂ catalysts was analyzed by an inductively coupled plasma (ICP) atomic emission spectrometer (PLASMA-SPEC-II). An appropriate amount of sample was dissolved into aqua regia, and the mixture was diluted with nitric acid to meet the detection range of the instrument. The obtained solution is then vaporized in the plasma of the monochromatic spectrophotometer and the emitted wavelengths, which are characteristic of the elements, are quantitatively analyzed.

II.3.2. Specific surface area (BET)

The specific surface areas of the catalysts were measured before and after catalytic test using BET (Brunauer, Emmett and Teller) method. These measurements were performed on an ASAP 2010 Micrometrics apparatus and consisted in Nitrogen adsorption at -193°C. Before analysis, the samples were outgased by heating for 3h at 300°C under N₂.

II.3.3. X-ray diffraction (XRD)

The crystalline phases of the catalyst were characterized by X-ray diffraction. XRD patterns were recorded using a Rigaku D/MAX-RB diffractor with Cu K α radiation source operating at 40 kV and 100mA. Measurements for the reduction of the Ir/CeO₂ catalyst were performed in a high temperature cell installed in the diffractometer. The sample was pressed into a pellet and mounted in the chamber. After heating to 200°C under a stream of He, 5 vol.% H₂/He was introduced into the chamber where the sample was stepwise heated to the desired temperatures (200-600°C) for 1 h before recording the XRD patterns. The mean

crystallite sizes of ceria were calculated from the Scherrer equation [100].

II.3.4. Fourier transform infrared spectroscopy (FT-IR)

Fourier transform infrared (FTIR) spectroscopy was used to follow the evolution of catalyst surface species during temperature programmed desorption of ethanol. The analyses were performed with a spectrometer (Brucker Vector 22) in diffuse reflectance (DRIFT) mode. Before the analysis, the sample was reduced with 5vol% H_2/He at 400°C for 1 h. After reduction, the system was cooled to room temperature under a flow of helium. The adsorption of ethanol was carried out at room temperature with a flowing mixture of ethanol/He for 1 h, which was obtained by passing He through a saturator containing ethanol. After adsorption, the DRIFT cell was purged with He for 30 min and then heated at a rate of 15°C /min up to 400°C. The spectra were recorded at room temperature, 100, 200, 300 and 400°C.

II.3.5. Temperature programmed reduction (TPR)

Hydrogen temperature programmed reduction (H_2 -TPR) was carried out with a conventional setup equipped with a TCD chromatograph. 100mg (40-60 mesh) samples were pretreated at 300°C for 1 h under N_2 flow (40mL/min). After cooling to room temperature and introducing the reduction agent (a 5 vol% H_2/N_2 mixture (40mL/min)), the temperature was then programmed to rise at 10°C /min up to 950°C. Hydrogen consumption versus time (and temperature) was followed by a TCD.

II.3.6. Temperature-programmed desorption (TPD) and surface reaction (TPSR)

Temperature-programmed desorption (TPD) and surface reaction (TPSR) of ethanol on the Ir/ CeO_2 catalyst were carried out in a micro-reactor equipped with an on-line mass spectrometer (Omnistar, Balzers). Before testing, the catalyst (100 mg) was reduced with 5vol% H_2/He (40 mL/min) at 400°C for 1 h. After reduction, the system was purged with He at 400°C for 30 min and cooled to room temperature. The adsorption of ethanol was carried

out at room temperature with a flow of ethanol/He mixture for 1 h, obtained by passing He through a saturator containing ethanol. After adsorption, the sample was purged with He (40 mL/min) for 30 min and then heated at a rate of 15°C /min up to 700 °C with a flow of pure He (for TPD), 3.0%H₂O/He, 1.0%O₂/He or 3.0%H₂O/1.0%O₂/He (for TPSR). The relative yields of C-containing products were calculated following the procedure of Yee et al. [101].

$$Y_i = \frac{A_i \times CF_i \times Cn_i}{\sum_j^n A_j \times CF_j \times Cn_j}$$

Where A_i is the area under the peak

CF_i is the correction factor

Cn_j is the carbon numbers in products

	CH ₃ CH ₂ OH	CH ₃ CHO	CH ₃ COCH ₃	CH ₄	CO	CO ₂
CF_i	2.1	2.3	3.6	1.9	1	1.4

II.3.7. Oxygen storage capacity (OSC)

As ceria is well known for its redox properties and its high oxygen storage capacity, oxygen storage capacity (OSC) was measured in a micro-reactor coupled to a quadrupole mass spectrometer (Omnistar, Balzers). Before analysis, the sample (100 mg) was reduced with 5%H₂/Ar (50 mL/min) at 650°C. The sample was purged for 15 min at 650°C using flowing Ar. A 5%O₂/Ar mixture (50 ml/min) was then passed through the sample, and the oxygen consumption was measured with a mass spectrometer at m/e=32.

II.3.8. Carbon deposits (TPO)

The formation of the carbonaceous deposits during steady-state catalytic experiments was quantified by temperature programmed oxidation (TPO) of the used catalyst. 100 mg of the used catalyst were loaded in a microreactor and the system was heated from 25°C to 650°C at a rate of 5°C /min with a flow of 5.0% O₂/Ar mixture (100 mL/min). The effluents were analyzed by the on-line mass spectrometry (Inficon quadrupole).

II.3.9. Transmission electron microscopy (TEM)

The catalysts were characterized using High Resolution Transmission Electron Microscopy (HRTEM), in order to determine their homogeneity, the distribution, the dispersion and the mean size of the ceria and metal particles. The measurements were carried out on a Philips Tecnai G²20 microscope operating at 300 kV. Samples were prepared by suspending the catalyst in ethanol and agitating in an ultrasonic bath. Several drops of the suspended catalyst were applied to a copper mesh grid with lacy carbon film, with the ethanol evaporating in between drops.

The microscope is coupled to a X-ray energy dispersive spectrometer, which can give the local elemental composition at nanoscale.

II.3.10. X-ray photoelectron spectroscopy (XPS)

The XPS spectra have been obtained using a PHI spectrometer (model 5400) equipped with an Mg/Al dual mode source and a small area analyzer with PSD detector. An achromatic Mg K_a X-ray source was operated at 300W. About 50mg catalyst was loaded in a quartz reactor and reduced under a 5%H₂/Ar mixture (50ml/min) at a ramp rate of 4°C/min up to 400°C and kept at this temperature for 1 h before cooling to room temperature.

Chapter III Characterization of fresh Ir/CeO₂ catalysts

As mentioned in the introduction section, one of the aims of the present thesis is to identify relationship between catalyst structure/composition and catalytic behavior for ethanol reforming. Therefore, we present in this chapter the detailed characteristics of: the Ir/Ce400, Ir/Ce550, Ir/Ce700 and Ir/Ce850 catalysts which ceria support was calcined at 400, 550, 700 and 850°C, respectively (see previous Chapter II) to elucidate the influence of ceria particle size.

All characterization data is obtained on fresh catalysts. The characterization of aged catalysts will be presented later, after the chapters on catalytic performances.

III.1. Physical and chemical characteristics of Ir/Ce400 catalyst

ICP. Analysis revealed that the amount of Ir in the Ir/Ce400 catalyst was 2.1 wt%, as targeted.

BET. The specific surface areas of the Ce400 support and the Ir/Ce400 catalyst were 158 and 146 m²/g, respectively, suggesting that the loading of Ir only slightly decreased the surface area of the ceria support. This might be assigned to a partial insertion of Ir ions or clusters of ions partly filling the structural and textural defects of the ceria support.

XRD. Fig. 1 shows the XRD patterns of the Ir/Ce400 catalysts. Only the diffraction reflexes of ceria with fluorite structure were observed for the as-prepared catalyst, and the average crystalline size was about estimated to 6 nm (Fig 1a). This is in good agreement with the value (5.2 nm) estimated from the BET surface area. The absence of Ir diffraction lines was expected from the highly dispersed form of iridium oxide for a non-reduced system.

When the Ir/Ce400 catalyst was reduced with hydrogen at 200 and 400°C, the crystallite sizes of ceria remained still at ~6 nm suggesting that no sintering occurred. However, the position of diffraction reflexes shifted to lower 2θ values and the diffraction

intensities became weaker. This was caused by defects formed through the reduction of the surface CeO₂, since the radius of Ce³⁺ ions (0.114 nm) produced by ceria reduction was larger than that of Ce⁴⁺ ions (0.097 nm) [102-106]. At 600°C, the reflexes for CeO₂ in the catalyst reduced became sharper, and the calculated crystallite size of ceria increased to 9.6 nm. In all cases, there was no detection of reflexes for metallic Ir suggesting that the Ir particles were highly dispersed on ceria, as it is confirmed by the further analyses on aged samples indicating mean particle sizes of 2-3nm.

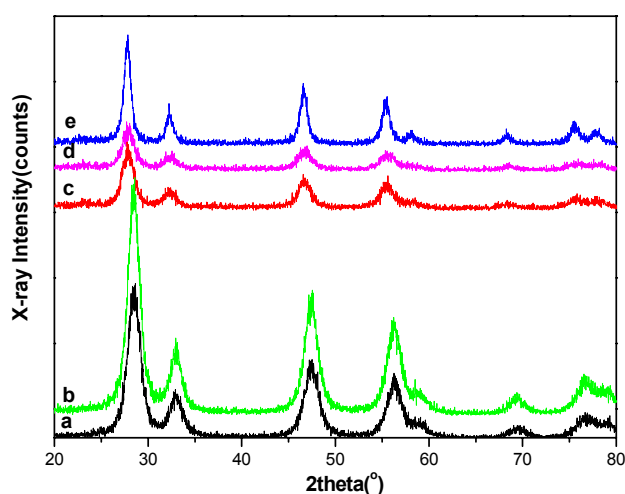


Figure 1 XRD patterns of Ce400 (a) the as-prepared Ir/Ce400 catalyst (b) and the Ir/Ce400 catalysts after reduction with hydrogen at 200°C (c) 400°C (d) and 600°C (e).

HRTEM. Fig. 2 shows the HRTEM images of the as-prepared Ir/Ce400 catalyst. The sizes of ceria particles were in the range of 5-10 nm, in good agreement with XRD and BET measurements. The spherical ceria particles were poorly crystalline and their composites were oriented randomly and interfaced epitaxially. Ir particles were not observed on this unreduced sample in line with XRD analysis. However, EDX analysis (Fig 3) confirmed the presence of Ir all over the surface of CeO₂.

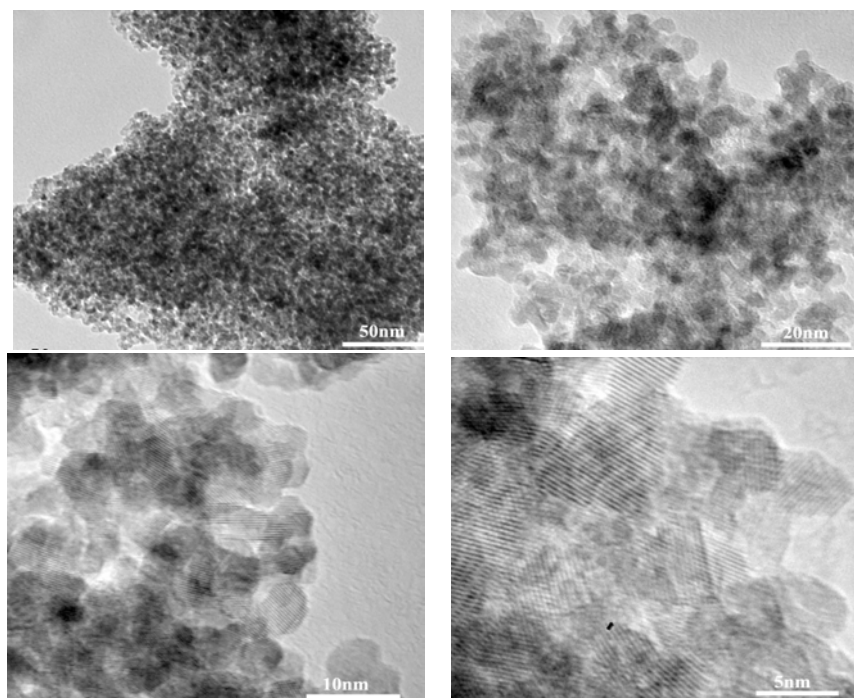


Figure 2 HRTEM images of the fresh Ir/Ce400 catalyst.

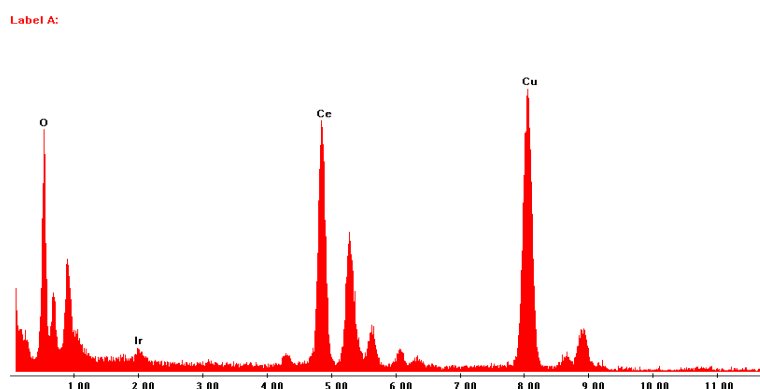


Figure 3 EDX spectrum of the Ir/Ce400 catalyst

TPR. Fig. 4 compares the TPR profiles of the Ir/Ce400 catalyst and the Ce400 support. Pure Ce400 showed a broad reduction peak around 483°C with a hydrogen consumption amounting to 420 μmol/g corresponding to a stoichiometric reduction of CeO₂ to CeO_{1.93}. Another broad reduction peak appeared at 789°C with a hydrogen consumption of 464 μmol/g, indicating the further reduction of CeO_{1.93} to CeO_{1.85}. The former is usually assigned to the reduction of surface ceria and the latter is related to the reduction of bulk ceria [106]. To the contrary, three intensive reduction peaks were observed for the Ir/Ce400

catalyst at 77, 345 and 769°C, respectively. The reduction peak at 77°C corresponded to a H₂ consumption of 993 μmol/g, which was much larger than the quantity of hydrogen required for the stoichiometric reduction of IrO₂ to Ir (218 μmol/g). The remaining hydrogen (775 μmol/g) is obviously used to reduce CeO₂ to CeO_{1.87}. Most likely this reduction proceeds at the ceria surface and subsurface, as generally proposed in the literature showing the existence of reduction gradients between surface and bulk [98]. Therefore, this main hydrogen consumption could be assigned to the combined reduction of IrO₂ and surface ceria. The hydrogen consumption corresponding to the reduction peak at around 345°C was 202 μmol/g, which indicated a further surface reduction of CeO_{1.87} to CeO_{1.84}. The high temperature reduction at 769°C could be regarded as the bulk reduction of ceria and the consumed hydrogen amounted to 388 μmol/g. This value corresponds to the reduction of bulk ceria from CeO_{1.84} to CeO_{1.77}.

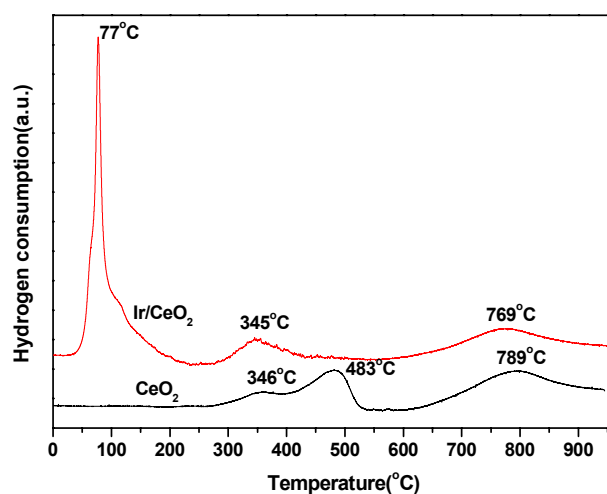


Figure 4 TPR profiles of the Ce400 support and of the Ir/Ce400 catalyst

Hence, the presence of Ir caused the reduction of CeO₂ to shift to a much lower temperature region, indicating that there was a strong interaction between Ir and ceria. This observation is also in good agreement with previous findings concerning the reduction behavior of ceria-supported noble metal catalysts [107,108,109]. Indeed, it can be supposed that hydrogen, once dissociated on metallic Ir, is able to spill over to CeO₂ and reduce it at lower temperatures.

OSC. Cerium oxide is well recognized to exhibit a very high oxygen exchange capacity [110-115]. This capacity is associated with the ability of cerium to act as an oxygen buffer through the storage/release of O₂ due to the Ce⁴⁺/Ce³⁺ redox couple [116]. It has been found that OSC can enhance the activity and stability of catalysts in reactions involving hydrogen production from ethanol [117]. In the present study, oxygen uptake was 235 and 596 $\mu\text{molO}_2/\text{g}$ for the pure Ce400 and the Ir/Ce400 catalyst, respectively. This strong increase in the OSC for the Ir containing ceria is in good keeping with the observation that an addition of noble metals promotes in general the ceria OSC significantly [118,119]. Though it can be analyzed as a proof of a strong metal/support interaction, the specific role of the noble metal in OSC enhancement remains a matter of debate. One possible explanation is that part of the added metal forms small oxide clusters within the fluorite structured ceria, acting as privileged pathway for oxygen diffusion and storing [114]. It also may be due to the smaller size of noble metal cations that participate to remove the strain associated with the increase of ionic size accompanying the Ce⁴⁺ \rightarrow Ce³⁺ transition [120,121].

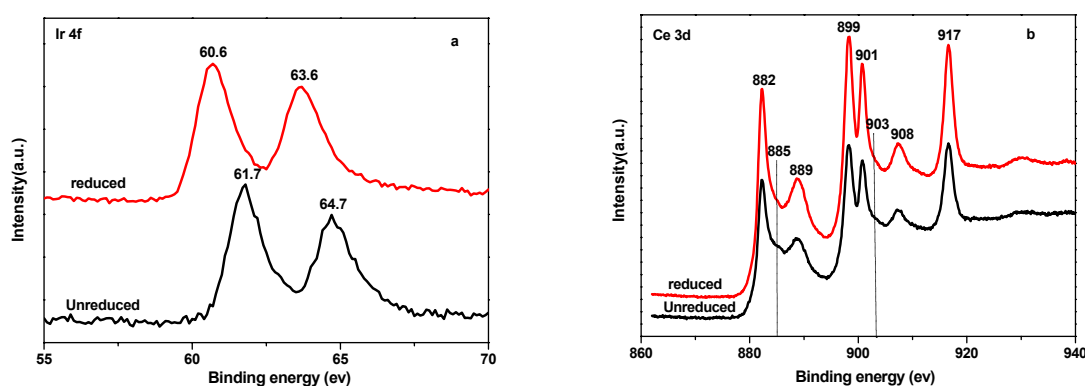


Figure 5 XPS of Ir4f (a) and Ce3d (b) for the reduced and unreduced Ir/Ce400 catalysts.

XPS. The Ir4f XP spectra of unreduced and reduced samples are shown in Fig 5a. The spectrum of the unreduced sample shows a doublet centered at around 61.7 and 64.7 eV. These peaks correspond to the binding energy of IrO₂ species. The spectrum of the reduced sample shows a doublet centered at 60.6 and 63.6 eV, characteristic of the binding energy of Ir⁰ metal. It indicated that most of the Ir oxide species were reduced to metallic Ir after reduction step.

Fig 5b shows the XPS spectra of the unreduced and reduced Ir/Ce673catalyst in the Ce3d region. The unreduced samples exhibit six peaks at around 882, 889, 899, 901, 908 and 917eV, which can be assigned to Ce3d_{5/2} 4f², Ce3d_{5/2} 4f¹, Ce3d_{5/2} 4f⁰, Ce3d_{3/2} 4f², Ce3d_{3/2} 4f¹, Ce3d_{3/2} 4f⁰ respectively for Ce⁴⁺ species [117-119]. In addition to these six peaks, the reduced sample exhibits shoulders at around 885 and 903eV due to the formation of Ce³⁺ species. This is in line with the TPR results showing that the ceria surface is partially reduced upon a hydrogen treatment at 400°C.

From the previous characterization results, one could conclude that iridium species were highly dispersed on the ceria surface and the redox capacity of CeO₂ support was greatly enhanced due to the strong interaction between iridium and ceria. In fact, the Ir-CeO₂ interaction would be helpful to increase the catalyst activity in hydrogen production from ethanol.

III.2. Effect of ceria particle sizes

Since a key feature of the Ir/CeO₂ systems is related to a strong metal/support interaction, it seemed of interest to follow the impact of ceria particle size controlled by the temperature of calcination upon the main characteristics of the fresh catalysts.

Catalyst	Surface area (m ² /g)
Ir/Ce550	102
Ir/Ce700	45
Ir/Ce850	16

Table 1 surface areas of the catalysts

Table 1 gives the surface area of the Ir/CeO₂ catalysts which support were calcined at different temperatures. The surface area of the samples decreased in the following order: Ir/Ce550 > Ir/Ce700 > Ir/Ce850.

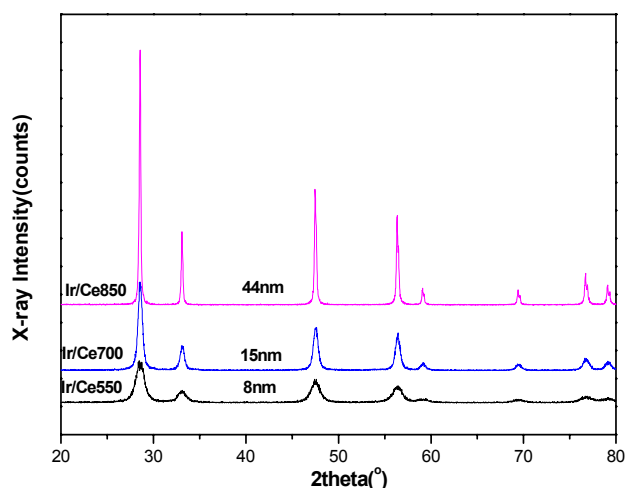


Figure 6 XRD patterns of the Ir/CeO₂ catalysts with different ceria particle sizes.

XRD. Fig 6 presents the XRD patterns of the Ir/CeO₂ catalysts displaying different ceria particle sizes, due to changes in the temperature of pre-calcination for the ceria. The XRD patterns showed that only a fluorite-type oxide structure of CeO₂ was present in all samples. Upon rising the calcination temperatures, the CeO₂ reflexes became sharper, as expected for particles with increasing size. The ceria crystallite size increased in the following order: Ir/Ce550 (8nm) < Ir/Ce700 (15nm) < Ir/Ce850 (44nm). In all cases, the absence of Ir diffraction lines indicated that the iridium remained highly dispersed and amorphous for a non-reduced system. There was only a slightly increase for the ceria particle sizes from Ir/Ce400 to Ir/Ce550 catalyst. However, for the Ir/Ce850 catalyst, the support particle sizes were significantly enlarged.

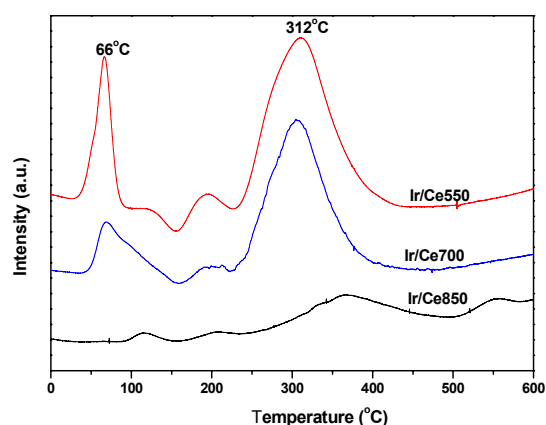


Figure 7 H₂-TPR profiles of the Ir/CeO₂ catalysts with different ceria particle sizes.

TPR. Fig 7 compares the H₂-TPR profiles of the Ir/Ce550, Ir/Ce700 and Ir/Ce850 samples. Two main reduction peaks were observed at 66°C and 312°C, respectively, for the Ir/Ce550 catalyst. As already discussed for the Ir/Ce400 catalyst, the low temperature peak (66°C) was assigned to the combined reduction of Ir and Ce surface species, while the reduction peak at 312°C was attributed to the reduction of the CeO₂ surface. The shift in the reduction peak for the Ir/Ce700 catalyst towards higher temperature indicated the slight decline of the interaction between iridium and ceria. However, a strong decrease in intensity of the surface ceria reduction was observed in the case of the Ir/Ce850 catalyst. This observation might suggest that the decline of the metal-support interaction harmed the ability of the supported metal to activate H₂ and then spill it over to the support. On the other hand, Ir/Ce850, which was calcined at higher temperature and had larger ceria particle size, should have more perfect crystalline structure with fewer oxygen defects and hence smaller amount of mobile surface oxygen species.

HRTEM. Fig 8 presents the HRTEM images of the Ir/Ce550, Ir/Ce700 and Ir/Ce850 catalysts. The sizes of ceria particles increased with rising calcination temperature, in good agreement with XRD measurements. Extended IrO₂ particles were not observed on Ir/Ce550, Ir/Ce700 catalysts in line with XRD analysis. However, EDX and HRTEM image analysis also confirmed the presence of Ir on the surface of CeO₂. Both IrO₂ particles (2-4nm) on the ceria borders and iridium clusters between CeO₂ particles were observed for the Ir/Ce850 catalyst. This indicates that even after major ceria sintering, the dispersion of Ir is not or only slightly changed. A further deduction is that on well dispersed ceria systems (reference Ir/Ce400), the mean particle size can be considered as in the range 2-4 nm, since much smaller particles (below 2nm) are known to be unstable for noble metals.

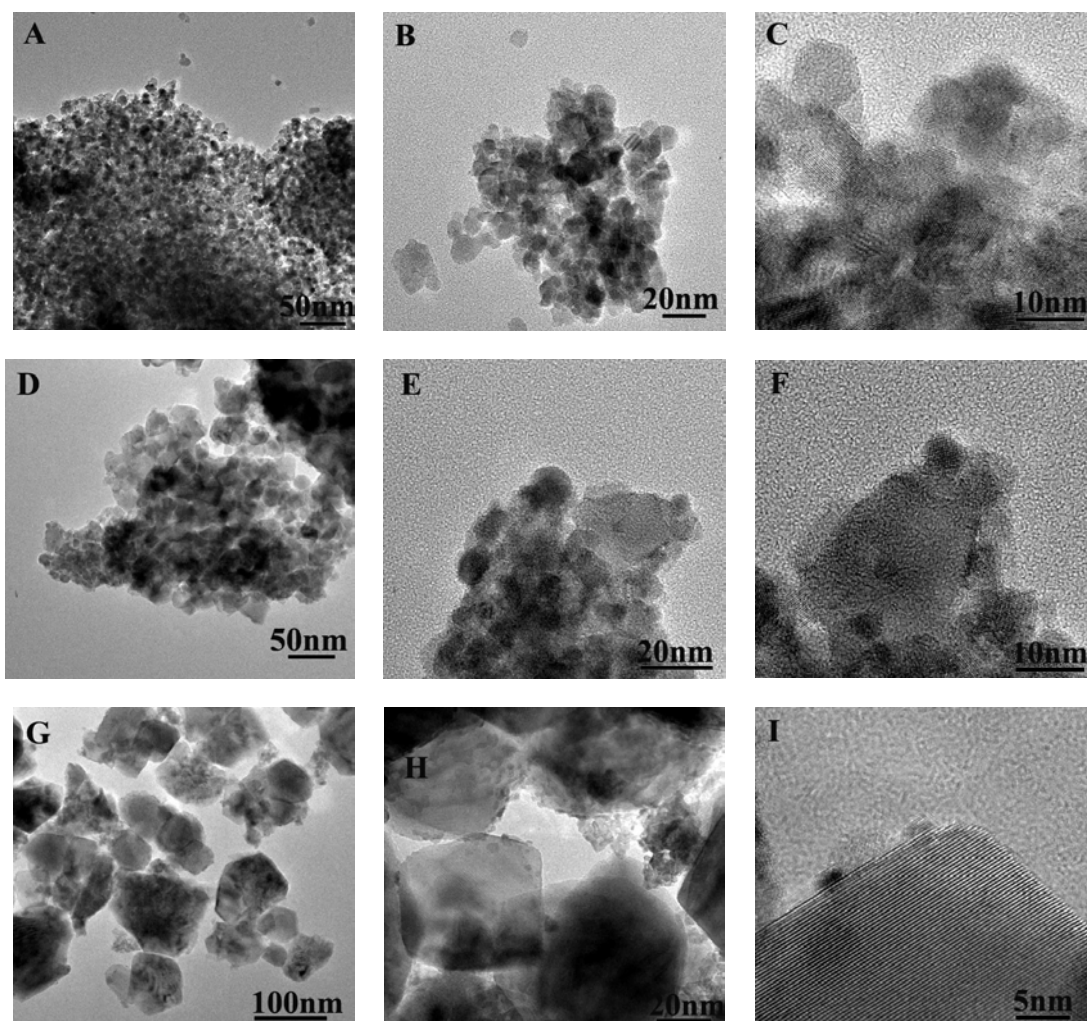


Figure 8 HRTEM images of the catalysts: (A-C) Ir/Ce550 (D-F) Ir/Ce700 (G-I) Ir/Ce850

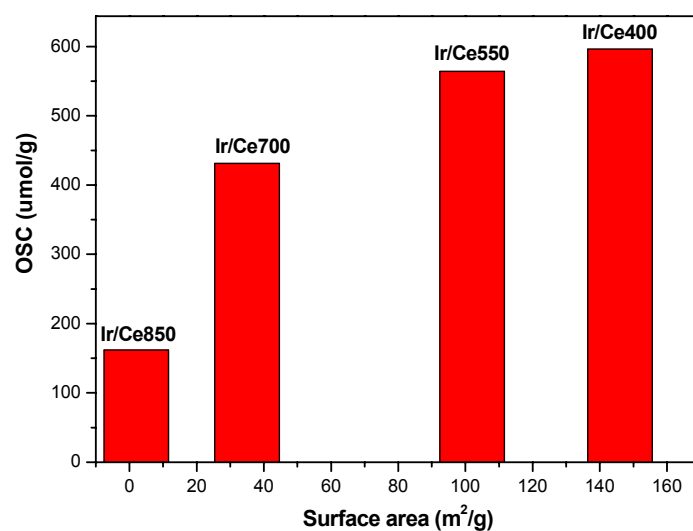


Figure 9 OSC versus surface area of the Ir/Ce550, Ir/Ce700 and Ir/Ce850 catalysts

OSC. Fig 9 presents the relationship of the oxygen storage capacity and the surface area

of Ir/CeO₂ catalysts with different ceria particle sizes. The oxygen storage capacity decreased in line with the surface areas. It is also interesting to note that the oxygen storage capacity is only slightly decreased up to an aging temperature of 700°C but drops dramatically when ceria is calcined at 850°C. Mamontov et.al. [122] proposed that the oxygen defects of the ceria annihilated at high calcination temperature due to recombination of the interstitial ions with the vacancies. In ceria, some oxygen ions may relocate themselves from the tetrahedral sites to the octahedral sites, leaving the oxygen vacancies in the tetrahedral sites and the oxygen interstitial ions in the octahedral sites. The interstitial oxygen ions are the “active” ions that provide necessary mobility crucial to the function of ceria as oxygen storage medium. If the annealing temperature is not high enough they may not be able to overcome a potential barrier to get into the regular tetrahedral sites, and remain in the octahedral sites. Only when the sample is treated at sufficiently high temperature, thermally activated interstitial oxygen ions may enter regular tetrahedral sites and recombine with vacancies.

It is clearly observed that there is little influence of the catalyst's physical and chemical properties if the calcination temperature of CeO₂ increases from 400 to 550°C. However, both the catalyst structure and the redox properties significantly changed after the ceria was calcined at 850°C. Surface area and the oxygen storage capacity drastically decreased. The influence of this change for the catalyst activity and stability in ethanol oxidative steam reforming will be discussed later.

III.3. Conclusion

This chapter mainly summarized the characterization results of the fresh Ir/CeO₂ catalyst in order to investigate the physical and chemical properties of the catalysts. Several observations deserve to be outlined.

i) For the XRD results, there are no diffraction lines of active metal species in all cases (including Ir/Ce400 Ir/Ce550 Ir/Ce700 and Ir/Ce850 catalysts). HRTEM images give further evidence that the noble metals stayed highly dispersed.

ii) With the addition of noble metal (Ir), the reduction property of ceria is greatly

promoted which is attributed to the unique metal-CeO₂ interaction. Once the noble metal supported on the surface CeO₂ is reduced, H₂ molecules can be effectively activated on metal species. The dissociated H atoms subsequently spillover to the surface CeO₂ at the metal-CeO₂ interface, promoting the reduction of surface CeO₂ to Ce³⁺ at relatively low temperature [123].

iii) For the Ir/CeO₂ catalysts, the oxygen storage capacity of ceria only slightly decreases if the calcination temperatures of CeO₂ increased not beyond 700°C. However, the OSC drops sharply during the aging at a temperature of 850°C. The oxygen storage capacity is correlated to the oxygen defect concentration. In ceria, the concentration of oxygen defects and the amount of “active” oxygen (interstitial oxygen ions) remain almost unchanged up to 700°C. While ceria exhibits a dramatic drop in the concentration of vacancies and interstitial ions following higher temperature treatment (850°C) due to the interstitial oxygen ions to reach the tetrahedral sites and recombine with vacancies.

Similar characterization data will be provided later for catalysts aged after ethanol reforming in order to understand the effect of catalysis on these various catalysts.

Chapter IV Comparison between SR, POX and OSR over Ir/CeO₂ catalyst in fixed bed reactor

In order to compare steam reforming, partial oxidation and oxidative steam reforming of ethanol over Ir/Ce400 catalyst under conditions close to a potential application, the influence of the reaction temperature and catalyst stability were investigated with an undiluted reactant feed. Parts of these results have already been published [124,125].

The search for relationship between catalyst structure and catalytic performance is a permanent challenge, since ideally it should allow one to foresee catalytic performances from the catalyst composition and a structural description. This kind of investigation requires indeed an advanced characterization of both fresh and used catalysts.

In general, the size of support particle, i.e. BET area, is assumed to play an important role in hydrogen production when bi-functional mechanism is in place [126]. For instance, Kugai et al [45] investigated the effects of nanocrystalline CeO₂ supports for oxidative steam reforming of ethanol. The results demonstrated that Ni-Rh catalysts supported on small CeO₂ particles showed better ethanol conversion and hydrogen selectivity than those catalysts having metal clusters supported on larger particles. Mamontov et al also proposed that the calcination temperature of CeO₂ support had a great influence on the oxygen storage capacity of CeO₂ [122].

In this chapter, we also examine the effects of ceria particle size on the catalytic performance of ethanol SR, POX and OSR, within the context of the above mentioned search for a structure-activity relationship. For that purpose, it is required to fix the other structure parameters such as the active metal content. This study was therefore carried out by keeping constant Ir loading.

IV.1. Homogeneous reaction

Homogeneous reactions are very important when studying the ethanol reforming and

special attention must be paid to reduce the dead volume to avoid or at least minimize them. We investigated the homogeneous reaction under the OSR conditions. Results obtained with an empty tubular reactor are presented in Fig 1.

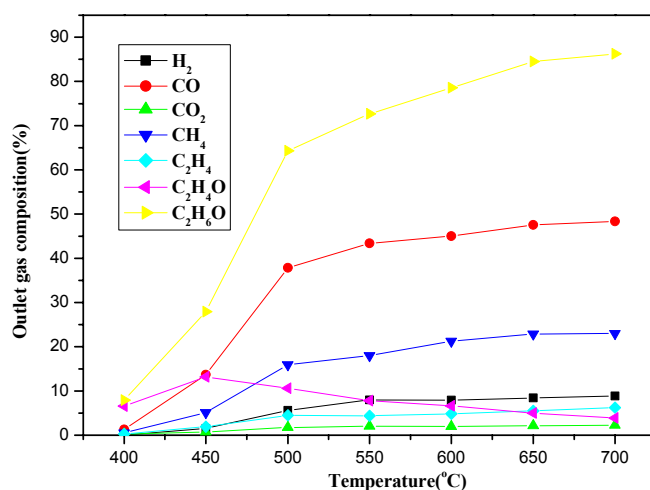


Figure 1 Conversion of ethanol and outlet gas composition vs temperature at conditions where homogeneous reactions prevail: Ethanol/H₂O/O₂=1:1.8:0.6, GHSV=6000 ml/g_{cat}·h

Ethanol decomposed at temperatures higher than 450°C reaching a conversion of 90% at 700°C with a total conversion of oxygen. There is a high concentration of CO (about 40%), but the hydrogen concentration remains very low (about 10%) due to the high reaction selectivity to hydrogenated products such as methane or ethylene. Monitoring the C₂H₄ formation is also rather important; as ethylene acts as a very strong promoter for coke formation.

Fatsikostas et al. [59] also studied the homogeneous reaction influence under ethanol steam reforming conditions (EtOH:H₂O=1:3). Homogeneous activity is initiated at about 600°C and becomes significant at temperatures higher than 700°C. Homogeneous activity at low temperature is primarily directed towards a dehydrogenation producing acetaldehyde, while at higher temperature dehydration and cracking or dissociation also take place.

IV.2. Steam reforming of ethanol over Ir/Ce400 catalyst

IV.2.1. Effect of reaction temperature on activity

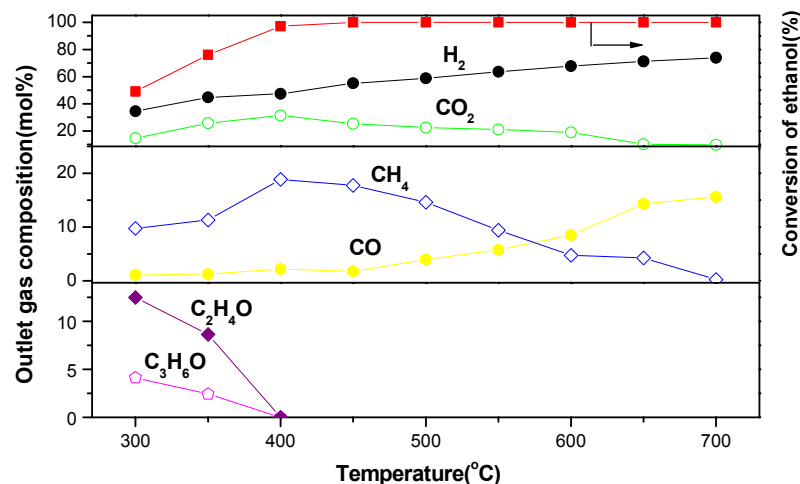
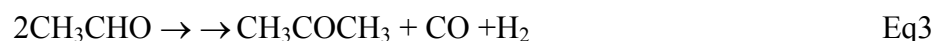


Figure 2 Effect of the reaction temperature on the product distribution for ethanol SR over the Ir/Ce400 catalyst. Reaction conditions: Ethanol/H₂O =1:3.0, GHSV=6000 ml/g_{cat}·h

Fig 2 illustrates the product distribution from ethanol SR with a stoichiometric water/ethanol feed at a molar ratio of 3.0. The concentration of H₂ increased progressively with temperature. At temperatures below 400°C, acetaldehyde, acetone and methane were formed. This suggests a primary dehydrogenation of ethanol to acetaldehyde (Eq1), as will be analyzed in details in chapter V dedicated to reaction mechanism. The acetaldehyde is being further decomposed to methane and carbon monoxide (Eq2) or converted to acetone through aldolisation processes [127](Eq3).



At 400°C and above, ethanol, acetaldehyde and acetone were no more formed since the C2 intermediates were decomposed into fragments desorbing as H₂, CO (equilibrated by WGS reaction (Eq4) and into CH₄ also equilibrated via methane SR (Eq5).





Thus, at 700°C, the concentration of H₂ approached 73% and the concentration of CH₄ decreased to 0.3% due to methane SR as predicted by thermodynamics [23].

The concentration of CO increased monotonously up to 16% and the concentration of CO₂ decreased to 10%, as expected from the WGS equilibrium changes with temperature. No ethylene formation was observed probably due to the basicity of ceria, which inhibited the dehydration of ethanol. Another possible explanation was that ethylene could be rapidly be reformed once it was formed. Effectively, it will be shown later that at very short contact time (at a tenfold higher GHSV), a formation of ethylene can be detected.

IV.2.2. Long term stability test

The development of stable catalysts is one of the most important issues in the production of hydrogen from ethanol, particularly for stoichiometric feed compositions where no excess water and/or oxygen is available to remove carbon deposits that are detrimental to the catalytic stability.

The stability of the selected Ir/ceria system was tested at very different contact times, i.e., under conditions where the conversion of ethanol is complete or only partial.

Ethanol SR at low GHSV. At high contact time i.e. for a GHSV of 6000ml/g_{cat}·h, ethanol was fully converted all along the testing period. Figure 3 shows the concentration of H₂, CO₂, CH₄ and CO in the outlet streams of ethanol SR up to 60 h on stream at 550 and 650°C.

When operated at 550°C (Fig 3, a), the outlet gas compositions remained very stable along the 60 h on stream. The concentrations of H₂, CO₂, CO and CH₄ in the outlet gas were 63%, 18%, 9% and 10% respectively, without any acetaldehyde and acetone. By increasing reaction temperature to 650°C (Fig 3, b), methane reforming was favored and the concentrations of H₂, CO, CO₂ and CH₄ in the outlet stream of ethanol SR were about 70%, 15%, 10% and 5%, respectively while the conversion indeed was still kept complete over the testing period.

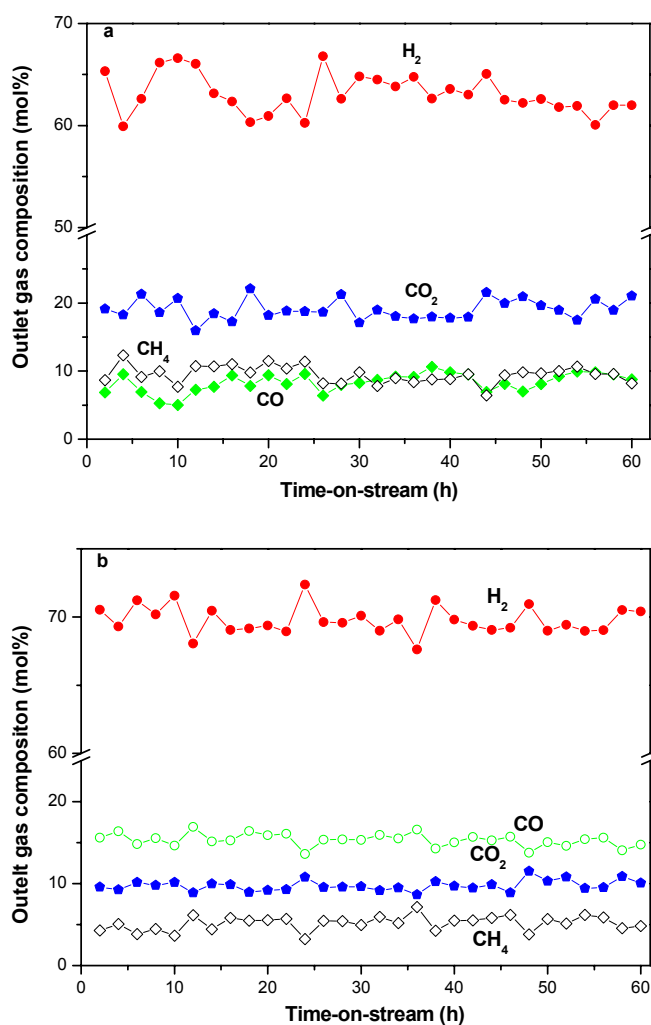


Figure 3 Changes in outlet gas composition for SR of ethanol over the Ir/Ce400 catalyst. Reaction conditions: 550°C (a), 650°C(b), Ethanol/H₂O=1:3, GHSV=6000 ml/g_{cat}·h

Ethanol SR at high GHSV. At much lower contact time (12.5 times lower than for the previous stability results) i.e. for a GHSV of 75000ml/g_{cat}·h, ethanol was only partly converted all along the testing period, involving the presence of C₂ intermediates for the SR reaction at 650°C, which can be considered as the most demanding conditions in term of stability.

As shown in Fig 4, the activity decreased significantly during the initial period of 3-5 h on stream, then slowly and regularly deactivated over the all remaining testing period. After about 60h on-stream reaction, there was only a little fluctuation in products distribution. As can be seen in Fig 4, under the high GHSV conditions, the production of acetaldehyde and methane were not negligible, which confirmed that acetaldehyde and methane are primary

products [128-130] and that under these demanding conditions, the thermodynamic equilibrium is not achieved.

The reasons for the initial deactivation followed by the very slow one deserve to be investigated by means of catalyst characterization after aging period.

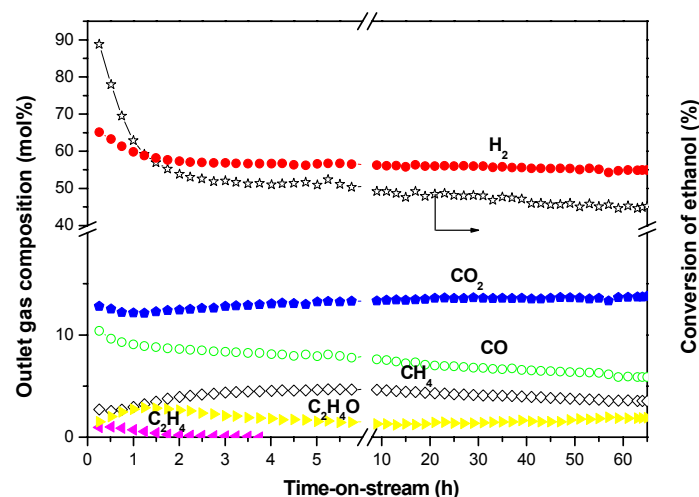
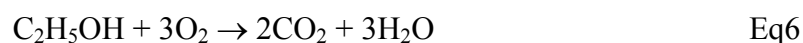


Figure 4 Changes in the outlet gas composition for SR of ethanol over the Ir/Ce400 catalyst. Reaction conditions: 650°C, Ethanol/H₂O=1:3, GHSV=75000 ml/g_{cat}·h

IV.3. Partial oxidation of ethanol over Ir/Ce400 catalyst

IV.3.1. Effect of reaction temperature on activity

Fig 5 shows the reaction results of POX of ethanol over the Ir/Ce400 catalyst with an ethanol/O₂ molar ratio of 1:0.6. Carbon dioxide and water (not quantified) were formed as the main products at low temperatures, indicating the combustion of ethanol (Eq6) [15,131].



About 3% acetaldehyde was produced by dehydrogenation of ethanol, which disappeared completely at 500°C. The formation of acetone through decarbonylation of acetaldehyde was also observed, and vanished at 450°C. The formation of CH₄ and CO evidenced the decomposition of acetaldehyde. Complete conversion of ethanol, acetaldehyde and acetone was achieved at 500°C. At temperatures above 500°C, the concentrations of methane and CO₂ decreased continuously due to the occurrence of

methane reforming with carbon dioxide and/or water, and the relative concentrations of H₂, CO and CO₂ were monitored by the reversible WGS reaction. At 700°C, the outlet gas consisted of 56% H₂, 29% CO, 13% CO₂ and 2%CH₄.

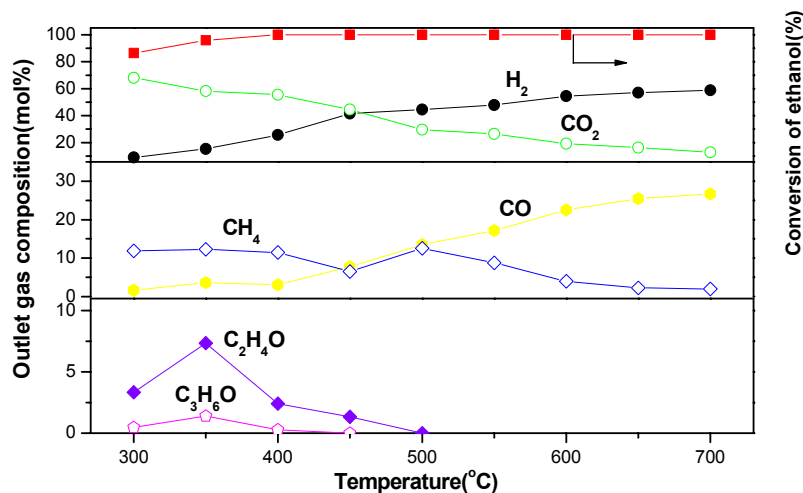


Figure 5 Effect of reaction temperature on the product distributions for POX of ethanol over the Ir/Ce400 catalyst. Reaction conditions: Ethanol/O₂=1:0.6, GHSV=6000 ml/g_{cat}·h

IV.3.2. Long term stability test

The stability tests were performed at high contact time to ensure total conversion of ethanol. Fig 6 presents the concentration of H₂, CO₂, CH₄ and CO in the outlet streams of partial oxidation of ethanol within 60 h on-stream operated at 550 and 650°C. In all the cases, there was no apparent deactivation, as expressed by a change in the effluent dry products composition.

Long term catalytic test at high GHSV ensuring partial conversion of ethanol was not carried out in fixed bed reactor due to technical issues. However, very stable long term performance was obtained at partial conversion in a micro-reactor (see Chapter VI) for OSR which combines SR and POX. Therefore it is quite likely that the Ir/Ce400 catalyst also displays an excellent stability for partial oxidation of ethanol, even with stoichiometric feed compositions. Further experiments are required for strengthening that conclusion.

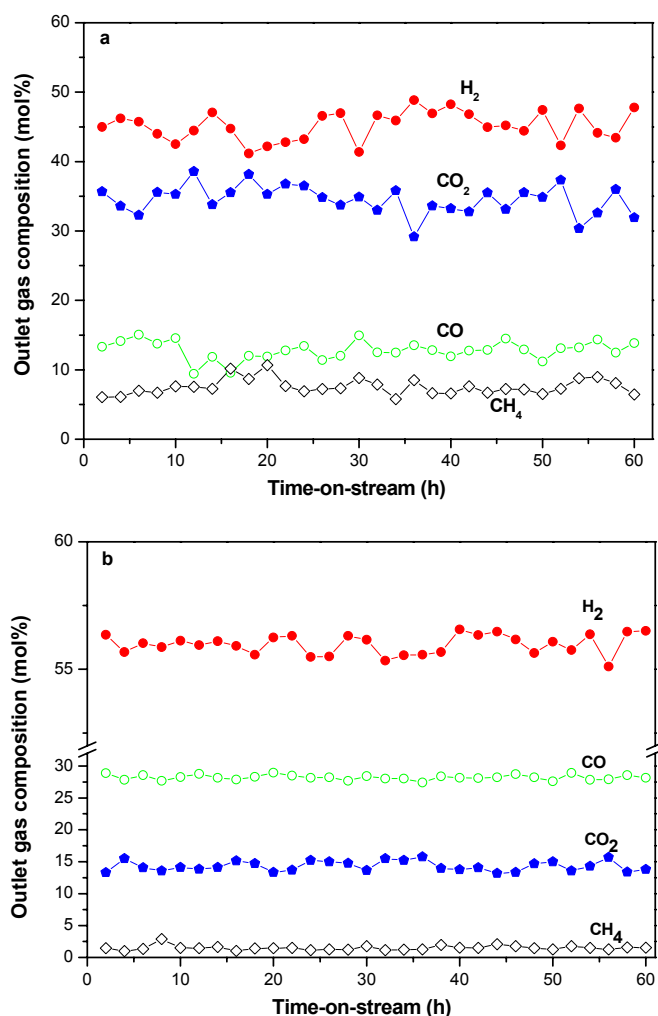


Figure 6 Changes in outlet gas composition for POX of ethanol over the Ir/Ce400 catalyst. Reaction conditions: 550°C (a) 650°C (b), Ethanol/O₂=1:0.6, GHSV=6000 ml/g_{cat}·h

IV.4. Oxidative steam reforming of ethanol over Ir/Ce400 catalyst

IV.4.1. Effect of reaction temperature on activity

The influence of temperature on catalytic performance over Ir/Ce400 catalyst in the oxidative steam reforming of ethanol is shown in Fig 7. It can be seen that both the conversion of ethanol and the concentration of H₂ increased progressively with temperature. By increasing temperature up to 700°C, the hydrogen concentration in the effluent approached to 65%. Concerning the distribution of C-containing products, significant amount of CO₂ was formed at lower temperatures, suggesting that ethanol was mainly oxidized into CO₂. Meanwhile, the concentration of acetaldehyde, formed through

dehydrogenation of ethanol, decreased rapidly from 12% at 300°C to practically zero at 450°C. Simultaneously, traceable amount of acetone was produced through the condensation of acetaldehyde at 300°C, which further increased to 4% at 400°C and disappeared at 500°C.

The formation of methane through the decomposition of ethanol was observed to be significant (about 18%) at 300°C, but the amount of CO was lower than that of methane, implying the occurrence of the water gas shift reaction. At 500°C, the outlet stream only contained 10%, 26%CO₂, 57%H₂ and 7%CO.

With further increasing the temperature, rapid increase in the CO concentration and slow decrease of carbon dioxide concentration were observed. This clearly indicated that the steam reforming of methane and the reverse water gas shift reaction took place as the major reactions, as predicted by thermodynamics. At 700°C, methane was almost completely reformed into hydrogen and CO, and the outlet gas consisted of 65%H₂, 18%CO, 16%CO₂ and 1%CH₄.

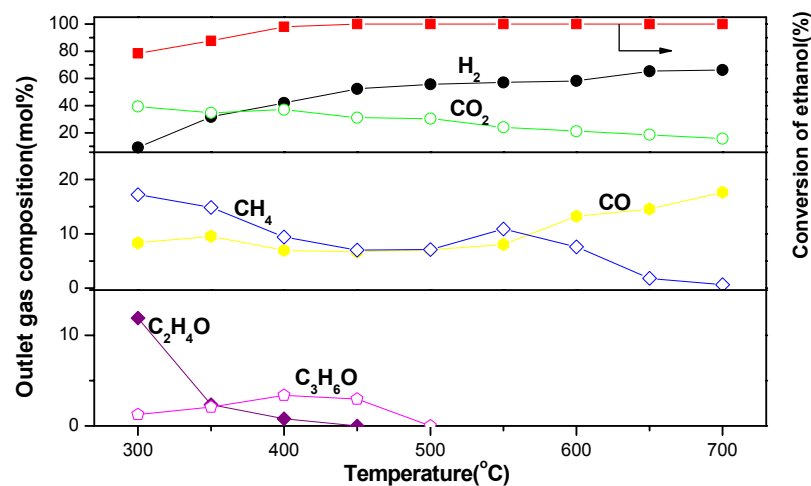


Figure 7 Effect of reaction temperature on the product distribution for oxidative steaming reforming of ethanol over the Ir/Ce400 catalyst. Reaction conditions: Ethanol/H₂O/O₂=1:1.8:0.6, GHSV=6000 ml/g_{cat}·h

IV.4.2. Long term stability test

Long-term stability test of oxidative steam reforming of ethanol was conducted over the Ir/Ce400 catalyst at 550 and 650°C, respectively, at low GHSV, ensuring complete conversion of ethanol and C₂ intermediates into CH₄, CO, CO₂ and H₂.

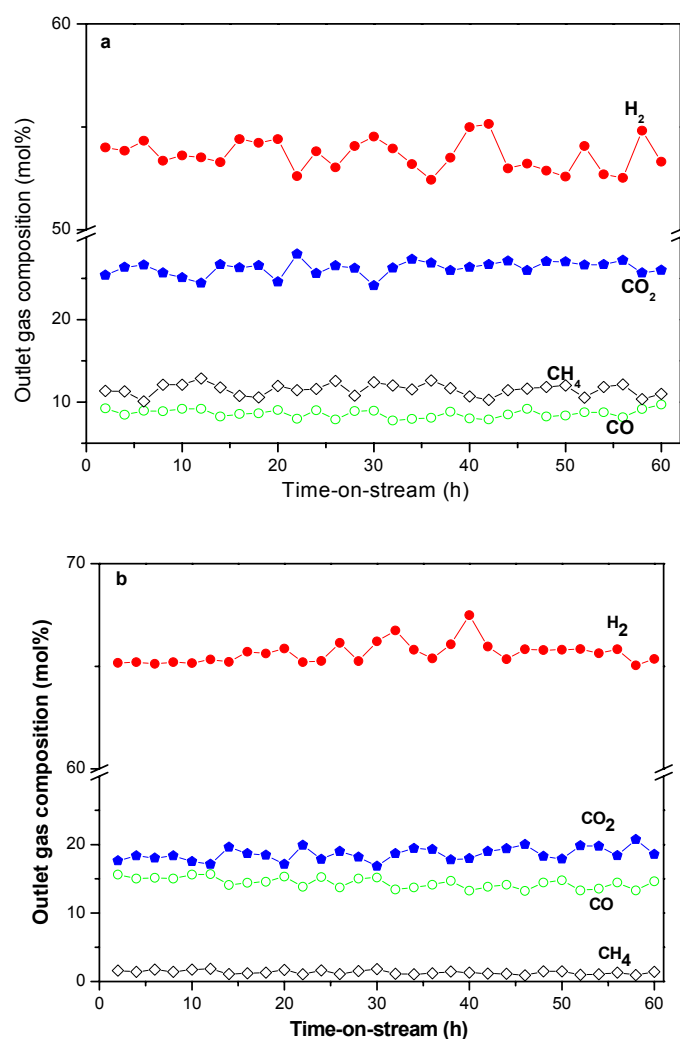


Figure 8 Changes in outlet gas composition for oxidative steam reforming of ethanol over the Ir/Ce400 catalyst. Reaction conditions: 550°C (a) 650°C(b), Ethanol/H₂O/O₂=1:1.8:0.6, GHSV=6000 ml/g_{cat}·h

Fig 8a shows the product concentrations in the outlet stream reforming of ethanol over the Ir/CeO₂ catalyst at 550°C. The concentrations of H₂, CO₂, CH₄ and CO were about 55%, 26%, 11% and 9%, respectively. When operated at 650°C (Fig8b), methane was almost totally reformed and the outlet stream contained about 65%H₂, 18%CO₂, 15%CO and only negligible amount of methane (about 2%). The outlet gas composition was kept stable for 60h on stream.

In a summary, the Ir/CeO₂ catalyst exhibited excellent catalytic performance for ethanol SR, POX and OSR reactions, even with stoichiometric feed compositions. Under reaction conditions, acetaldehyde was the primary product below 400°C, which mainly decomposed to methane and carbon monoxide at higher temperatures, whereas methane reforming and water gas shift were the major reactions above 500°C. The Ir/CeO₂ catalyst also showed rather high stability for the 3 reactions carried out at low GHSV in the 550-650°C temperature range, under complete conversion conditions without apparent deactivation for 60h on stream. In contrast, at very high GSHV, under partial ethanol conversion conditions, deactivation was observed for SR, but apparently not for POX and OSR.

IV.5. Comparison between SR, POX and OSR over Ir/Ce400 catalyst

Temp (°C)	Ethanol conversion (%)			TOF* (S ⁻¹)		
	SR	OSR	POX	SR	OSR	POX
150	0.8	4.1	8.6	0.1	0.6	2.8
200	2.7	8.9	10.5	0.4	1.4	3.4

a : GHSV=36000 ml/g_{cat}·h

b: The average size of Ir particle was 2nm, for all cases, as measured from HRTEM images of the used catalysts

Table 1 Ethanol conversions and TOF of SR, POX and OSR

Table 1 compares the turnover frequencies (TOF) for the three reactions at low temperature, and high GHSV, ensuring low conversion for differential conditions. As expected, the TOF of Ir followed the order POX>OSR>SR, the TOF of POX being more than 10 times larger than that of the SR reaction. This is consistent with the TPSR result (which will be discussed in the next chapter) where the presence of oxygen was shown to greatly promote the surface reaction of ethanol, due to its easy activation both on reduced

ceria and on Ir particles.

In such a scheme, the reaction of ethanol mainly occurs at the CeO₂-Ir interface where i) Ir is mainly responsible for breaking the ethanol/acetaldehyde C-C bond and ii) CeO₂ activates H₂O/O₂ and produces active oxygen to oxidize carbonaceous fragments. Hence, the strong Ir-CeO₂ interaction favors these cooperative reaction steps and accelerates the conversion of ethanol.

	POX	OSR	SR
Y _{H2}	0.78	0.89	0.92

Table 2 Hydrogen yields for the SR, POX and OSR reactions over Ir/Ce400 catalyst (650°C)

Hydrogen yields for the SR, POX and OSR reactions over Ir/Ce400 catalyst are reported in Table 2. As already predicted from the stoichiometric equations specific of each reaction (see introduction section), the results show that the hydrogen yields increased in the order POX<OSR<SR.

Although steam reforming of ethanol (SR) exhibited the highest hydrogen yield, this reaction was however an endothermic process which requires large input of external energy.

In contrast, partial oxidation of ethanol (POX) does not need added heat but leads to the poorest hydrogen yield.

From the point of energy efficiency and hydrogen yield, oxidative steam reforming of ethanol (OSR) seems therefore to be the best choice for the industrial application, still ensuring relatively high hydrogen yield, but being close to a thermo-neutral process.

IV.6. Influence of ceria particle size for OSR over Ir/CeO₂ catalysts.

From the previous results of ethanol oxidative steam reforming over Ir/Ce400 catalyst, no deactivation was observed after a long term stability test under complete ethanol conversion (at low GHSV). However, as will be seen later, some initial deactivation was observed under partial conversion conditions (at high GHSV), but followed by a long lasting stabilization of performances.

This stability at low GHSV might be due to several factors among which an optimized Ir-ceria interfacial area which would favor oxygen and water activation to prevent coke formation and inhibit active metal sintering. In order to get further insight in this analysis, three iridium catalysts supported on CeO₂ support with different ceria particle sizes (Ir/Ce550, Ir/Ce700, Ir/Ce850) but with the same Ir dispersion were tested to check the influence of support particle size for the ethanol oxidative steam reforming.

IV.6.1. Effect of reaction temperature on product distributions

Fig 9 shows the catalytic performance of these Ir/CeO₂ catalysts on ethanol oxidative steam reforming reaction. It was found that both the ethanol conversion and the product distributions were similar for the Ir/Ce550 and Ir/Ce700 catalysts, which was also in line with the previous results obtained over the Ir/Ce400 catalyst. The concentration of hydrogen increased progressively with temperature and the complete conversion of ethanol was achieved at 450°C. More importantly, the production of undesirable reaction byproducts, i.e. acetaldehyde and acetone disappeared completely at 500°C. At higher temperature region, there was a rapid increase in the concentration of CO and a gradual decrease in the concentrations of CH₄ and CO₂. This indicates clearly that the reforming of CH₄ and the reverse WGS occurred significantly. It meant that increasing the ceria particle size from 6nm to 15nm had little influence for the catalytic activity in the oxidative steam reforming of ethanol.

However, the catalytic performance considerably decreased on Ir/Ce850. Increasing ceria particle size from 8nm to 44nm resulted in a marked decrease of the ethanol conversion at medium temperature (Fig.9a.), the full conversion being reached only at 650°C instead of 450°C for the two other systems.

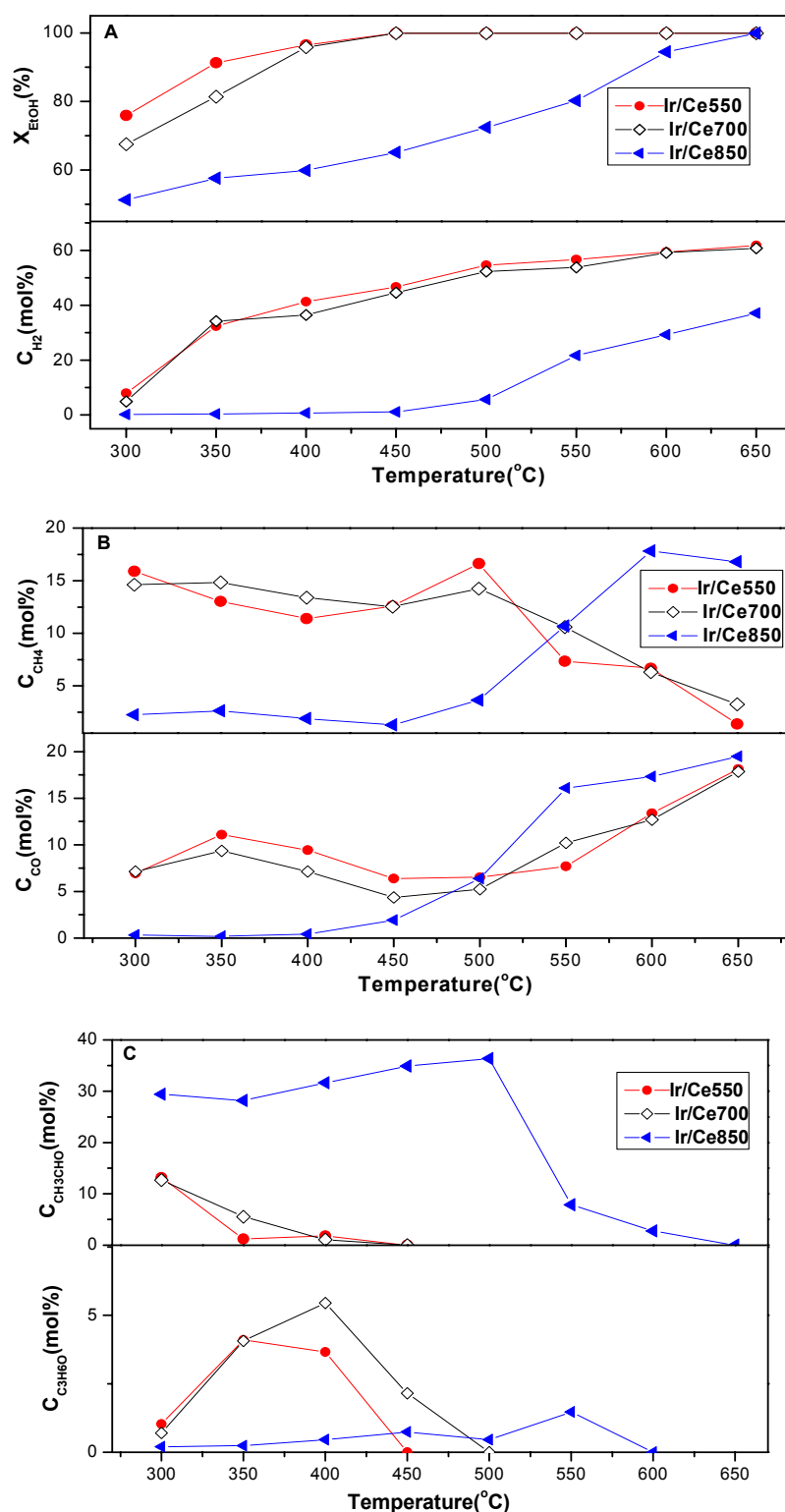


Figure 9 Effect of reaction temperature on the product distributions for OSR of ethanol over Ir/Ce550, Ir/Ce700 and Ir/Ce850 catalysts.

At 300°C, the main product in the outlet gas was acetaldehyde and almost no H₂ and methane production (Fig.9c.). It did not significantly change with increasing the reaction temperature to 500°C. This indicated that the drastically increase of the ceria particle size

weakened the catalyst ability of C-C bond dissociation caused by the decline of the metal-support interactions. Upon heating temperature, the concentration of acetaldehyde decreased continuously and the formation of CH₄ and CO evidenced the decomposition of acetaldehyde. As a result, the concentration of acetaldehyde in the outlet gas dropped to practically zero at 650°C. But there was still large methane formation (Fig 9b), which resulted in the lower hydrogen selectivity. It could be attributed to the relatively poor methane reforming capacity of the Ir/Ce850 catalyst. Lower oxygen storage capacity and Ir-ceria interaction hindered the activation of methane and water.

These results clearly demonstrate that when the ceria is sintered to a certain extent (corresponding to an oxide dispersion below about 2%), even well dispersed Ir particles cannot anymore ensure the proper interfacial cracking of C₂ intermediates from ethanol activation over ceria. This unambiguously points out the key role of ceria not only for activating ethanol and oxidizing it into acetaldehyde, but also for providing to the Ir/ceria interface enough OH groups and lattice oxygen to ensure the oxidation of carbonaceous C₁ into CO. These elementary steps will be analyzed in details in the chapter V.

IV.6.2. Effect of ceria particle size on long term stability tests

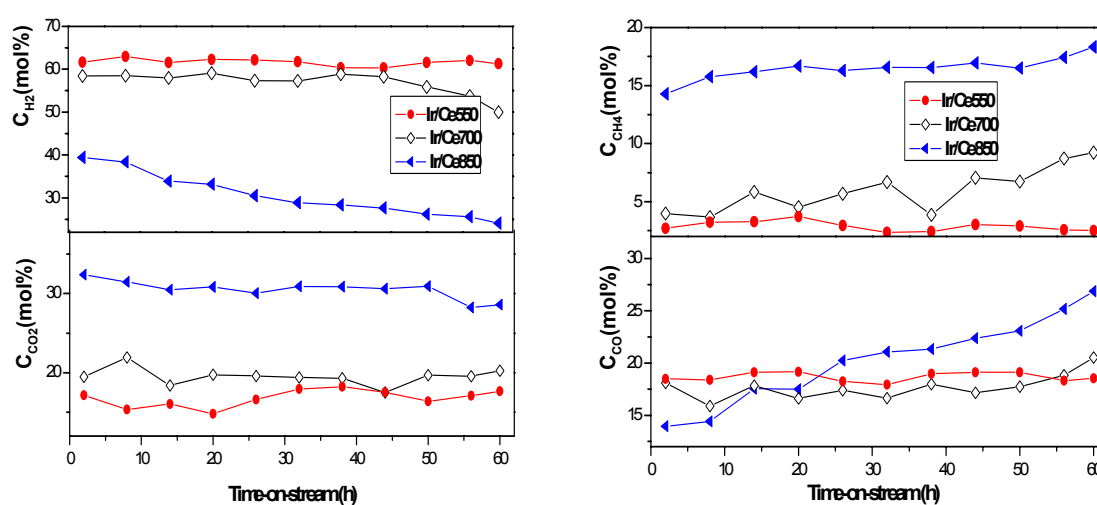


Figure 10 Changes in outlet gas composition for oxidative steam reforming of ethanol over the Ir/Ce550, Ir/Ce700 and Ir/Ce850 catalysts. Reaction conditions: Ethanol/H₂O/O₂=1:1.8/0.6, temperature: 650°C, GHSV=6000 ml/g_{cat}·h

The effect of time on stream on the outlet concentrations is depicted in Fig 10. For the Ir/Ce550 catalyst, there was no significant change in product distributions, while the conversion was kept complete over the testing period. The concentrations of H₂, CO₂, CO and CH₄ in the outlet gas of ethanol OSR were 62%, 18%, 17% and 3%, respectively, which followed the thermodynamics.

For the Ir/Ce700 catalyst, there was no variation of the gas phase distribution and the molar concentration of main products during the first 45h of reaction was 59% H₂, 19% CO₂, 17% CO and 5% CH₄. Then the concentration of hydrogen decreased gradually to 50%. Simultaneously, there was a slight increase of the CO and methane concentrations. This indicated a small deactivation of the Ir/Ce700 catalyst took place.

However, the Ir/Ce850 catalyst exhibited a relatively lower stability as compared to the two other catalysts. Hydrogen concentration continuously declined from 40% to 24% during the period on stream. In the meantime, the increase of CO and methane concentrations indicated that WGS and methane reforming reactions became unfavorable.

Hence, the conversion of ethanol decreased and other undesirable products began to appear. After 60h of test, ethanol conversion was about 95%. The outlet gas contained 1-2% acetaldehyde and 2-3% ethylene. The formation of acetaldehyde was due to the decline of catalyst ability to break the C-C bond.

Again, the poor dispersion of ceria for that case has probably deeply altered the interface Ir/ceria sites. We might propose that the C-C bond activation was inhibited due to a lack of available lattice oxygen for a too sintered ceria support (much less defects slowing down diffusion of lattice oxygen and surface OH groups).

The appearance of ethylene, typical of ethanol dehydration favored on acid sites would suggest that the basicity of the sintered Ir/Ce850 catalyst decreased due to a weaker metal-support interaction.

IV.7. Catalyst characterization after aging tests

IV.7.1. Characterization of SR, POX and OSR aged Ir/Ce400 catalyst

In order to explain the excellent activity and stability of Ir/Ce400 catalyst on SR, POX and OSR reactions, several characterizations (XRD, HRTEM, TPO) were done on the used catalysts.

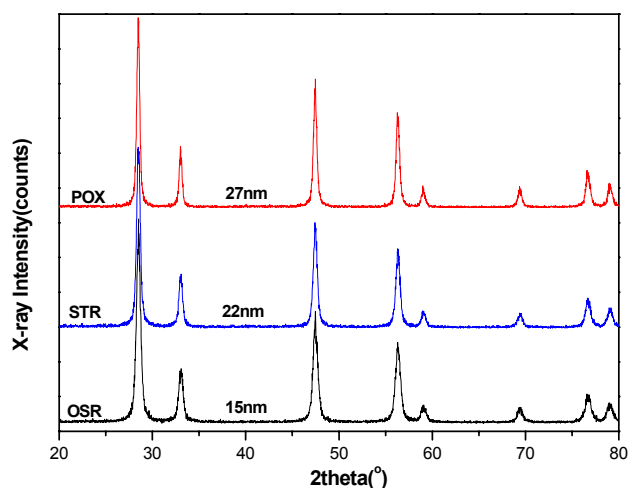


Figure 11 XRD patterns of the Ir/CeO₂ catalysts used for POX, SR and OSR reactions at 650°C for 60 h on-stream.

XRD. Fig. 11 shows the XRD patterns of the Ir/Ce400 catalyst used for SR, POX and OSR at 650°C. No diffraction reflexes of Ir were observed as before testing, providing evidence that no aggregation or sintering of Ir particles occurred during the aging tests. In contrast, the crystallite size of ceria, which was ~6 nm in the fresh catalyst, increased significantly with time on stream, depending on the reaction atmosphere. For SR and POX reactions, the particle size of ceria increased to 22 and 27 nm, respectively, whereas it increased only slightly to 15 nm for OSR reaction.

This sintering in ceria might explain partly the above described rapid initial decay in conversion under high GHSV conditions on the ethanol steam reforming reaction. As a matter of fact, sintering generally proceeds with a high order versus time on stream which may lead to an accelerated process in the initial period followed by a leveling off to a pseudo steady-state.

It could also be suggested that the deactivation of ceria redox property might be

associated with the removal of defects occurring in a narrow temperature range, but this process is not expected to occur under the present testing conditions [131].

Other decay phenomena related to coke deposits would be considered after proper coke analysis.

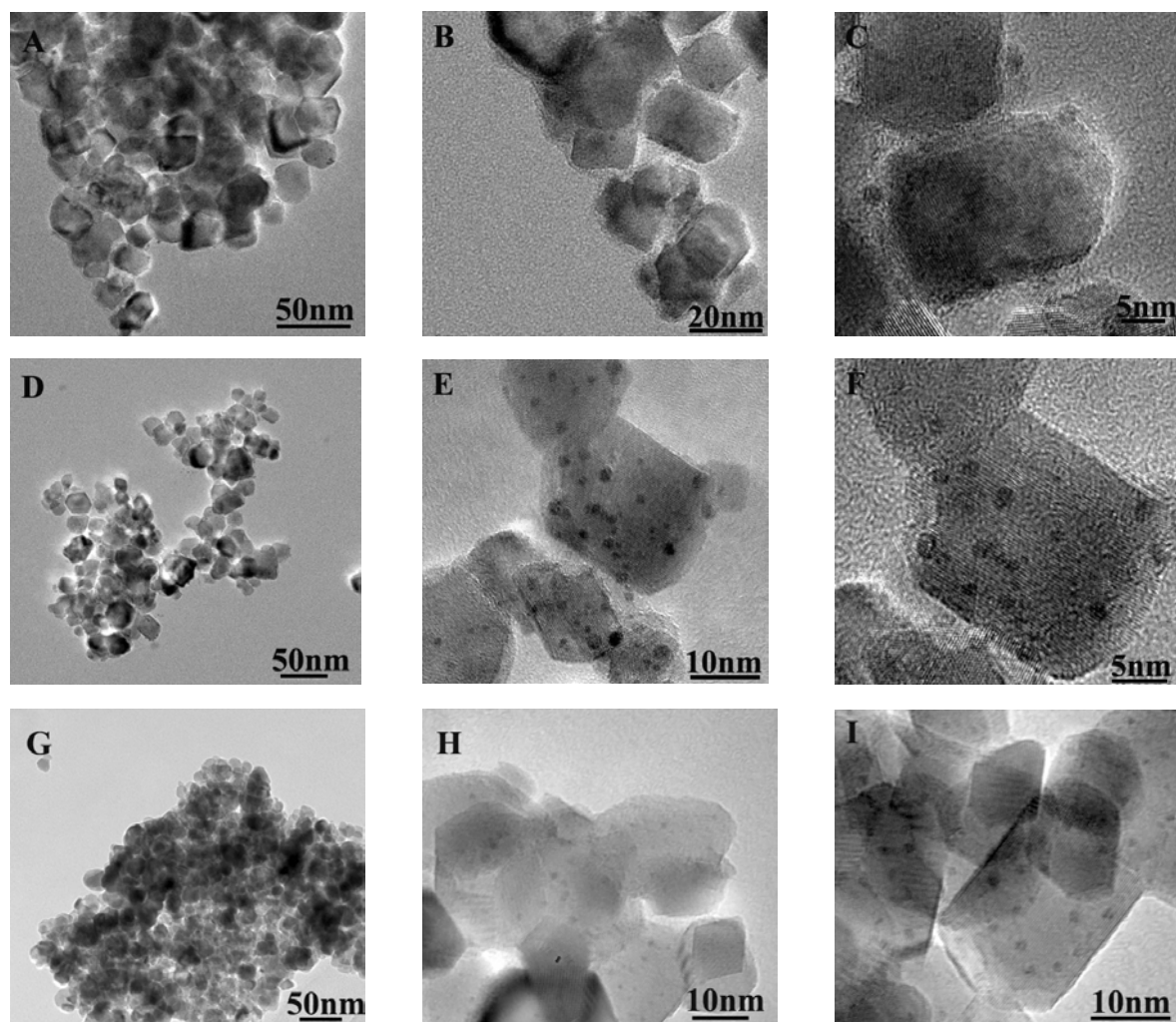


Figure 12 HRTEM images of the Ir/Ce400 catalysts used for POX (A-C), SR (D-F) and OSR (G-I) reactions at 650°C for 60 h on-stream.

HRTEM. Fig12 presents the HRTEM images of the used Ir/Ce400 catalysts. In addition to the significant increase in particle size, the morphology of the ceria particles also shifted from spherical in the as-prepared sample to polygonal crystallites after the tests.

The sample used for the OSR reaction appeared to be less agglomerated than those for the SR and POX reactions, in agreement with the XRD measurements. Probably, the small ceria particles with high surface energy in the fresh catalyst tended to aggregate into larger

particles under the reaction conditions through a hydrothermal process [132].

During the POX reaction, hot spots occurring in the catalytic bed are likely to cause the ceria sintering. Under SR conditions, water is also likely to initiate aggregation of ceria via the formation of cerium hydroxyl phases.

The relatively less marked ceria sintering in the catalyst used for OSR reaction might be due to the co-existence of H₂O and O₂ in the feed, which would maintain milder reaction conditions compared with the POX and SR reaction, ensuring a slower sintering of ceria.

As for Ir particles, they could be observed on the aged samples (at variance with the fresh ones, except for the Ir/Ce850) because the ceria particles were sintered enough to allow us to differentiate Ir from Ce aggregates. The observed Ir particles presented a mean size in the 2-3 nm range, exactly similar to the size observed or deduced for the fresh samples.

It can therefore be concluded that the Ir phase remained highly dispersed on the surface of ceria for all testing and aging conditions. This demonstrated the existence of a strong Ir-CeO₂ interaction prevented the sintering of Ir particles during the course of the reaction.

No carbonaceous deposits were observed in the HRTEM pictures for samples aged under POX and OSR conditions, ruling out any contribution of carbon deposits to deactivation under these conditions.

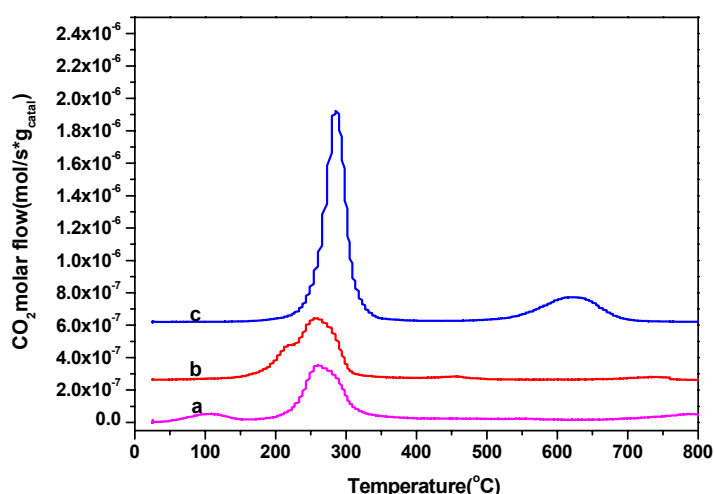


Figure 13 Temperature-programmed oxidation of the used Ir/Ce400 catalysts for ethanol SR at 650°C as a function of time on stream and GHSV. (a) 3 h, GHSV:6000 ml/g_{cat}·h (b) 60 h, GHSV:6000 ml/g_{cat}·h and (c) 60 h, GHSV:75000 ml/g_{cat}·h on-stream .

TPO. In order to detect eventual carbonaceous formation over the samples aged under ethanol steam reforming, which was the most favorable case as compared with the OSR and POX reactions, TPO experiments were carried out after various types of aging conditions.

Fig13 shows the TPO profiles of the aged catalysts for ethanol SR at 650°C, either under low GHSV (after 3 and 60h on stream) or high GHSV (after 60h on stream) conditions.

As can be seen, the main quantity of CO₂ produced was observed in all cases in the 200-300°C temperature interval but other forms of carbons were also detected after testing under high GHSV conditions.

Carbon deposition after low GHSV tests: For low GHSV conditions (Fig 13a and b), this amount was quite time on stream independent (3.4 and 3.3 mgC/g_{cat} for 3 and 60 h on stream, respectively). It can therefore be concluded that this form of carbon deposits, easily oxidized, is directly related to the catalytic activity, i.e., it corresponds to the accumulation of surface reaction intermediates on the catalyst surface, rapidly established after few hours on stream. It could be even further observed that in fact, two distinct forms of easy oxidized carbon deposits formed upon time on stream. The very small amount giving CO₂ below 150°C after 3 h on stream (Fig 13a) and shifted to below 250°C after 60h on stream (shoulder of main peak at 220°C on Fig 13b) might be related to carbon ad-species directly formed on Ir particles (like CH_x or CO_{ads}). They would be very easily combusted after 3h on stream, whereas they would react with oxygen at slightly higher temperature after 60h on stream due to ceria sintering and slower oxygen transfer from ceria to Ir particles. In this respect, the large peak between 200 and 300°C would correspond to C1 carbon containing intermediates accumulated at Ir-ceria interface as will be seen in Chapter V dealing with reaction mechanism.

Carbon deposition after high GHSV tests: After aging test at high GHSV (Fig. 13c), the intermediate CO₂ peak increased by a factor of two (6.8mgC/g_{cat}), whereas a new peak appears at much higher temperature, around 620°C (1.9mgC/g_{cat}). Under high GHSV conditions, the reforming of ethanol was shown to be only partial with still significant

amounts of intermediate C₂ products formed. For that reason, the observed increase of “active” carbon which was oxidized at medium temperature would simply be related to the fact that instead of accumulating C₁ ad-species at low GHSV (with residence time large enough to allow C-C bond rupture), the catalyst surface accumulated essentially C₂ species under high GHSV conditions, due to much shorter residence time.

In line with this explanation, the observation of more stable carbon deposits oxidized only around 620°C might be related to the formation of ethylene (as observed in the initial gas composition at high GHSV) which would be precursor of stable polymeric coke, accumulating regularly over the catalyst and explaining the slow but regular deactivation observed under these conditions (Fig. 4).

It might be deduced from the above discussion that moderate GHSV conditions should be preferred to allow a complete reforming of C₂ adsorbed intermediates into C₁ ad-species, therefore avoiding ethylene formation and "hard" coke deposition. These conditions lead to quite stable performance over 60 h on-stream indeed for POX and OSR but also for the most demanding SR of ethanol with stoichiometric feed compositions.

IV.7.2. Characterization of OSR aged Ir/CeO₂ with different ceria sizes

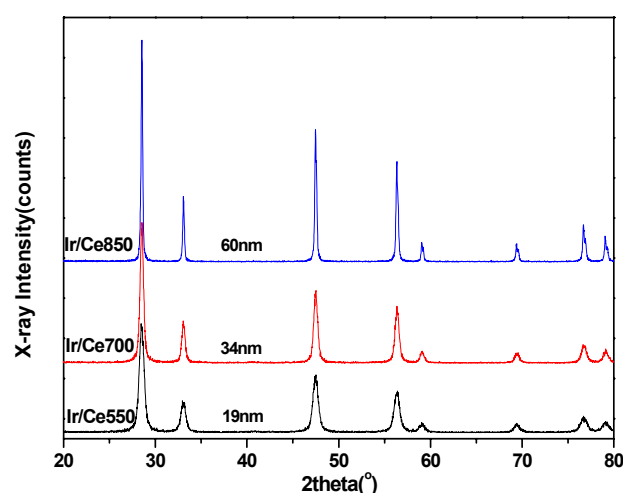


Figure 14 XRD patterns of the Ir/Ce550 Ir/Ce700, Ir/Ce850 catalysts used for OSR reactions at 650°C for 60 h on-stream, Ethanol/H₂O/O₂=1:1.8/0.6

XRD. Fig14 presents the XRD patterns of the used Ir/CeO₂ catalysts with different

ceria particle sizes for OSR at 650°C. The diffraction peaks were similar to the fresh catalysts. Once more, only the cubic fluorite structure was detected. There was still no diffraction peak of Ir as before testing confirming that no significant aggregation or sintering of Ir particles occurred during the aging tests.

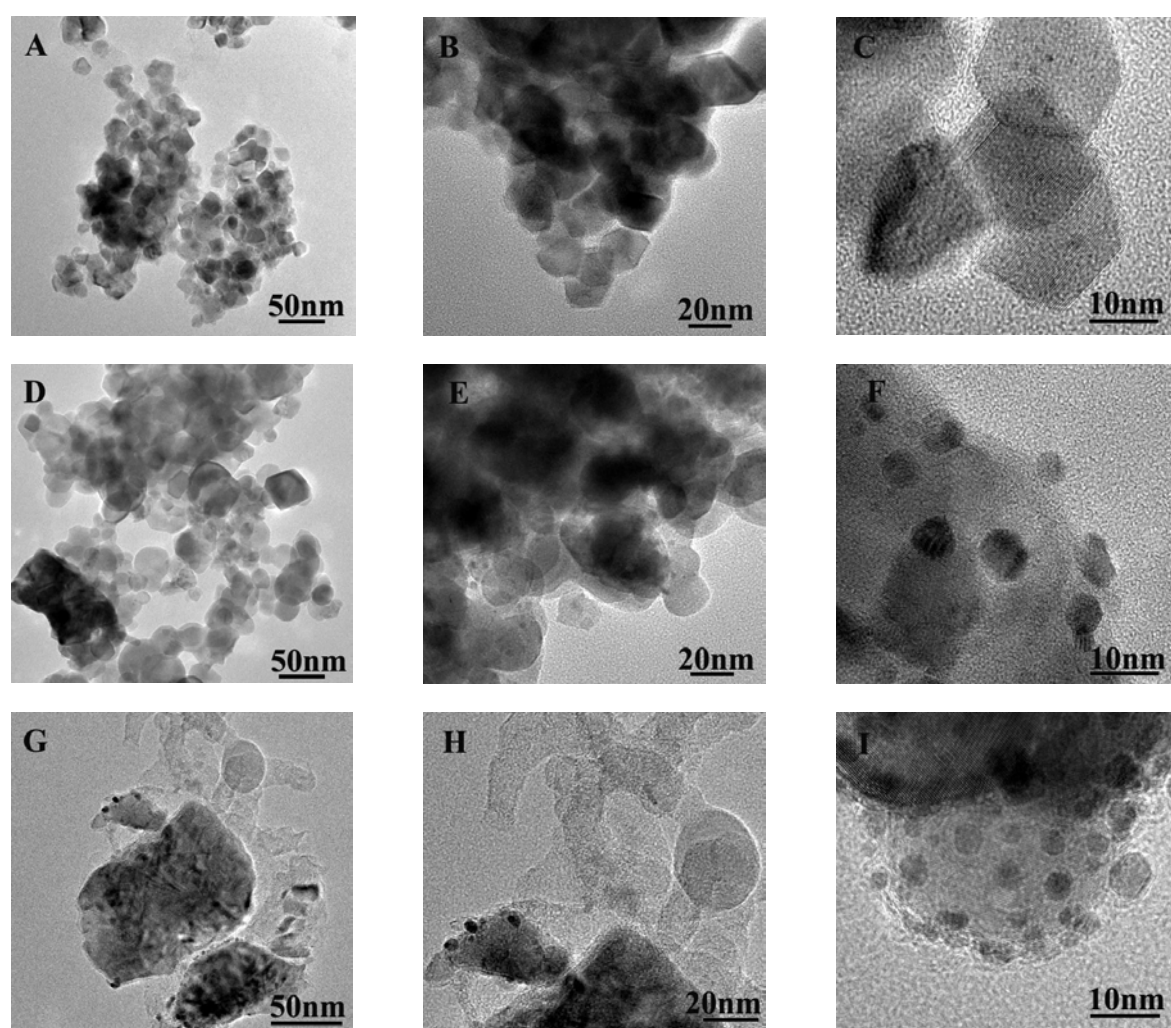


Figure 15 HRTEM images of the Ir/CeO₂ catalysts used for OSR reaction. (A-C) Ir/Ce550, (D-F) Ir/Ce700 and (G-I) Ir/Ce850. Reactions at 650°C for 60 h on-stream, Ethanol/H₂O/O₂=1:1.8/0.6

HRTEM. Fig.15. shows the HRTEM images of the used Ir/CeO₂ catalysts with different initial ceria dispersion.

For the used Ir/Ce550 catalyst, the observation of Ir particles with size of 2-3 nm confirmed that the Ir phase remained highly dispersed on ceria. In addition, no evidence of carbonaceous deposits was gained.

For the used Ir/Ce700 catalyst, a thin layer of encapsulating coke was observed around the catalyst, which might contribute to the slight deactivation noted during the test.

For the used Ir/Ce850 catalyst, HRTEM observations revealed two types of carbon species: either carbonaceous layers on the surface of the grains (Fig.15I.), either filaments (Fig.15H.).

During the 60 h on-stream OSR aging tests, let us recall that only the Ir/Ce550 catalyst exhibited stable performance with stoichiometric feed composition. Like for the Ir/Ce400 catalyst, the effective removal of carbon from Ir particles due to an optimized Ir-ceria interface explains this stable performance.

For the Ir/Ce700 catalyst, only a slight deactivation was detected after 45h test and the particle size of CeO₂ support increased from 15nm to 34nm at last. The formation of carbon deposits as detected by HRTEM explains this deactivation, together with or due to ceria sintering. Thus it can be stated that for the ceria dispersion higher than about 3-4% corresponding to particle size of about 30nm, there was almost no influence of ceria dispersion on catalytic OSR performance.

Above this "threshold", like for the Ir/Ce700 catalyst and over all for the Ir/Ce850 catalyst, a weakened Ir-ceria interaction would decrease the effectiveness of metal particles cleaning mechanism [42,133], leading to deactivating coke accumulation, as shown by HRTEM.

This process is likely to be related to a lower OSC of ceria after deep sintering. A slower OH groups or oxygen surface diffusion might also contribute to this process [134-136]. So the deactivation of the Ir/Ce850 catalyst could be due to the coke formation.

IV.8. Conclusion

In this chapter, many catalytic effects such as the comparison between the TOF under differential conditions for the three POX, SR and OSR reactions and the aging profiles for various reaction conditions (low and high GHSV) were tentatively related i) to structural characteristics of the tested systems, such as iridium and ceria dispersion and ii) to reaction

induced effects such as coke deposition.

The main features could be summarized as follows:

i) A high catalytic activity and stability was observed for the SR, POX and OSR reactions for catalysts exhibiting a ceria dispersion higher than about 3-4% and for operating conditions ensuring a full conversion of ethanol (low GHSV).

ii) Since no Ir sintering and coke formation were detected for these systems and for these operating conditions and despite a moderate ceria sintering along the long lasting tests, these good performances were assigned to a strong interaction between iridium and ceria. More precisely, a moderately sintered ceria would allow the Ir phase to benefit from its high capacity both to promote the activation of water and oxygen and to provide oxygen fluxes at Ir-ceria interface necessary for carbon removal on and around the Ir phase.

Thus, the Ir/Ce400, Ir/Ce550 and Ir/Ce700 exhibited similar catalytic performance since all of them present ceria dispersion above the mentioned "threshold".

In contrast, the Ir/Ce850 catalyst (ceria dispersion around 2%) showed a much lower stability and activity, due to deactivating coke formation.

iii) A strong effect of operating conditions was also revealed showing that for any case where the conversion of ethanol was not complete (e.g. for high GHSV values), more coke accumulates on the aged surfaces. It includes first a non deactivating coke (oxidized at moderate temperature) probably accumulated at Ir-ceria interface and corresponding to non dissociated C₂ intermediates adspecies (the further mechanistic study will give evidence for that process). A second type of "hard" coke, stable and encapsulating catalyst particles probably arise from ethylene formation and further polymerization.

Therefore structure-activity relationships were revealed from this investigation, pointing out that optimized systems require both i) a ceria dispersion maintained above a threshold level (which might be further improved by dopant additive as generally proposed in the literature) and ii) operating condition ensuring full conversion of ethanol. iii) By comparing the TOF values and hydrogen yields for the OSR, SR and POX reactions, a clear compromise has to be made between hydrogen yield and energy management. The OSR

reaction seems therefore to be the best choice for still ensuring relatively high hydrogen yield, but with an energy management favored by a close to thermo-neutral balance.

Chapter V Effects of noble metal nature: comparison between Rh/Ce400 and Ir/Ce400 catalysts

In order to precisely evaluate the role of the metal in systems based on noble metal supported on ceria, we investigated the properties of a catalyst having the same metal molar content supported on the same ceria support as for the reference 2%Ir/Ce400: the 1%Rh/Ce400 catalyst. In this chapter we report the main trends observed for this system, focusing on the similarities and differences with the iridium catalyst.

V.1. Catalytic performance

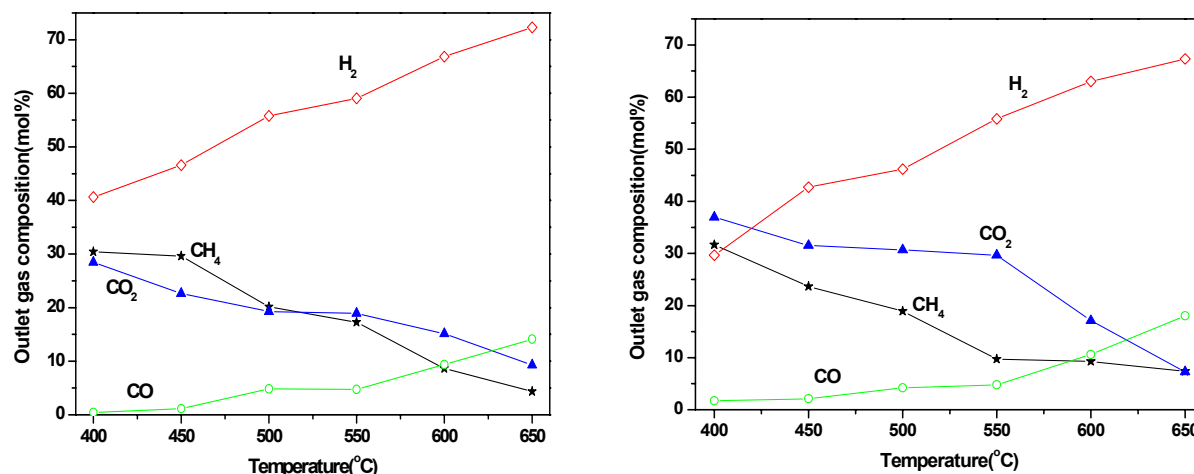


Fig 1 Effect of reaction temperature on the product distributions for SR of ethanol over the 1%Rh/Ce400 catalyst, reaction conditions: Ethanol/H₂O = 1:3.0, GHSV = 6000 ml/g_{cat}·h (left); oxidative steam reforming of ethanol, reaction conditions: EtOH: H₂O: O₂ = 1:1.8:0.6, GHSV: 6000 ml/g_{cat}·h (right)

Fig 1 shows the catalytic performance of ethanol SR and OSR over the 1%Rh/Ce400 catalyst.

i) In the high temperature domain (above 500°C), the same catalytic behavior is observed for the two Ir and Rh systems (see Chapter IV Fig 2 and 7 for comparison). In both cases, methane steam reforming and reverse water gas shift reactions control the product distribution, as predicted from thermodynamics.

ii) in the low temperature domain (below 500°C), the rhodium catalyst exhibited a slightly higher activity since the temperature at which the ethanol conversion to C₁ products was 100°C lower than for the iridium catalyst. Hence, lower CO concentration was observed for the OSR below 450°.

This effect is likely not to involve a distinct mechanism but can simply be explained by a higher C-C bond dissociation capacity for Rh as compared to Ir, as generally agreed in the literature [65, 66]. As a matter of fact, we will see in the next chapter dedicated to mechanism that the key step (after ethanol primary activation on ceria) is related to the C-C bond activation of acetate species at the ceria/metal interface.

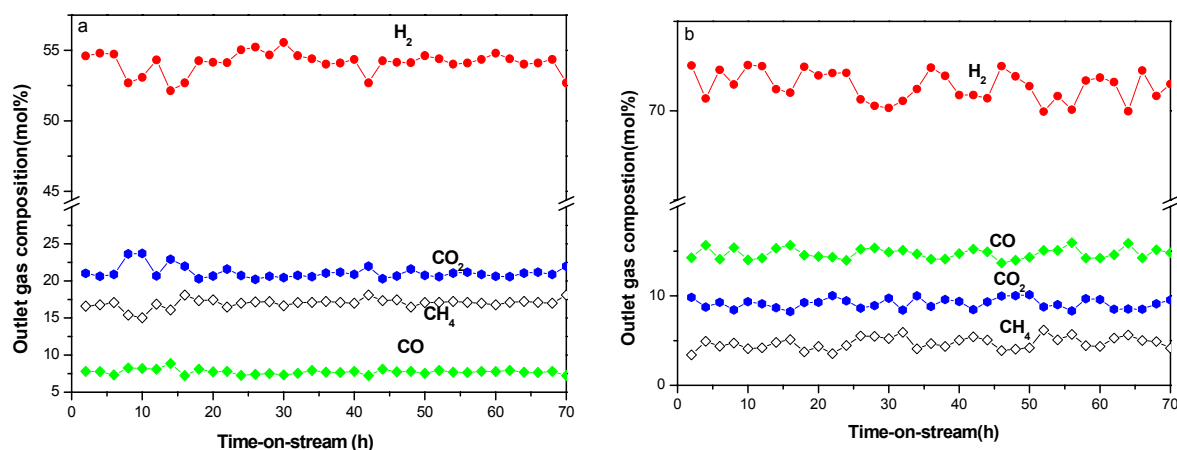


Figure 2 Stability test for steam reforming of ethanol. (a) 550°C (b) 650°C. Reaction conditions: EtOH: H₂O=1:3, GHSV: 6000 ml/g_{cat}·h

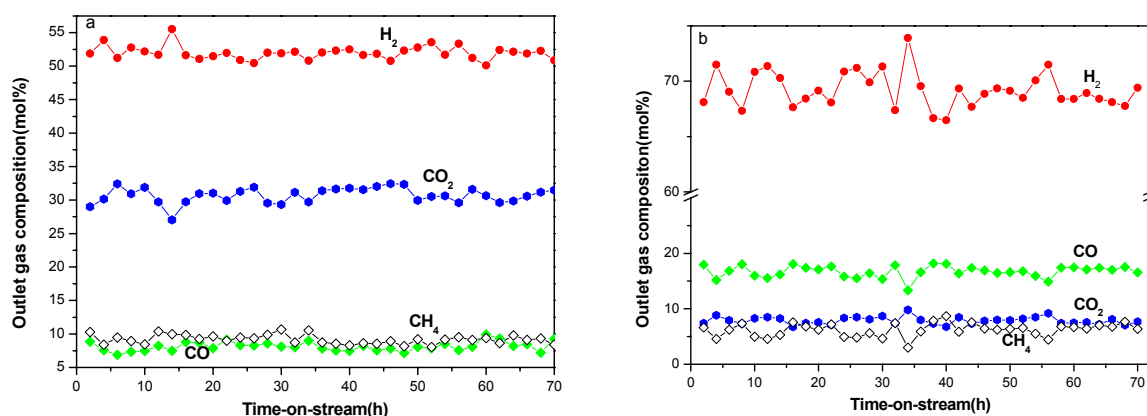


Figure 3 Stability test for oxidative steam reforming of ethanol. (a) 550°C (b) 650°C. Reaction conditions: EtOH: H₂O:O₂=1:1.8:0.6, GHSV: 6000 ml/g_{cat}·h

Figures 2 & 3 present the results of stability test for SR and OSR reactions respectively, under conditions where ethanol conversion is complete (low GHSV).

As can be seen, no significant changes in the product distribution were observed during the whole test. It can be concluded therefore that the same stability in the catalytic performance with time on stream was observed in the 550-650°C temperature range for the Rh/Ce400 catalyst as for the Ir/Ce400 one (see Chapter IV Figs 3 and 8 for comparison). In line with the above mechanistic comments, it can be added that the Rh/ceria interface, like the Ir/ceria one, ensures easily the full conversion of ethanol, and therefore guaranties a stable catalytic behaviour (without coking) under OSR conditions.

V.2. Characterization of Rh/Ce400 catalyst before and after testing

Structure properties of the fresh and used Rh/Ce400 catalyst were investigated by the same techniques as for the reference iridium system.

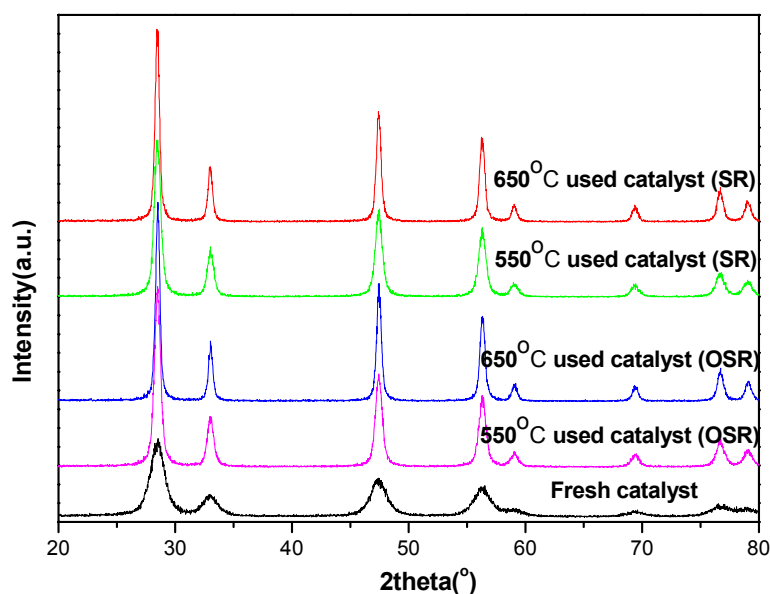


Figure 4 XRD patterns of the fresh and used Rh/Ce400 catalyst after OSR and SR long term testing.

Figure 4 shows the XRD patterns of the fresh and used Rh/Ce400 catalyst after OSR and SR long term testing.

No diffraction reflexes of Ir were observed in any case, but a slight increase of ceria particle size (from 7 to 21 nm) occurred, which was also observed over the Ir/Ce400 catalyst (from 6 to 22 nm, as reported in Chapter IV Figure 11).

The same conclusion can therefore be formulated: under low GHSV conditions, the small sintering of ceria had no significant impact on catalytic performance, respect the noble metal dispersion remains high, which is the case for both iridium and rhodium cases.

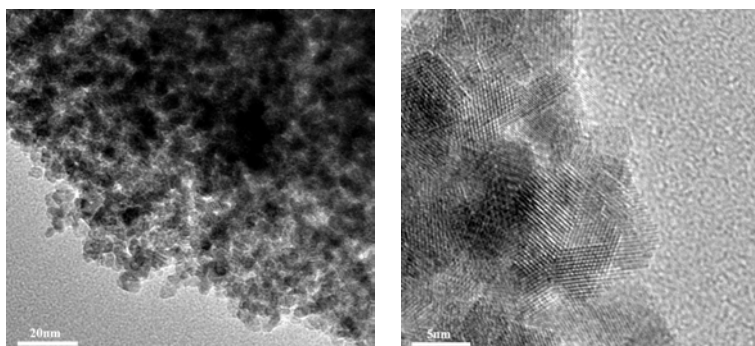


Figure 5 HRTEM images of Rh/Ce400 catalysts

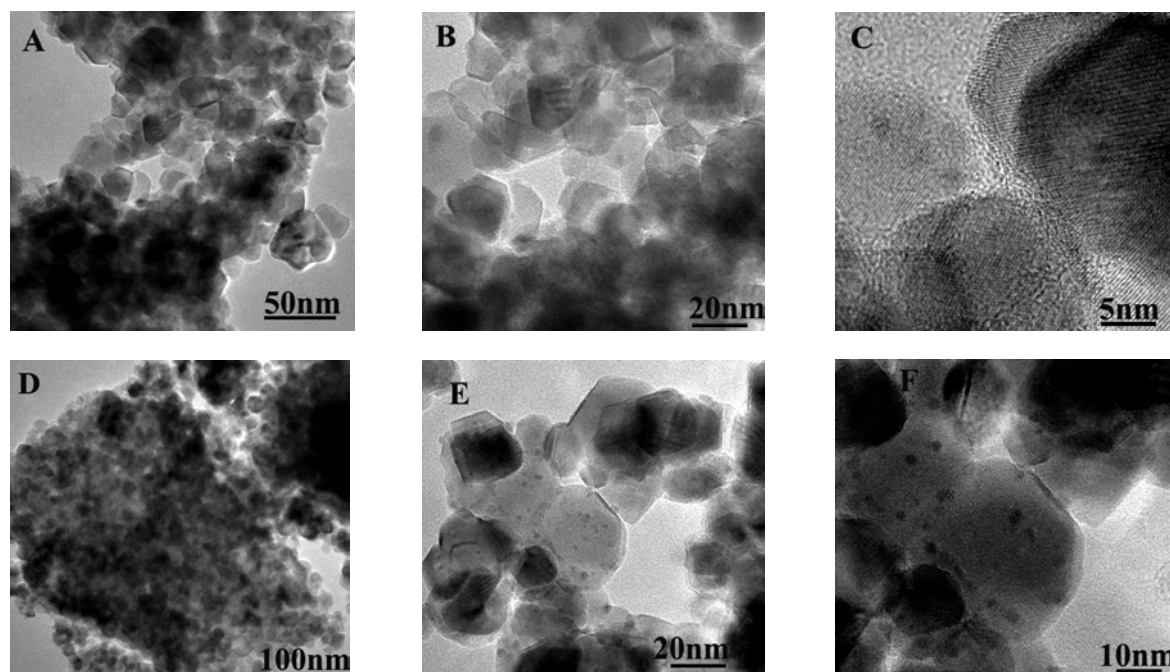


Figure 6 HRTEM images of the used Rh/Ce400. (A-C): Ethanol steam reforming (D-F): Ethanol oxidative steam reforming.

Figures 5 & 6 report the HRTEM images of Rh/Ce400 before and after stability test. Before reaction, it is hard to see rhodium phase due to the high dispersion. Hence, neither Rh sintering nor coke formation was detected besides the small ceria sintering for the aging catalysts.

As said previously and further discussed in Chapter IV, a moderate sintering of ceria still allows it to promote the activation of water and oxygen for providing active oxygen at metal-ceria interface for carbon removal on and around the metal phase. The ceria support

also prevented the rhodium sintering via the strong metal-support interaction, as observed for the iridium case.

V.3. Conclusion

In this chapter, it was shown that the Rh/Ce400 catalyst exhibited the same catalytic performance as Ir/Ce400 under low GHSV conditions (6000 ml/g_{cat}·h) and at high temperature (thermodynamic regime). In turn, at lower temperature (below 500°C) the higher C-C bond rupture capacity of the rhodium catalyst lead to a higher overall activity and a lower CO selectivity. We will investigate in more details these mechanistic features in the next chapter.

The same structure changes with time on stream were observed for the two compared systems. It was concluded that the slight ceria sintering was not detrimental for the catalyst performance, due to the fact the metal/ceria interfaces were still acting efficiently for full conversion of ethanol and C₂ adspecies and for coke removal on the metal phase.

Thus, it can also be concluded at that stage that the same ethanol mechanism applies for the two compared noble metal/ceria systems, which will not be the case for other types of catalysts like Rh/alumina or Ni-Cu/silica, as will be seen in the next chapter.

Chapter VI. Investigation of ethanol conversion mechanism over Ir/CeO₂ catalyst and comparison with other systems

Several technologies can be used to produce hydrogen from ethanol such as steam reforming (SR), partial oxidation (POX) and oxidative steam reforming (OSR) [11,49,137]. As already pointed out in the introduction section, the routes for the production of hydrogen from ethanol involve a complex reaction system [59,117,138,139]. Besides ethanol steam reforming, several reaction pathways exist depending on the catalysts and reaction conditions. Routes include an ethanol decomposition to methane, CO and H₂; the ethanol dehydrogenation to acetaldehyde; the water gas shift reaction; an ethanol dehydration to ethylene or acetone and acetic acid formation from ethanol. Some of these reactions lead to the formation of by-products, which can cause a catalyst deactivation. For example, one of the reasons of coke formation is the polymerization of ethylene produced from the ethanol dehydration or the decomposition of methane.

Furthermore, an advanced knowledge of the reaction mechanism is fundamental for designing optimized catalysts involved in the hydrogen production from ethanol. Infrared spectroscopy, temperature programmed desorption (TPD), temperature programmed surface reaction (TPSR) under unsteady-state and steady state reaction conditions, which are in essence in situ techniques, have been employed to identify the main reaction routes and the corresponding intermediates and products. These investigations might also provide kinetic data for the reactions of ethanol over the selected Ir/CeO₂ catalyst. A comparison with other active catalytic formulas is also considered for identifying the specificities of the selected system.

The major outcomes of this investigation are reported in this chapter.

VI.1. FTIR of ethanol activation under temperature programmed conditions

VI.1.1. Ethanol adsorption over Ce400

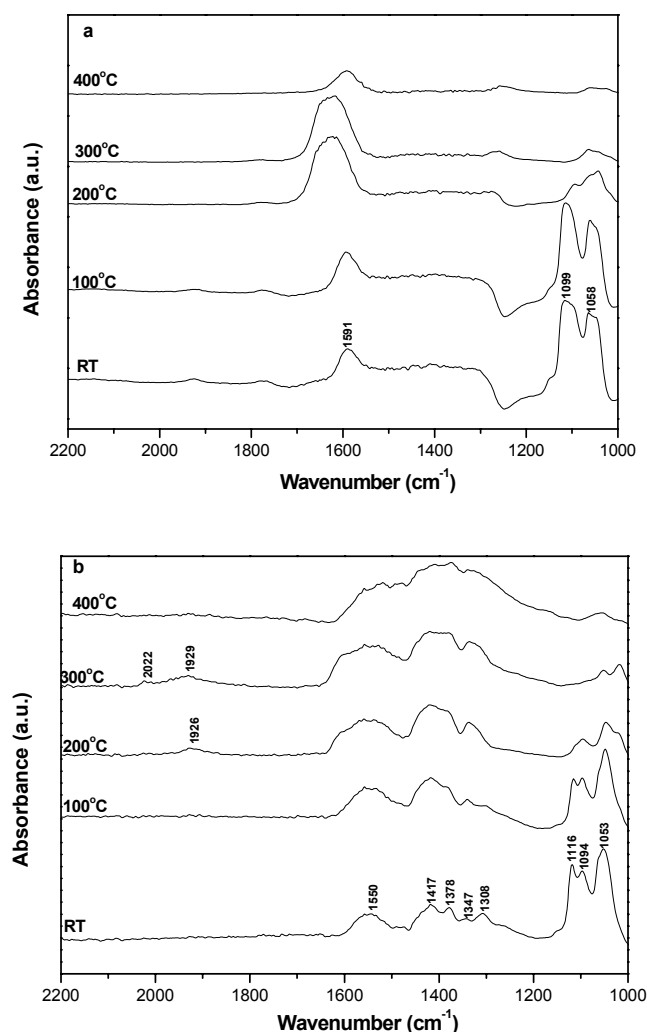


Figure 1 FTIR spectra of ethanol adsorption on Ce400 (a) and Ir/Ce400 (b)

Fig. 1a shows the IR spectra of ethanol adsorbed on pure Ce400. At room temperature, a series of bands in the range 1050-1150 cm⁻¹ can be unambiguously assigned to ethoxy species (Table 1). Two types of ethoxy species were formed, being characterized by (C-O) bands at 1099 and 1058 cm⁻¹ as monodentate and bidentate species, respectively [42,140]. These two bands correspond to a combination of ν C-C and ν C-O stretching vibrations, and to the ν C-O stretching vibration of a bidentate system where the O atom is shared between two adjacent cerium cations (Table 1). Indeed, the adsorption of ethanol on ceria may occur

easily through the activation of the hydroxyl group to form these ethoxy species bonded to surface cations [65].

Another set of bands was observed in the range 1300-1600 cm⁻¹, with a main one at 1591 cm⁻¹, typical of adsorbed acetate species according to [141]. It demonstrates that the dissociation of ethanol and the production of acetate species are quite fast steps and take simultaneously place on the ceria surface.

The pathway from adsorbed ethoxide to acetate species, though not clearly tracked during this study, is likely to proceed through i) the direct oxidative dehydrogenation of ethoxide by ceria lattice oxygen into acetaldehyde and ii) the reaction between adsorbed or desorbed acetaldehyde and hydroxyl species on ceria, in line with the proposal of Jacobs et al. [141]. For the case of ceria supporting a noble metal phase, hydroxyl groups could be formed via the dissociation of H₂ on Ir and a subsequent spillover of atomic hydrogen to the ceria surface, reducing the cerium atoms associated with hydroxyl groups from Ce⁴⁺ to Ce³⁺ during the reduction. For the present case of pure CeO₂, mobile oxygen and hydroxyl groups still remain available after the reduction at 400°C, which makes the above mentioned sequential processes still likely.

Hence, both ethoxy and acetate species are readily formed on the CeO₂ surface upon adsorption of ethanol at room temperature. This demonstrates that the dissociation of ethanol and the reaction of adsorbed ethoxy species are easily proceeding steps and take place simultaneously on the surface of ceria.

Upon heating, the intensity of the ethoxy species decreased progressively and almost vanished at 400°C. The intensity of the acetate species increased with increasing temperature up to 300°C, and then decreased, indicating their decomposition. However, no bands associated to carbonates appeared, even at 400°C. This confirms that ethoxy and acetate species are the only adsorbed intermediates formed on ceria upon adsorption of ethanol.

VI.1.2. Ethanol adsorption over Ir/Ce400

Fig. 1b shows the IR spectra of ethanol adsorbed on the Ir/Ce400 catalyst. As mentioned above, bands corresponding to surface ethoxide species (1378 cm^{-1} ($\delta_s\text{CH}_3$), 1116 cm^{-1} associated with a shoulder at 1096 cm^{-1} (νCO -monodentate), 1053 cm^{-1} (νCO -bidentate)) were observed. As there was almost no surface oxygen on ceria after the reduction, the bands at 1308 cm^{-1} (δCH_3), 1417 cm^{-1} ($\nu_s\text{OCO}$), 1550 cm^{-1} ($\nu_{as}\text{OCO}$) [66,101] were attributed to the acetate species formed through the reaction between short-lived acetaldehyde and hydroxyl groups.

The new band at 1347 cm^{-1} (monodentate carbonates) indicated the further reaction of the acetate species and $-\text{OH}$ groups to yield carbonate species, and, as will be seen by effluent analysis in TPD, methane. This statement strongly suggests the key role of interface sites between i) ceria where the C_2 species are formed and progressively oxidized and ii) the Ir phase able to cleave the C-C bonds of the C_2 species to produce CH_x ad-species further hydrogenated into CH_4 and the carbonate species. Here, the required hydrogen ad-species can be tentatively assigned to spill-over of OH groups to Ir particles, followed by a decomposition of the hydroxyl groups into Ir-H and Ce=O boundary species. The preliminary reduction of the ceria before TPD experiments would favor this decomposition.

Further evidence for the bi-functional process at Ir/ceria interface was obtained by heating the surface. As shown in Fig. 1b, the intensity of the bands attributed to ethoxy species decreased greatly upon heating. At 200°C , the band at 1116 cm^{-1} almost disappeared. When the temperature was increased to 300°C , more ethoxy species were transformed and in the meantime CO carbonyl species were formed. Effectively, metal carbonyl bands at 1929 (bridged) and 2022 (linear) cm^{-1} were clearly observed, and the ethoxy species disappeared almost completely at 400°C . On the other hand, the intensity of the bands associated with acetate and carbonate species gradually increased, indicating the still growing production of acetate and carbonate species via the reaction between intermediate acetaldehyde and hydroxyl groups. The formation of the carbonyl species clearly involves the Ir phase and it can be reasonably proposed that at these medium

temperatures, oxygen ad-species coming from the ceria interface sites can easily oxidize the CH_x ad-species arising from acetate decomposition.

At 400°C, the bands origination from acetate species also drastically decreased. The band characteristic of carbonate species at 1347 cm⁻¹ became dominant. This observation indicated that the acetate species were not only decomposed into methyl groups adsorbed on the Ir surface but also into carbonate species adsorbed on the ceria surface, through a C-C bond breaking initiated by Ir particles (which indeed was not observed on pure ceria, as stressed before).

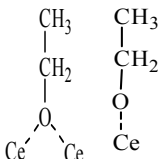
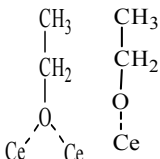
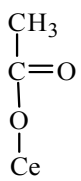
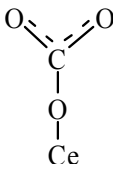
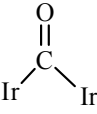
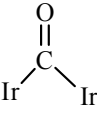
Vibrational Mode	Ir/Ce400	Ce400	
Ethoxy species			
vCO-monodentate	1116	1099	
vCO-bidentate	1053	1058	
δ_sCH₃	1378	---	
Acetate species			
δCH₃	1308	---	
v_sOCO	1417	---	
v_{as}OCO	1550	1591	
Carbonate species			
v_sOCO-monodentate	1347	---	
CO			
vCO linear	2022	---	
vCO bridging	1926	---	

Table 1 Vibration frequencies (as wave numbers in cm⁻¹) of surface species produced by the adsorption of ethanol on Ce400 and Ir/Ce400.

To summarize, it was shown that ethoxy species were formed immediately on the ceria support upon the adsorption of ethanol. Then, a fraction of these ethoxy species was readily transformed into acetate, through intermediate acetaldehyde formation. These acetate

ad-species can be further decomposed according to a bifunctional process into methyl groups and carbonate species at ceria/Ir interface, in the presence of hydroxyl groups even at room temperature. Increasing the temperature to 200-300°C led to the oxidation of the methyl groups into metal carbonyl ad-species onto the Ir surface, further released into CO, as observed by effluent analysis, later reported in TPD experiments.

VI.2. TPD and TPSR over Ir/Ce400 catalyst

VI.2.1. TPD of ethanol over Ir/Ce400 catalyst

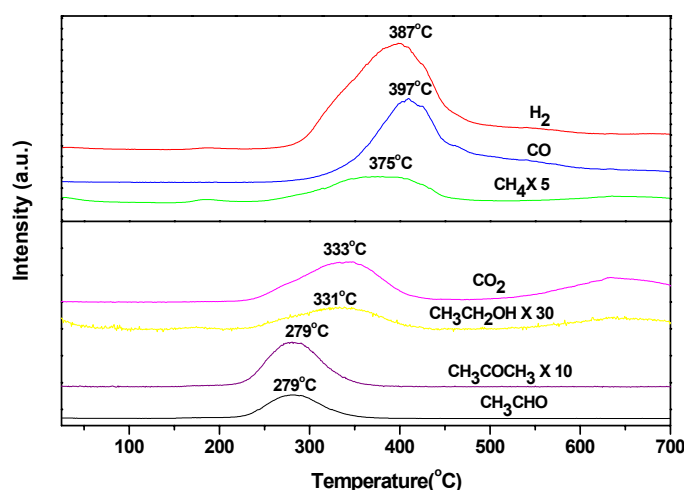


Figure 2 TPD profiles of ethanol adsorption on Ir/Ce400 catalyst

The interaction of ethanol with the surface of the support (CeO₂) and the active metal (Ir) was also investigated by temperature-programmed desorption of adsorbed ethanol at room temperature.

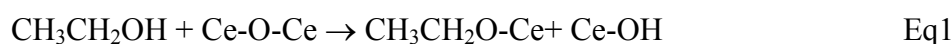
The TPD spectrum of ethanol on the pre-reduced Ir/Ce400 catalyst is shown in Fig2. A simultaneous desorption of acetaldehyde and acetone was observed at ~279°C. As stated during the IR study, the former product is due to the oxidative dehydrogenation of ethoxy species. The later is likely to come from the further condensation of acetaldehyde to acetone, which is known to occur on basic surfaces like ceria via sequential aldolisation, oxidation to C4 acetate intermediate and decarbonylation to acetone processes [127].

Desorption of CH₄ and CO₂ also began at ~279°C, presenting a maximum at 333 and 375°C, respectively. At slightly higher temperature, a significant formation of H₂ and CO

was observed at 387 and 397°C, respectively. This sequence is clearly related to the decomposition of the acetate and carbonate species initially formed from the ethoxy species, as explained by the IR study.

All these steps can be tentatively illustrated by the following reaction sequence:

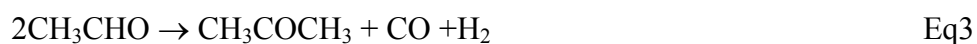
i) ethoxy species formation on ceria



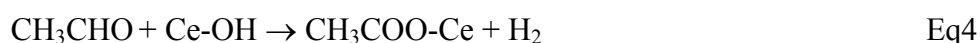
ii) transient formation of acetaldehyde on ceria



iii) formation of acetone from acetaldehyde condensation/aldolisation



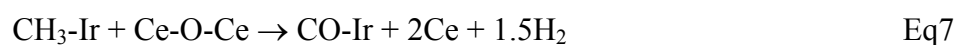
iv) formation of acetates from acetaldehyde on ceria



v) decomposition of acetates at Ir-ceria interface into methyl groups and carbonates



vi) methane and syngas formation on Ir surface



where “Ce” means actually a reduced Ce ion or a Ce vacancy.

Further mechanistic considerations deserve to be made here:

i) Two domains of CO₂ formation were observed from carbonate decomposition (Fig.2). The low temperature one should correspond to carbonates formed on weakly basic interface sites as corresponding to Eq5. This low basicity might come from an electron transfer from ceria to metal particles. In turn, the high temperature CO₂ should be released

from carbonate formed on the strong basic sites of ceria not affected by Ir. These more stable carbonates would be formed from re-adsorption of CO₂ formed at low temperature.

ii) Several recent works on ethanol decomposition over ceria-supported Rh or Pt catalysts reported TPD peaks corresponding to the formation of CH₄, CO and H₂ at around 200°C and above 230°C [42]. The low and high temperature desorption peaks were attributed to the decomposition of ethoxy species and acetate species, respectively.

In this work, only one intense peak of H₂, CO and CH₄ was obtained in the temperature range of 330-400°C. The superior redox properties of the present Ir/Ce400 system as above discussed could possibly explain the differences observed. It is quite possible that only a small fraction of the ethoxy species decomposed into CH₄, CO and H₂ at room temperature, but most of the ethoxy species were rapidly transformed into acetate or carbonate species on the surface of ceria upon heating, as already outlined. Hence, the formation of H₂, CO, CO₂ and CH₄ at 330-400°C can be mainly due to the respective decomposition of the accumulated acetate and carbonate species.

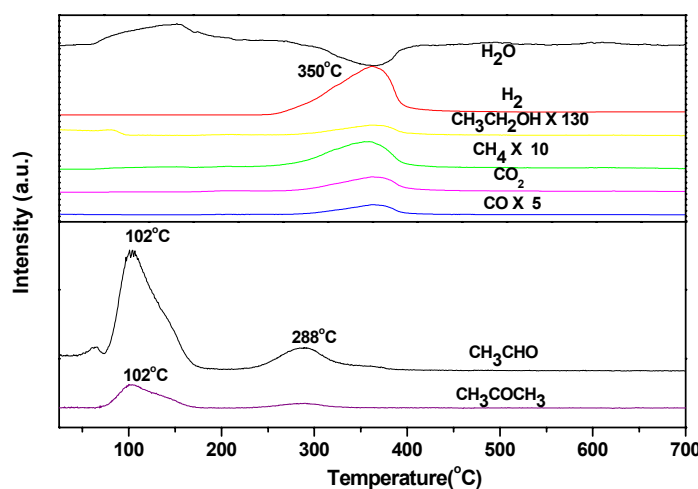


Figure 3 TPSR of adsorbed ethanol on the Ir/Ce400 with a flow of 3.0 %H₂O/He

VI.2.2. TPSR over Ir/Ce400 catalyst

The reaction of ethanol reforming was investigated by TPSR of pre-adsorbed ethanol with water or oxygen over the Ir/Ce400 catalyst.

H₂O/He TPSR. As shown in Fig. 3, the addition of water to the carrier gas shifted the

formation of acetaldehyde and acetone to a temperature of 100°C, i.e., much below the TPD peak at 280°C. This indicates that water enhances the dehydrogenation of ethoxy species to acetaldehyde, favoring the easy desorption of acetaldehyde. A significant consumption of water occurred at ~350°C with the formation of considerable amounts of H₂ and CO₂ at ~353°C, as expected from the WGS reaction converting the CO formed from ethoxy species into CO₂ and H₂ in the presence of excess H₂O. Indeed CO₂ formation has to be considered as resulting from the reaction according to the carbonate formation/decomposition equilibrium. Meanwhile, trace amounts of CH₄ provide evidence of acetate decomposition occurring mainly in this temperature range.

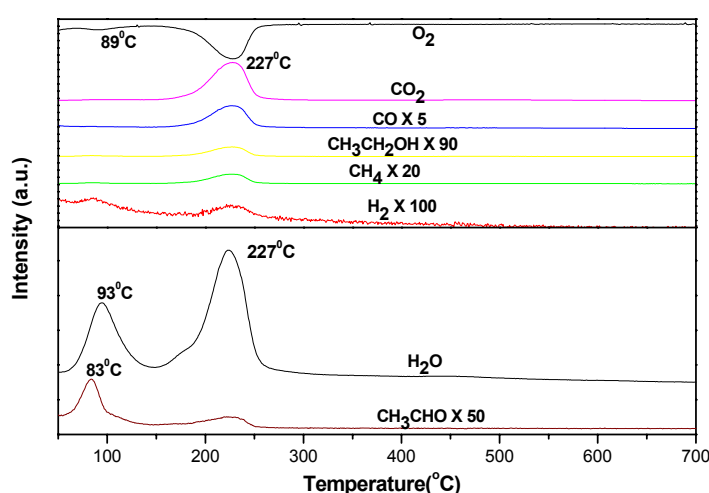


Figure 4 TPSR of adsorbed ethanol on the Ir/Ce400 catalyst with a flow of 1.0% O₂/He.

O₂/He TPSR. Fig. 4 shows the TPSR profile of the reaction of adsorbed ethanol with the O₂/He mixture. Formation of acetaldehyde was observed at ~83°C. In parallel, the consumption of oxygen at 90°C and the appearance of water at 93°C indicated clearly that oxidative dehydrogenation of ethoxy species into acetaldehyde occurred by consuming oxygen from the feed.

Upon further increase of temperature, a significant consumption of oxygen at 227°C was accompanied by the formation of large amounts of water and carbon dioxide. This indicated that the oxidation of the various species (ethoxy, acetate and CH_x fragments) into CO₂ and H₂O was considerably enhanced in the presence of gaseous oxygen. In fact, this finding might be expected from the activation of oxygen both on Ir and on the ceria phase.

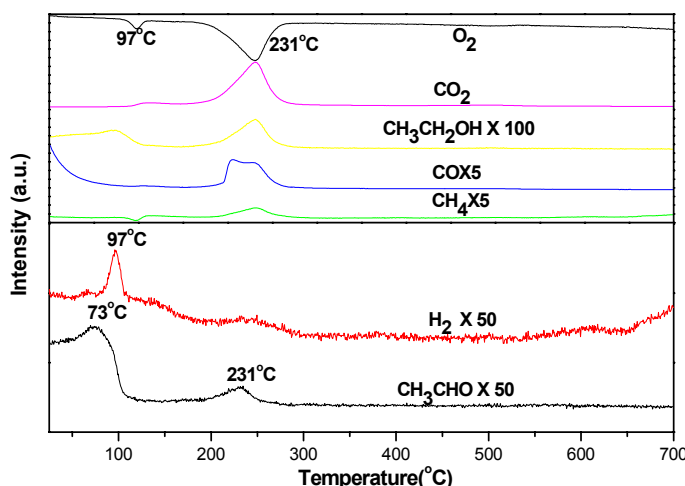


Figure 5 TPSR of adsorbed ethanol on the Ir/Ce400 with a flow of 3.0 %H₂O/1.0%O₂/He.

H₂O/O₂/He TPSR. The TPSR profile of adsorbed ethanol with a H₂O/O₂/He mixture showed similar features as that one with the O₂/He reactant gas. Oxidative dehydrogenation of ethoxy species to acetaldehyde took place at ~73°C. Direct dehydrogenation of ethoxy species to acetaldehyde might also occur as evidenced by the production of hydrogen at 97°C [125]. A fraction of the hydrogen produced was oxidized to water, as confirmed by the simultaneous consumption of oxygen at 97°C. The main consumption of oxygen at 231°C resulted from the oxidation of remaining adsorbed species to carbon dioxide. Much smaller amounts of methane and carbon monoxide were formed from less favored reforming processes. Again, the presence of oxygen in the reactant flow shifted the surface reactions of adsorbed ethanol to much lower temperatures.

Main features of TPD/TPSR experiments. By comparing TPD and TPSR profiles of adsorbed ethanol, some important features can be revealed.

Since ethoxy, acetate and carbonate species were formed readily upon adsorption of ethanol on the Ir/Ce400 catalyst at room temperature, the surface reactions of these intermediates with oxygen species provided either by ceria or the feed would determine the features of releasing products.

In the TPD case, i.e., in the absence of oxygen in the carrier gas, conversion of large part of the ethoxy species to acetate and further on to carbonate species followed by their decomposition was the main reaction pathway with increasing temperature.

The addition of water to the carrier gas shifted acetaldehyde desorption to 102°C and enhanced the decomposition of acetates that took place at ~350°C. In the presence of oxygen, the oxidative dehydrogenation of ethoxy species to acetaldehyde occurred at 83°C, and the decomposition of acetates followed by the oxidation of the resulting fragments took place at ~227°C, thus more than 100°C below the temperature established for the TPSR process under steam reforming conditions.

This effect could be explained by the effective activation of gaseous oxygen or water on the Ir/Ce400 catalyst. Thus, a permanent flux of activated oxygen will maintain the ceria surface in an oxidized state. As a result, ethoxy and acetate species on the surface could be oxidized and/or decomposed readily at much lower temperatures. Meanwhile, the absence of acetone observed in the case of experiments with oxygen-containing atmosphere further confirmed the rapid surface reaction/desorption of acetaldehyde. Note that thermal effects arising from the exothermicity of the oxidation reactions are not expected to contribute significantly to the observed shift towards lower temperature for TPSR in the presence of gaseous oxygen. As a matter of fact, due to the small quantity of adsorbed ethanol on the catalyst surface, a negligible heat effect is expected with respect to the normal convective heat transfer through the permanent flux of inert gas.

Products	Carbon product yield (%)			
	TPD		TPSR	
	He	3.0% $\text{H}_2\text{O}/\text{He}$	1.0% O_2/He	3.0% $\text{H}_2\text{O}/1.0\%\text{O}_2/\text{He}$
Carbon monoxide	45.1(397°C)	5.2(353°C)	6.9(227°C)	8.9(191,263°C)
Carbon dioxide	9.8(333°C)	68(353°C)	83.8(227°C)	81.8(231°C)
Methane	26.5(375°C)	17.2(347°C)	6(227°C)	5.4(231°C)
Acetaldehyde	13.9(279°C)	3.5(102,288°C)	3(83,220°C)	3.6(73,231°C)
Ethanol	0.6(331°C)	2(350°C)	0.3(227°C)	0.4(231°C)
Acetone	4.2(279°C)	4.1(102°C)	---	---

Table 2 Product distributions for TPD and TPSR of adsorbed ethanol.

All above trends are reflected in a more quantitative way in Table 2 presenting the carbon yields estimated from the TPD/TPSR profiles of ethanol with the temperature

corresponding to the peak maxima. In all cases, the minor products acetaldehyde and/or acetone were formed in the low temperature range of 77-277°C. The low yield of acetaldehyde amounting to 15% (TPD) and 3-4% (TPSR) of the total carbon yield confirmed the effectiveness of the Ir assisted carbon-carbon bond dissociation. CO, CO₂ and CH₄ are the dominant products, desorbing at relatively higher temperatures. For the TPD, these C1 products contributed to 81% of the total carbon product yield. Under the TPSR conditions, however, CO, CO₂ and CH₄ contributed to more than 90% of the total carbon yield with CO₂ being the major product. The yield of CO₂ increased with rising oxygen content in the carrier gas, confirming the effectiveness of oxygen activation both on ceria and metal phases to oxidize the fragments of C2 species decomposition.

VI.3. Comparison of OSR over Ni-Cu/SiO₂, Rh/Al₂O₃, Rh/Ce400 and Ir/Ce400

In the IRCELYON group, Akdim [142] and Fierro et al, [51] already reported that various catalysts based on noble (Rh) and non noble (Ni-Cu) metal supported over neutral (SiO₂) and amphoteric (Al₂O₃) supports, respectively, led to stable and highly performing systems for the oxidative steam reforming of ethanol. By considering our own results obtained on Ir/Ce400 and Rh/Ce400 catalysts, we tried to analyze why these completely different systems, as to catalyst formulation (nature of the active phase, content of metals), may lead to excellent performances under ethanol OSR conditions, as shown in Table 3. For that purpose, we compared the specific features of the different systems under TPD-DRIFT conditions [69].

VI.3.1. Catalytic performances under OSR conditions

Hydrogen yields on the 16.7%Ni2.1%Cu/SiO₂ (labelled as Ni_{16.7}_Cu_{2.1}_Si) and 5%Rh/Al₂O₃ (labelled as Rh₅_Al) and 2%Ir/Ce400 (labelled as Ir₂_Ce) catalysts obtained at two different temperatures are reported in Table 3. As already outlined, the results showed that these catalysts exhibited excellent hydrogen yields, quite close to values predicted by

thermodynamics, ranked in the order Ni<Rh<Ir.

Temperature (°C)	Rh ₅ _Al	Ni _{16.7} _Cu _{2.1} _Si	Ir ₂ _Ce	Thermodynamics
650	0,85	0,78	0.89	0.93
700	0,90	0,85	0.94	0.96

Table 3 Hydrogen yields over Rh₅_Al and Ni_{16.7}_Cu_{2.1}_Si catalyst as a function of reaction temperature

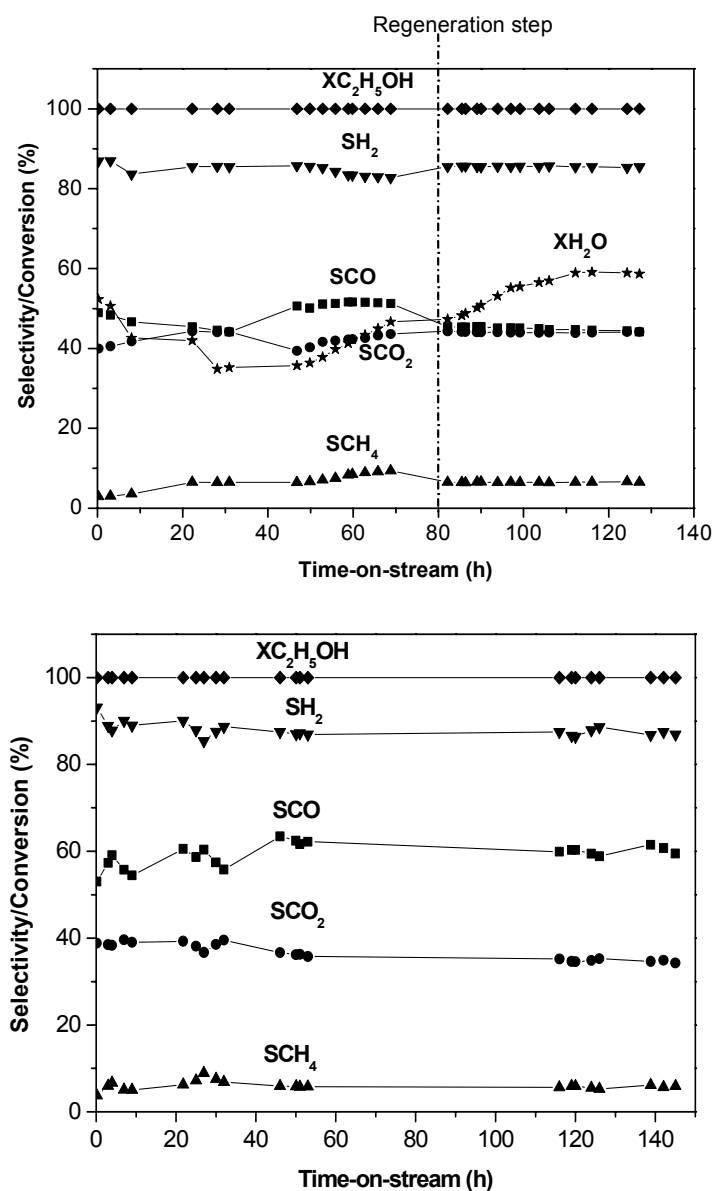


Figure 6 Conversion of ethanol and product selectivity vs time on stream (T=700°C, C₂H₅OH: H₂O: O₂=1:1.6:0.68 GHSV: 60000 ml/g_{cat}·h) over A: Ni_{16.7}Cu_{2.1}Si and B: Rh₅Al

The stability of the Ni_{16.7}Cu_{2.1}Si, Rh₅Al and Ir₂Ce catalysts was evaluated as a function of time on stream at various temperatures. It was found that Ni_{16.7}Cu_{2.1}Si and

Rh₅_Al catalysts seemed perfectly stable when operated at 700°C and (Fig6) with complete ethanol conversion. The results obtained at 700°C for Ni_{16.7}_Cu_{2.1}_Si catalyst (Fig.6 A) revealed in addition a slight change in selectivity during the first 80h on stream: H₂ and CO₂ selectivity decreased slowly, whereas CO and CH₄ selectivity increased slightly. After a regeneration step carried out at 80h on stream oxidizing the catalyst under O₂/Ar= 5/95 flow for 1 h, a further exposure to the reaction mixture did not result in any further changes in selectivity, till 120h on stream. For the Rh₅_Al catalyst (Fig. 6B), selectivity to hydrogen was not altered after 140h of stability test and remained constant at about 90%. Over the Ir₂_Ce catalyst, a perfectly stable performance was obtained at 650°C for 60h on stream (GHSV: 6000h⁻¹) as discussed in the previous chapter.

Thus, all three investigated catalysts were shown to be active, stable and selective under ethanol OSR conditions for the production of a hydrogen-rich process gas, when operated between 650 and 800°C. The main challenge was therefore to understand why these systems containing different active metals (noble or non-noble) and supports (neutral, amphoteric or basic) were performing well, while numerous other systems were found much less stable and selective under the same OSR conditions [69].

VI.3.2. Overall comparison of DRIFT-TPD analysis for three catalysts

While the three catalysts Ni_{16.7}_Cu_{2.1}_Si, Rh₅_Al and Ir₂_Ce catalysts showed comparable performances under steady-state ethanol OSR conditions, marked differences in either product distribution (under TPD conditions), and surface intermediates identified during DRIFT-TPD analysis revealed that these overall good performances might depend on various parameters and mechanisms. Table 4 summarizes these differences.

Catalysts		Ni _{16.7} _Cu _{2.1} _Si	Rh ₅ _Al	Ir ₂ _Ce
OSR activity and stability		Full conversion Stable at 700°C	Full conversion Stable at 700°C	Full conversion Stable at 650°C
Active phases		Ni ^o -Cu ^o NiOH/CuOH NiOOH	Rh ^o + interfacial sites Rh/Al ₂ O ₃ + Al ₂ O ₃	Ir ^o + interfacial sites Ir/CeO ₂ + CeO ₂
TPD products	CH ₃ CHO	<1%	<1%	14%
	acetone	Not detected	Not detected	4.2%
	ethylene	3.5%	7.8%	Not detected
	methane	~1%	~1%	~10%
	CO ₂ (LT)	yes	yes	no
	CO ₂ (MT)	yes	yes	yes
	CO ₂ (HT)	yes	yes	yes

Table 4 General features highlighting differences for the selected catalysts

Carbon deposition. The relatively weak deactivation observed for Ni_{16.7}_Cu_{2.1}_Si catalyst could be easily resolved by the oxygen regeneration. (treatment under oxygen rich flow after a long term OSR run). This points out that for this specific case, in the absence of active oxygen continuously fed by an active support like for the ceria system, some harmful coke deposition occur with time on stream. For that reason, the Ni_{16.7}_Cu_{2.1}_Si catalyst has to be operated at a higher temperature than the Ir₂_Ce system.

Active phases. It was found that the reaction proceeded via different routes depending on the nature of the active phase. The main reactions of adsorbed ethanol and intermediate species take place on the nickel sites for the Ni_{16.7}_Cu_{2.1}_Si catalyst. The contribution of complex nickel hydroxy-silicate sites for producing ethylene at low temperature is also likely [69]. The silica support just ensures active metal phase (Ni and Cu) dispersion but does not participate directly in the reaction, apart from storing loosely adsorbed ethanol at low temperature. Copper added to the Ni/SiO₂ formulation increases markedly the lifetime of the catalyst for ethanol OSR [69]. Copper appears to adjust the properties of nickel particles facilitating Ni redox cycles necessary for the reaction of ethanol and intermediate species.

In contrast, for the noble metal based systems (Rh₅_Al, Ir₂_Ce), the metal phase

remains essentially in a metallic state, while the support plays a key catalytic role to store intermediates from ethanol decomposition and assists in water activation.

Mechanistic specificities. In line with the above statement, adsorption of ethanol on the catalysts gives rise to form ethoxy species, which are produced on nickel sites for the Ni_{16.7}_Cu_{2.1}_Si catalyst and on the support sites for the other two catalysts. A fraction of ethoxy species can be further dehydrogenated to produce acetaldehyde, readily reacted with oxygen from support to produce acetate and carbonate species. Here, the nature of the support is essential: on the amphoteric alumina surface, few carbonates are stored while large amounts of stable carbonates accumulate on the ceria surface. The same trend is observed for the acetate ad-species.

Upon increasing the temperature, the decomposition of above intermediate products leads to the appearance of CH₄, CO, CO₂ and H₂.

A key singularity is observed for the Ir₂_Ce system, which produces relatively large amounts of methane and acetaldehyde under TPD conditions. This underlines the ability of ceria to promote the oxidative dehydrogenation and also the easy occurrence of H spillover (via OH groups as generally assumed) towards the metal phase. That additional H is supposed to hydrogenate the methyl groups originating from the cracking of acetate species. For the two other catalysts, this reaction does not occur (insufficient surface activity for alumina and/or spillover rate and total inertness of silica). In contrast the formation of ethylene (as coke precursor) is observed only for the two Ni_{16.7}_Cu_{2.1}_Si and Rh₅_Al systems, most likely on acid surface sites: nickel hydroxy-silicate and aluminium hydroxyl groups, respectively.

It can be stressed here that the formation of acetone is specific for the Ir₂_Ce catalyst, since this product was never observed for the two other tested systems. Acetone can be produced along a ketonisation process, proceeding for instance by the thermal decomposition of metal acetates or from acetaldehyde according to an aldolisation process [127,143].

Another specificity of the Ir₂_Ce catalyst was its stability under ethanol OSR conditions

at lower temperature than for the two other selected systems (650 vs 700°C, respectively). This might be due to a permanent "cleaning" effect, i.e. carbon removal, owing to ceria's excellent oxygen exchange capacity [144,145]. As a matter of fact, carbon deposits formed on metal surface could reduce partially the oxide support to produce CO₂ and oxygen vacancies. Then water and/or oxygen can easily react with those vacancies to reoxidize ceria around metal particles. Such a redox process occurring at the metal-support interfacial perimeter acts for the oxidation of carbon deposits, but also for hydroxyl spillover from oxide to metal phases, as required by the bi-functional mechanism typical of this catalytic system.

As far as CO₂/CO production is concerned, here again, there are many differences deserving to be outlined:

i) For the Ni_{16.7}_Cu_{2.1}_Si system, an obvious high activity for low and medium temperature WGS was revealed by TPD analysis. This feature can be easily assigned to the Ni-Cu alloyed phase, able to activate CO and water via a process involving formate intermediates probably arising from Ni hydroxyl groups reacting with Ni carbonyls. The role of Cu was clearly proved by the much larger production of CO₂ at medium temperature for the alloyed system as compared to the copper free Ni/SiO₂ system. This WGS activity remains high (under OSR conditions) for this Ni-Cu based system at high temperature due to the efficiency of the redox cycles of the Ni-Cu phase.

ii) For Rh₅_Al, the production of CO₂ is reasonable at medium temperature under TPD conditions, essentially due to the decomposition of unstable carbonates accumulated on the alumina support. In contrast, at higher temperature, under OSR conditions, the production of CO₂ by WGS remains below the equilibrium value, most likely due to the limited possibility of water transfer on the interfacial alumina sites around the Rh particles.

iii) For the Ir₂_Ce system, CO₂ release is unfavourable at low temperature under TPD conditions, obviously due to the trapping effect of the basic sites on ceria, accumulating stable carbonates. However, at high temperature, the quite large production of CO₂ under OSR conditions clearly reflect the direct activity of the whole ceria surface to activate water

and to allow mobile OH groups to spill over the Ir particles for ensuring H₂ and CO₂ production.

Proper effect of noble metal nature with similar ceria support: Ir/Ce400 compared to Rh/Ce400

As shown in the previous Chapter V, the Rh/Ce400 catalyst exhibited a slightly higher ethanol conversion and less CO formation at low temperature compared with Ir/Ce400. According to the previous mechanism analysis, it was probably that rhodium had higher C-C bond rupture capacity than iridium due to electronic property. In other words, the d electrons of Rh might be shared to a larger extent with the antibonding orbitals of C2 intermediates increasing C-C bond dissociation. Similar electronic mechanism can explain the less CO formation. For the water gas shift reaction, there is the larger electronic interaction between Metal-CO and hydroxyl groups on rhodium than iridium.

VI.4. Preliminary kinetic analysis on Ir/Ce400 catalyst

It is obvious that the design of catalysts and reactors require information on the kinetic properties of the reaction of interest. For the present case of ethanol reforming, little kinetic information is available [71]; therefore, we have performed preliminary kinetic measurement for the ethanol steam reforming reactions over the Ir/Ce400 catalyst.

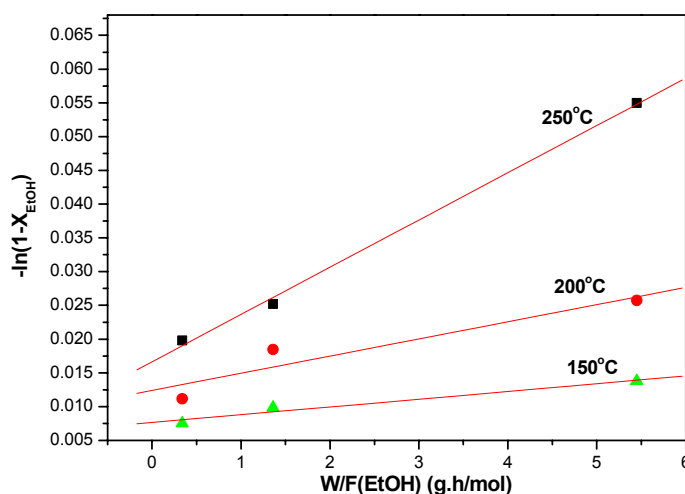


Figure 7 Semi-logarithmic plot of the mole fraction of unreacted ethanol as a function of w/F at various temperatures.

The chosen experimental conditions were checked to ensure the absence of significant external and internal diffusion limitations. Fig 7 displays the effect of the contact time on the ethanol conversion at various temperatures, formalized through the following Eq9

$$-\ln(1-x) = (k \cdot w)/F \quad \text{Eq9}$$

where x is the degree of ethanol conversion; w is the catalyst weight; F is the flow rate.

The linear relationship between the degree of ethanol conversion and contact time indicates a first-order reaction with respect to ethanol, the slope of each line being the rate constant k [101,146].

The first-order dependence on ethanol is in agreement with results of other researchers. Sun et al.[25,70] have reported that the rate of ethanol conversion over Ni based catalysts is first order with respect to ethanol. Morgenstern and Fornango [147] earlier studied the reaction kinetics over Cu plated Raney Ni and suggested a sequence of two first-order reactions: dehydrogenation of ethanol to acetaldehyde and decarbonylation of acetaldehyde.

Indeed mechanistic studies demonstrated that the activation of ethanol at low temperature in form of ethoxy species was a readily proceeding, which might contradict a first order in respect to ethanol. But in the mean time, DRIFT investigations clearly demonstrated that there was no more ethoxy accumulation in the reacting domain (above 400°C), which is quite consistent with the observation of an apparent order of one for the rate of ethanol conversion.

The reaction order for water was not investigated at this stage due to the difficulty to quantify the water.

By changing the reaction temperature, a first evaluation of the apparent activation is obtained by means of the Eq10:

$$\ln(k_2/k_1) = (E_a/R) \cdot (T_2 - T_1)/(T_1 \cdot T_2) \quad \text{Eq10}$$

where R is the perfect gas constant and T is the reaction temperature.

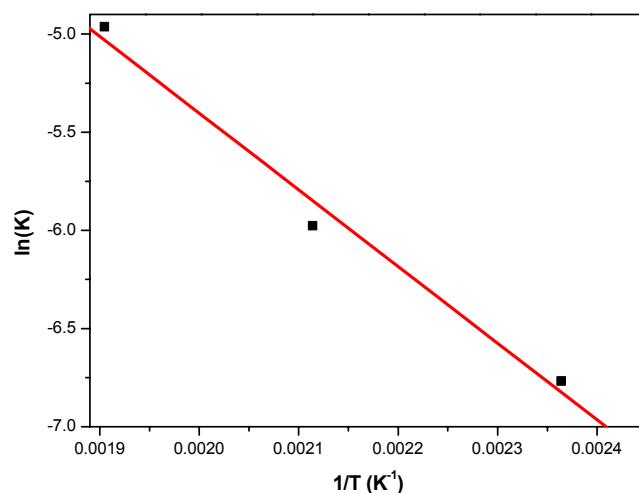


Figure 8 Semi-logarithmic plot of the rate constant as a function of temperature

Hence, the apparent activation energy of reaction E_a can be computed to be 32.54 kJ/mol as illustrated in Figure 8. In spite of the different temperature range, Baltacioglu et al. [35] using a Pt-Ni/Al₂O₃ catalyst obtained an activation energy (39.3 kJ/mol) perfectly similar to the value obtained in this work. Doca et al, working with Mn/CuO catalyst also found an energy activation value quite similar (33.5 kJ/mol). On the other hand, Sun et al. [70] found a much smaller value (7 kJ/mol) over a Ni/Y₂O₃ catalyst, which might be due to the presence of extraneous effects (diffusion of mass and heat in catalyst particle and mixing in the reactor). Nevertheless, the relatively low value for the apparent activation energy of the ethanol SR reaction confirms that the activation of ethanol is an easy process, which is in line with the fact that thermodynamic equilibrium is easily achieved.

VI.5. Conclusion

Based on the above mechanistic and kinetic analysis, the following conclusions can be proposed:

i) Ethanol conversion over the Ir/CeO₂ catalyst is a bi-functional mechanism involving both the active metal (Ir) and the support (CeO₂):

- Over the ceria surface, ethanol conversion proceeds according to the sequence: ethanol → ethoxy species → acetaldehyde → acetate species, i.e, represents mainly a C2

chemistry.

- After addition of iridium, acetate species decompose into methyl groups and carbonate species at the interface of Ir-CeO₂, which represents a transition from C2 to C1 products.

- Methyl groups were further hydrogenated to methane or oxidized to carbonyl species, releasing CO, over the iridium surface, which represents the conventional C1 chemistry over noble metal phase.

- When changing the noble metal phase from Ir to Rh, the same mechanism applies but the C2 to C1 chemistry steps are slightly more favored on the Rh system due to a higher ability to C₂ bond breaking.

ii) In contrast with the above bi-functional mechanism, a single functional mechanism was found for a metal supported on an inert (silica) or a non redox (alumina) material. Thus, for the Ni-Cu/SiO₂ system, the main reactions of adsorbed ethanol and intermediate species take place on the nickel sites. The silica support just ensures the well dispersion of active metal phase (Ni and Cu). For the Rh/Al₂O₃ system, only the OH from the support can play a role but the main steps for ethanol activation till syngas formation occur on the metal phase.

iii) The links between a reaction mechanism determined by dynamic methods (TPD, TPRS) and a kinetic model remains to be established. In this work, the ethanol steam reforming reaction was found to be first order with respect to ethanol with an activation energy of 32.5 kJ/mol. Further investigations at various water partial pressure are required. However, the sequence of elementary steps above mentioned might serve as a strong basis for setting a micro-kinetic model.

iv) The DRIFTS analysis performed under effective reforming conditions (SR or OSR conditions between 400 and 600°C) for the Ni-Cu/SiO₂ and Rh/Al₂O₃ systems [142] revealed that only OH groups and stable acetate species were observable on the working surface. This observation displays the limits of an operando DRIFTS investigation for reforming reactions where the surface accumulation of active species is extremely weak.

Chapter VII. Hydrogen production from ethanol over Ir/Ce400 catalyst in micro-reactors

Previous studies concerning the process of hydrogen production from ethanol reforming were mainly based on the kinetic experiments carried out in conventional fixed-bed reactors [148-150]. In a similar way, we performed mechanistic and kinetic experiments presented in the previous chapter in fixed bed reactors for the newly proposed Ir/CeO₂ catalyst, including studies using a *In-situ* DRIFT cell for the IR study.

As already stressed in the Introduction section, alternative reactors such as micro-structured ones have attracted considerable interest in hydrogen production due to their proved advantages in mass and heat transfer, smaller size favorable for integration and process intensification, energy and cost saving. Drawbacks were however identified as well such as the challenges in developing stable and performing coatings, metallic substrate inertness and issues in structured elemental platelets assembly.

Micro-structured reactors are characterized by three-dimensional structures in the sub-millimeter range. Currently multi-channel reactors are mainly used with channel diameters between 10 and several hundreds of micrometers.

From the literature analysis, it comes that the investigation of hydrogen production in micro-structured reactor was till today mainly focused on methane and methanol reforming [151-154].

In this chapter, we report the catalytic performance of the selected Ir/Ce400 catalyst observed in two lab scale micro-structured reactors, for comparison with the results obtained in a fixed-bed reactor.

The first set of experiments is dedicated to ethanol OSR, but reaction temperatures were limited to 550°C for technical reasons. The second set of experiments is dedicated to steam reforming in a micro-structured reactor allowing operations at higher temperature. For both cases, the comparison with fixed bed reactors was made under the same operating

conditions.

VII.1. Micro-reactors used in this study

VII.1.1. Micro-reactor housings

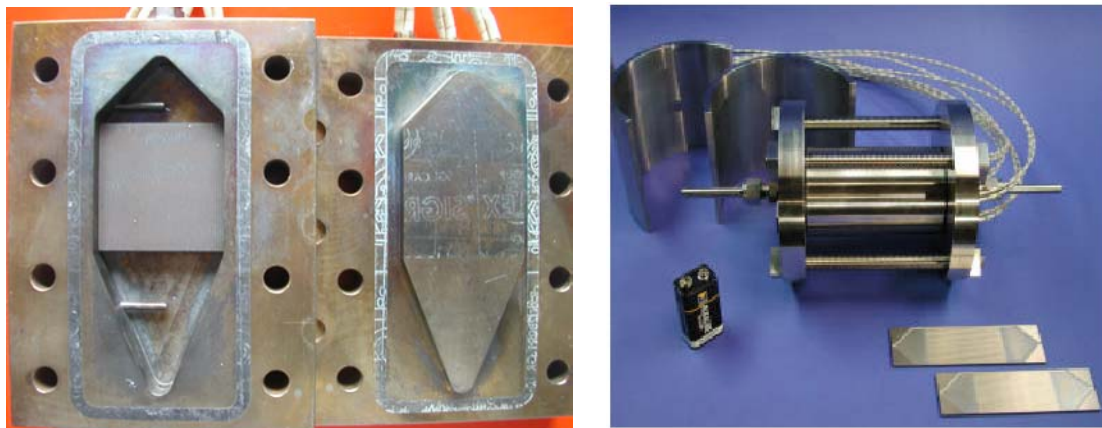


Fig 1 Micro-reactor housing used for ethanol oxidative steam reforming (left) and steam reforming (right)

The micro-reactor housings used for the oxidative steam reforming and steam reforming are depicted in Fig 1. Both housings were manufactured from stainless steel and have been designed and provided by the IMM company. They allow stacking of platelets, in the left case for oxidative steam reforming completed by cover platelet without channels. In the case of the right reactor for the steam reforming of ethanol a constant number of two platelets had to be used. Both devices were sealed against the lab atmosphere with a graphite gasket held in place by a gasket retainer. The housings also include welded-in Swagelok fittings for gas connections and sockets for four electronic cartridge heaters. Due to the design, the working temperature for the left reactor was limited to 600°C, and to 800°C for the right one.

Both reactors are "openable systems" for lab investigations allowing to run experiments repeatedly, just by changing the structured platelets stacks. Thus, advantages of this design are i) easy stacking and insertion into the testing unit; ii) easy opening and recovery of used platelets for further characterization. However, their drawback was a lacking of a temperature measurement well inside the stack for establishing temperature profiles along

the platelets. In addition, gas by-pass from one channel to another one cannot be discarded, in opposite to completely welded systems where each channel is completely isolated from neighboring channels.

VII.1.2. Micro-structured platelets

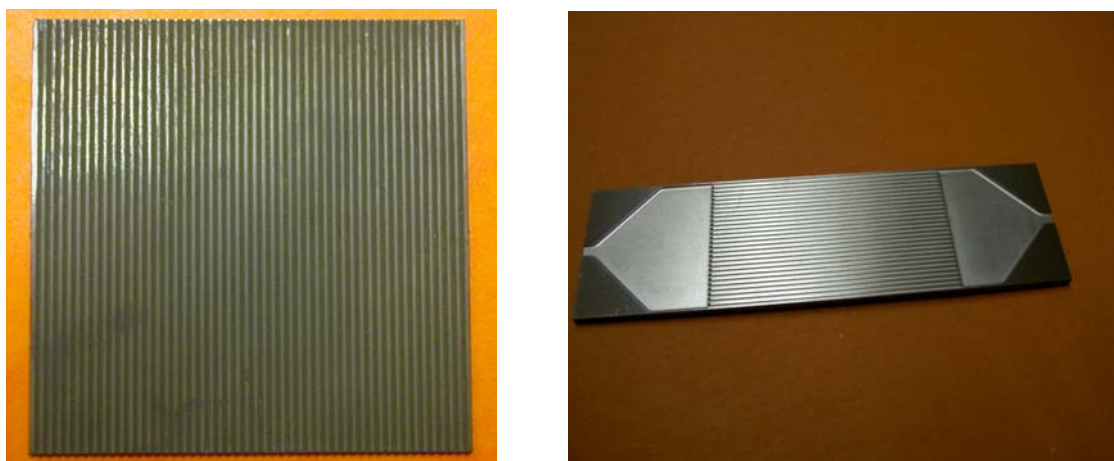


Fig 2 Micro-structured platelets used for ethanol oxidative steam reforming (left) and steam reforming (right)

Fig 2 presents the photography of platelets used in the test. Similar material and channel design (only the shape and dimension differ) were employed for both, low and high temperature, reactors. The platelets were made of aluchrom, 20%Cr, 30%Ni, 4%Al, 46%Fe.

The platelets used for the oxidative steam reforming have the following dimensions: 50mm*50mm*5mm. They contain 46 micro-channels per platelet with the following dimensions: 50mm length*0.5mm width*0.5mm depth.

The dimensions of the platelets used for ethanol steam reforming are: 100mm*30mm*2mm. There contain 28 micro-channels per platelet with the following dimensions: 100mm length*0.5mm width*0.5mm depth.

The micro-structured platelets are stacked between two or more non structured top platelets (depending on the number of catalytic platelets) and the stacks introduced in the housings before leak tests.

VII.2. Wash-coating of Ir/Ce400 catalyst onto micro-structured platelets

This paragraph refers to the wash coating technique used both for SR and OSR experiments

VII.2.1. Platelets pre-treatment

In order to eliminate impurities such as organic compounds, a three-step treatment was applied [155,156]. Agents used are acetone, acetic acid, ammonium hydroxide, phosphoric acid, and hydrogen peroxide. First, the platelets were washed with acetone. Next they were immersed in a bath of 5:1:1 deionized (DI) water: H_2O_2 : NH_4OH and rinsed in DI water followed by immersion in a solution of 5:1:1 DI water: H_2O_2 : H_3PO_4 : CH_3COOH in an ultrasonic bath and DI rinsing. Subsequently, the micro-channel platelets were annealed at 1000°C for 10h at a heating rate of $5^\circ\text{C} / \text{min}$. This thermal treatment triggered the segregation of an alumina layer on the metallic surface. Prior to starting the coating procedure, all supports were washed with ethanol, removing any superficial impurities caused by manipulation.

VII.2.2. Preparation of wash-coating slurry

For the preparation of the Ir/Ce400 slurries, several recipes were first tested to select one well adapted to the type of material to be coated, on the basis of a knowledge developed at IRCELYON in previous studies [156]

To prepare the slurry before coating, the Ir/Ce400 powder was milled to particle size $< 5\mu\text{m}$ using a wet ball-milling method and addition of the binder Tylose MH 300 P2 (methylhydroxyethyl cellulose). The powders were immersed into water (mass ratio Ir/Ce400: H_2O =1:4, binder: H_2O = 1:67) under vigorous stirring. The suspension was kept stirred for 12h prior to deposition at room temperature.

VII.2.3. Platelet coating

The coating was performed according to the following four step procedures:

i) The slurry was applied to the micro-channels of the platelets using a syringe. Even though the use of a syringe is not a commercially viable process in the production of bulk quantity of coated platelets, it is rather a convenient way to accomplish the catalyst deposition procedure at lab scale and leads to a good layer quality [157,158].

ii) Any excess of suspension was wiped off. It should be mentioned that conventional techniques using gas assisted fluid displacement in cylindrical geometries (monolith like) [159] is not suitable for an open channel geometry.

iii) The platelets were dried at ambient temperature in air.

iv) The coated micro-channel platelets were calcined at 400°C for 5h using a heating rate of 5°C /min.

Before reaction, two platelets were assembled in the reactor housings above described. Then the reactors were closed, tested for leaks tightness, eventually tightened until being leak-free and inserted in the ethanol OSR and SR set-ups described in the Experimental section.

VII.3. OSR over Ir/Ce400 in low temperature micro-structured reactor

VII.3.1. Influence of reaction temperature

Figure 3 reports the changes in the outlet dry gas composition as a function of the reactor temperature for the ethanol oxidative steam reforming over the Ir/Ce400 catalyst in the micro-structured reactor. The experiments were conducted in the temperature range of 300-550°C, since the temperature for this micro-reactor had to be kept below 600°C to prevent a degradation of the graphite seals and bolts assembling the housing.

Figure 4 compares the same values of outlet dry gas composition (without considering the C₂ products) with the values predicted by thermodynamics.

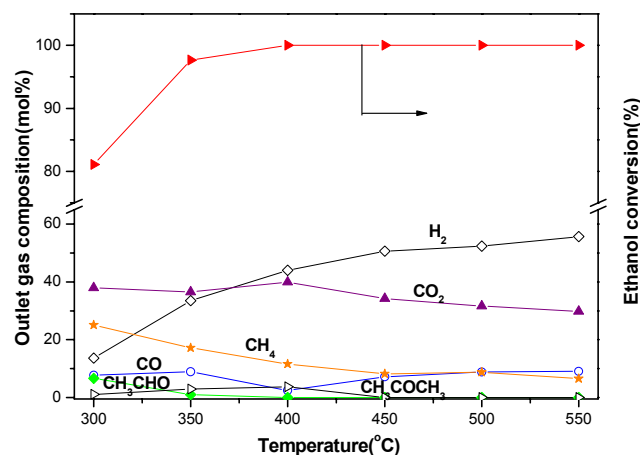


Figure 3 Effect of the reaction temperature on the concentrations of the products of ethanol oxidative steam reforming over Ir/Ce400 catalyst in a micro-reactor. Experimental conditions: EtOH/H₂O/O₂ = 1/1.8/0.6; GHSV = 6000ml/g_{cat}·h, p = 0.1MPa.

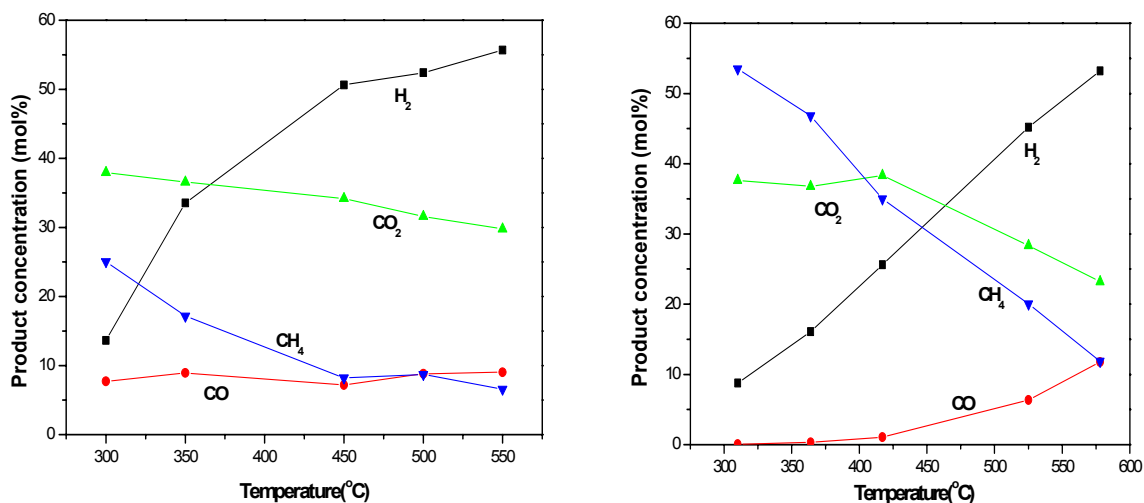


Figure 4 Comparison of thermodynamic equilibrium compositions (right) with actual product compositions (left) obtained in the oxidative steam reforming of ethanol over Ir/CeO₂ catalyst. EtOH/H₂O/O₂ = 1/1.8/0.6; GHSV = 6000ml/g·h, p = 0.1MPa.

As can be seen in Fig 3 & 4, the concentration of hydrogen increased progressively with rising temperature and a complete conversion of ethanol was achieved at 400°C, while thermodynamics predicts full conversion at any temperature, as seen in the introduction section. In the low temperature domain, oxygenates were formed at low concentration (below 10%) and disappeared above 400°C for case of acetaldehyde and 450°C for the case of acetone. Therefore the outlet dry gas only contained H₂ and C1 products from 450°C and above.

The formation of methane was important at mild and medium temperature, (25%) at 300°C, but to an extent significantly lower than predicted by thermodynamics (Fig. 4). Upon increasing temperature, the CH₄ concentration decreases regularly to reach thermodynamics values at high temperature.

In turn, the amount of CO was lower than that of methane at mild and medium temperature, but being much higher than predicted by thermodynamics. At higher temperature, its level was kept nearly constant around 10%, joining values predicted by thermodynamics at high temperature,

Finally the concentration of CO₂, like H₂, follows approximately the thermodynamics trends.

All these results can be analyzed in the following way:

i) at low and medium temperature, the thermodynamic equilibrium between methanation and reforming



which should be strongly displaced towards methane formation (see fig 4) is not achieved: This is revealed by the relatively low methane formation, which is the obvious indication that the tested catalyst is not designed for the methanation reaction (generally based on Ni systems). Our system is therefore kinetically controlled.

In turn the WGS equilibrium



which fixes the respective concentration of CO, CO₂, H₂ and H₂O, is much more achieved, as expected from this ceria based system known to be effective for the shift reaction via a bi-functional mechanism.

The partial conversion of ethanol at low temperature again indicates that the ethanol conversion is kinetically limited which favors the C₂ by-products as discussed in the mechanistic chapter.

ii) at high temperature, all gas concentrations are very close to thermodynamics values, indicating that the system is no more kinetically controlled for any of the reactions

involved, which makes that only stability issues have to be solved.

These results strongly outline the advantages of this OSR reaction implemented in a micro-reactor where the efficiency and the heat management of the catalyst allow the system to strictly reach the thermodynamics at lower temperature than with a fixed bed system. This leads directly to the possibility to produce hydrogen with a relatively low CO concentration. The drawback remains the methane production which should be still more minimized by decreasing the residual methanation function of the catalyst.

VII.3.2. Influence of contact time

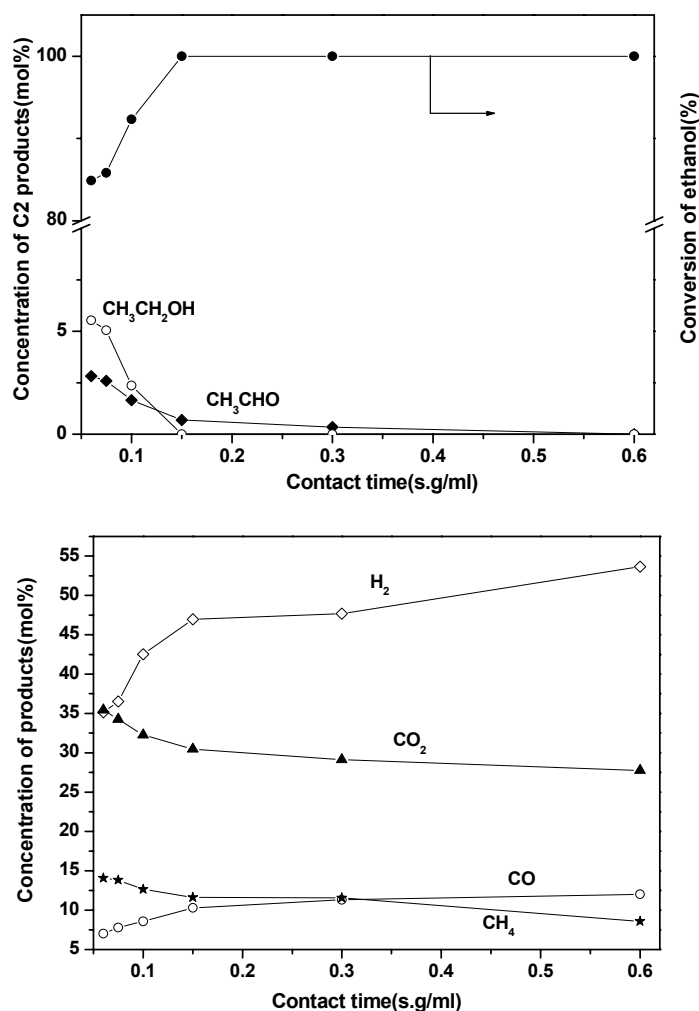


Figure 5 Influence of contact time for oxidative steam reforming of ethanol over Ir/Ce400 catalyst in micro-reactor. EtOH/H₂O/O₂ = 1/1.8/0.6; T:550°C; p = 0.1MPa.

Fig 5 reports both the change in ethanol conversion and the changes in detected product concentrations as a function of the contact time for a reaction temperature of 550°C.

The reasonably linear increase of conversion in the short contact time domain is expected for a catalytic regime as long as it passes the origin. Nevertheless, it seems not possible to extrapolate the points at shortest contact time to the origin and non-catalytic contributions might be present also. In turn, it can be deduced from extrapolation at zero contact time that a non negligible residual conversion occurs in the absence of catalyst. This fact would indicate gas phase combustion, which might even start in the hot tubes carrying the reactants to the reactor or the distributor zone, just preceding the catalytic micro channeled zone.

At higher contact time, ethanol is fully converted, reaching thermodynamic level. Concerning the product distribution, the major carbon containing product at very short contact time is carbon dioxide which strongly reinforces the occurrence of gas phase combustion. Methane formation can as well be assigned to direct thermal cracking of ethanol.

In the short contact time domain where the ethanol conversion is only partial, some acetaldehyde was also formed. This fact can be directly related to the sequential mechanism established in the previous chapter, indicating that ethanol is first converted to acetaldehyde, further oxidized into acetates before being reformed into syngas and carbon dioxide. The important formation of methane in that domain confirms that methane reforming is a slow and energy demanding process [161].

At higher contact time the catalytic syngas production establishes and part of the produced CO is further transformed to carbon dioxide according to the WGS equilibrium. Here the methane reforming becomes effective.

VII.3.3. Long term stability test

In order to test the stability of the Ir/Ce400 catalyst in a micro-reactor under OSR conditions, a long term reaction test was performed (Fig6).

During a first period of about 8h, the system was active enough to fully convert ethanol, which prevents drawing any direct conclusion on catalyst stability.

After that initial period, the system started to deactivate, but the decline leveled off after around 10h on stream and performances remained then perfectly stable at an ethanol conversion of 85% for the rest of the testing period (till 60h on stream). Concerning product distribution, the equilibrated syngas/ CO_2 distribution was mainly observed during the first full conversion period, while after reaching the effectively stable period at partial conversion, about 3% of acetaldehyde was produced and the H_2 and CO selectivity decreased slightly at the benefits of CO_2 and CH_4 formation.

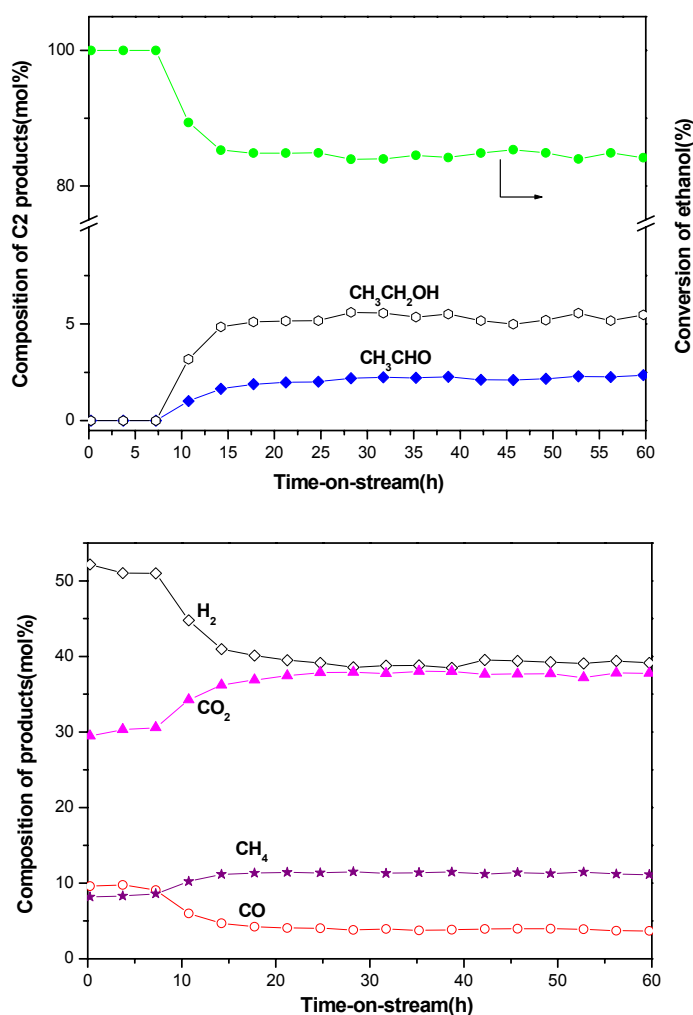


Figure 6 Outlet gas compositions as a function of time-on-stream for ethanol steam reforming over Ir/Ce400 catalyst in the micro-reactor. Experimental conditions: reaction temperature 550°C ; $\text{EtOH}/\text{H}_2\text{O}/\text{O}_2 = 1/1.8/0.6$; GHSV = $6000\text{ml/g}\cdot\text{h}$.

In order to understand this aging profile, the spent catalyst was collected after the test sampling part of the adlayer for XRD and TEM measurements. Results are reported in the next paragraph.

VII.3.4. Characterization of used catalyst after long term testing

Before sampling part of the catalyst adlayer, the used platelets were weighted and the remaining mass was compared to the one corresponding to the freshly coated platelets. The mass balance indicated a very small loss of about 0.2% of the catalyst coating, which confirms that the selected coating methodology was suitable and well implemented.

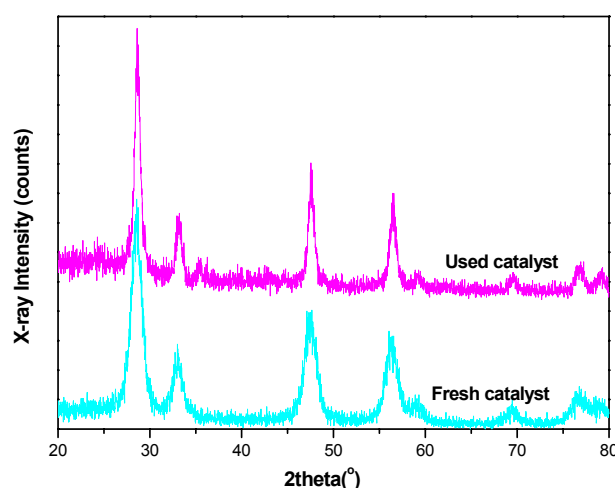


Figure 7 XRD patterns of the fresh and used Ir/Ce400 catalyst.

Figure 7 compares the XRD patterns of the fresh and used Ir/Ce400 catalyst. Only the patterns corresponding to the fluorite-structured CeO₂ could be observed after the test, like for the fresh catalyst. In both cases, the absence of Ir diffraction peak provides evidence that neither aggregation nor sintering of Ir particles occurred during the aging test. However, as for analyses carried out in the fixed-bed reactor (see chapter IV), the indexes of fluorite structure narrowed during the test and it was calculated that the ceria mean particle size increased from about 6nm to 15nm, which corresponds approximately to about 60% decrease in the BET area.

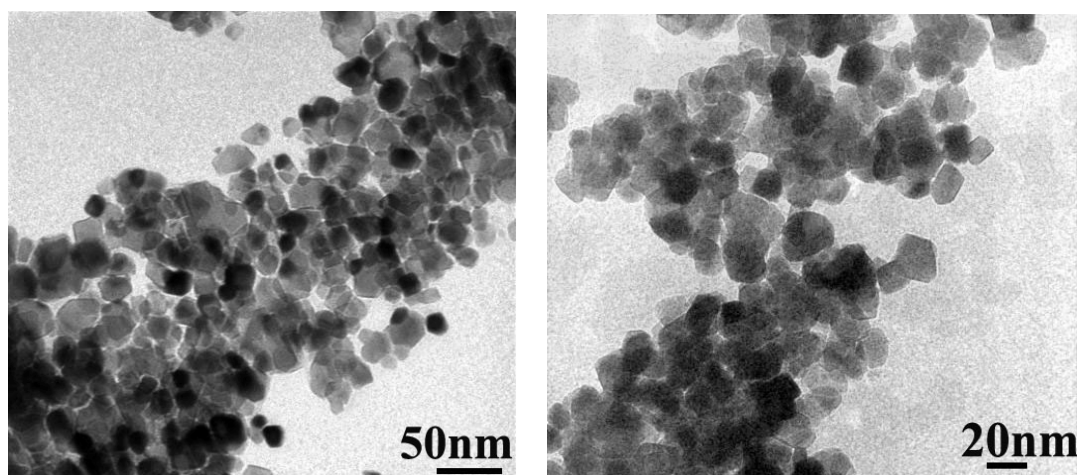


Figure 8 TEM images of the used Ir/Ce400 catalyst.

Figure 8 presents the TEM images of the catalyst after the stability test. It was clearly observed that there was no coke formation for the used catalyst. This result is in line with TPO results after long term tests in fixed bed reactor showing the absence of coke deposits under OSR conditions.

VII.3.5. Discussion on catalyst stability in micro-structured reactor

The above results indicated that the aging profile during the 60h on stream was neither caused by coke formation nor by sintering of the active metal. In contrast, the sintering of ceria occurred and has to be considered as a likely aging factor, at least during the initial period, till about 10 h on stream.

This structural factor might be related to the effective temperature inside the reactor. As a matter of fact, the initial product distribution (higher H_2 and CO selectivity) and higher activity (100% ethanol conversion) might be reasonably assigned to a higher initial temperature, due to a highly active material and a more exothermic process, at least in the catalytic zone close to the inlet.

In turn, during the stabilized period after 10h on stream, the system behaved as if a lower temperature was applied, as revealed by the partial ethanol conversion and the product distribution.

Finally, there remain interrogations to understand why the catalyst temperature changed

from the initial deactivating period till reaching a stable value after about 10 h on stream.

As seen in Chapters IV and V, the bi-functional mechanism applying for this Ir/ceria system involves a key participation of ceria to activate ethanol into ethoxy species, further dehydrogenated into acetaldehyde, then oxidized to acetates before the C-C bond activation proceeds at Ir-ceria interface. Therefore, the ceria sintering which is most likely to occur during the initial "pseudo stable" period (sintering processes are generally following kinetics with high orders versus time on stream) would progressively decrease the activity and probably the local temperature of the catalyst during this first 10h period. More precisely, it can be proposed that for the case of the high surface fresh ceria, the oxygen bulk and surface diffusion towards the Ir particles is much more favored than for the sintered ceria in the used catalyst. This would lead to a more favored exothermic partial oxidation process for the fresh catalysts, while for the used and stabilized one, it would be more endothermic, then leading to a decreased local temperature, and therefore a slightly decreased activity.

Again, the key information from this investigation in a micro-structured system is that the Ir/ceria catalyst, after an initial ceria sintering period, remains perfectly stable even under conditions where the ethanol is not fully converted. This result complements well the conclusions obtained under full ethanol conversion conditions in a fixed bed reactor in Chapter IV.

VII.3.6. Comparison between fixed bed and micro-structured reactor

The comparison of the catalytic behavior of the Ir/Ce400 catalyst in fixed-bed and micro-structured reactor under OSR conditions with strictly identical feed composition and contact time (GHSV=6000 ml/g.h.) is illustrated in Figure 9, based on the results from Chapter IV.

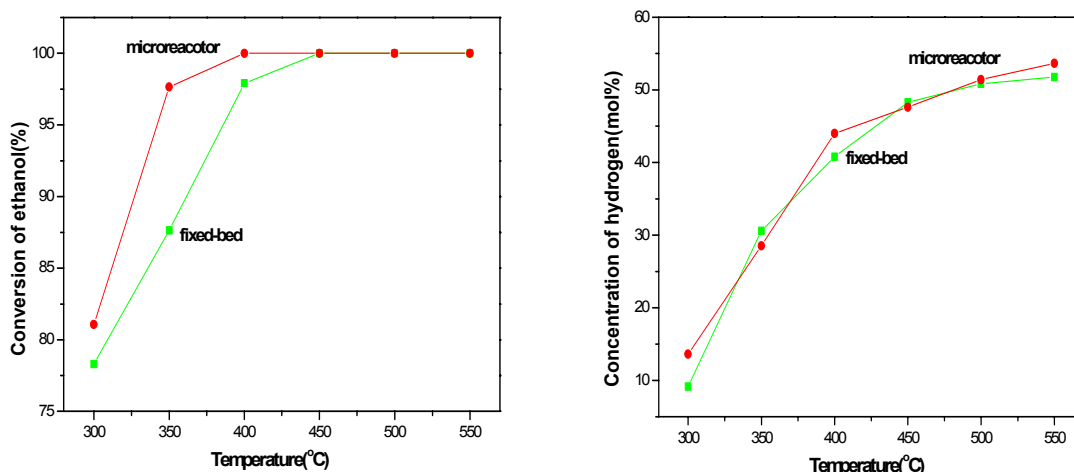


Figure 9 Ethanol conversion (left) and outlet hydrogen concentration (right) as a function of temperature for ethanol oxidative steam reforming over Ir/Ce400 catalyst in the micro-structured and fixed bed reactors. Experimental conditions: reaction temperature 550°C; EtOH/H₂O/O₂= 1/1.8/0.6; GHSV = 6000ml/g·h.

As can be seen, in the low temperature domain, the conversion of ethanol was significantly higher for the micro-structured reactor than in the fixed-bed reactor and ethanol was already converted to 98% at 350°C, while this level of conversion was reached only at 400°C for the fixed bed reactor. This indeed confirms that the improved mass transfer properties of the micro-structured reactor leads to markedly improved performances at low and mild temperature. At higher temperature, the complete conversion prevents from further comparison.

It might however be noted that at 550°C, during the long term testing experiments performed in the fixed bed (see Fig 7 in chapter IV) or in the micro-reactor (see Fig 6), the effective temperature of the fixed bed reactor was higher than the one observed in the micro-reactor, where a flatter temperature profile is generally achieved. This would explain why the ethanol conversion was permanently complete in the fixed bed, while it was decreased to about 85% after 60h on stream for the micro-structured system. Again, the less isothermal behavior of the fixed bed reactor as compared to the micro-structured one explains this difference in catalyst temperature for the two compared systems.

Other effects such as a smaller contact time per channel for the micro-structured system (actually 46 fixed micro-beds in parallels) cannot be discarded as contributing to the observed slight differences in performances.

VII.4. Comparison between SR over Ir/Ce400 in micro-structured and fixed bed reactors

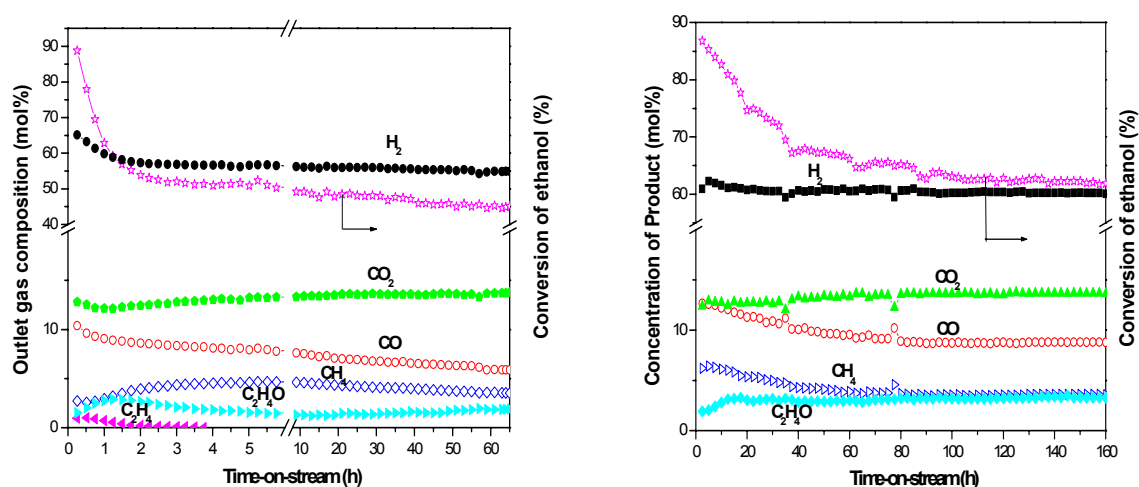


Figure 10 Outlet gas compositions and ethanol conversion as a function of time-on-stream for the steam reforming of ethanol over Ir/Ce400 catalyst in the fixed bed (left) and micro-structured (right) reactors. Experimental conditions: reaction temperature 650°C; EtOH/H₂O = 1/3; GHSV = 75000ml/g·h

Figure 10 compares the performance of the Ir/Ce400 catalyst in a fixed-bed reactor and in the micro-structured reactor for SR testing, under strictly identical feed composition and contact time. Note here that a very high GHSV of 75000ml/g·h (one order of magnitude higher than that for the previous OSR long term testing) was selected in order to avoid full conversion of ethanol, preventing from any correct analysis of deactivation.

As can be seen, despite very close initial performances, significant differences in the aging profiles can be outlined:

- A aging revealed by the fast initial decay in ethanol conversion is observed for the fixed bed reactor (during the first 2 h on stream), followed by a slow and continuous decay over the 60h on stream, while the deactivation in the micro-structured reactor is much slower and regular, with a long term stabilization after a hundred of hours on stream. Thus, it can be noted that the activity at 60h (maximum time on stream for fixed bed test) is about 50 and 65% for the fixed bed and micro-structured reactors, respectively.

In turn, no major difference is noted for the product distribution profiles, unless slight differences for the acetaldehyde and methane production. Indeed, as stressed before in the

mechanistic study, the observation of acetaldehyde under partial conversion of ethanol confirms its character of intermediate product. It may be noted as well that there is an initial production of ethylene in the fixed bed reactor, which corresponds to the faster decay period, as already stressed in Chapter IV.

For the present case of ethanol SR, at variance of the OSR case, carbon deposits are accumulated, as demonstrated by the TPO experiments reported in Chapter IV Figure 13 for the fixed bed reactor. Two types of carbon were identified, one which could be oxidized at low temperature (a carbide-like phase around the metal particles) and one more toxic and responsible of the catalysts aging which required higher temperatures to be oxidized. The production of ethylene is likely to explain the occurrence of this initial fast deactivation in the fixed bed reactor. In the micro-structured reactor, no TPO was performed for technical reasons. Note however that no change in pressure drop was observed in any case.

In addition to carbon deposition under SR conditions, the sintering of ceria might contribute as well to the deactivation process, since the activation of water is essentially ensured by ceria and the mobility of the resulting OH groups towards the Ir phase will suffer from the ceria sintering, despite a constant Ir dispersion.

To conclude this paragraph, a marked beneficial effect of using a micro-structured reactor under the severe SR conditions was demonstrated, most likely arising again from a better heat and mass management. As a matter of fact, the temperature profile for the fixed bed reactor was measured, as reported in Figure 11 (left), showing a temperature difference range of about 40°C. Though not measured in the present micro-reactor system under ethanol SR conditions (see paragraph IV 1.1), the temperature profile obtained in a micro-reactor under even more severe methane steam reforming conditions was only half as pronounced as that for the fixed bed (see Figure 11 (right)). This efficiency of micro-structured reactors for flattening temperature profile was demonstrated as well for methanol steam reforming by Dupont et al [162].

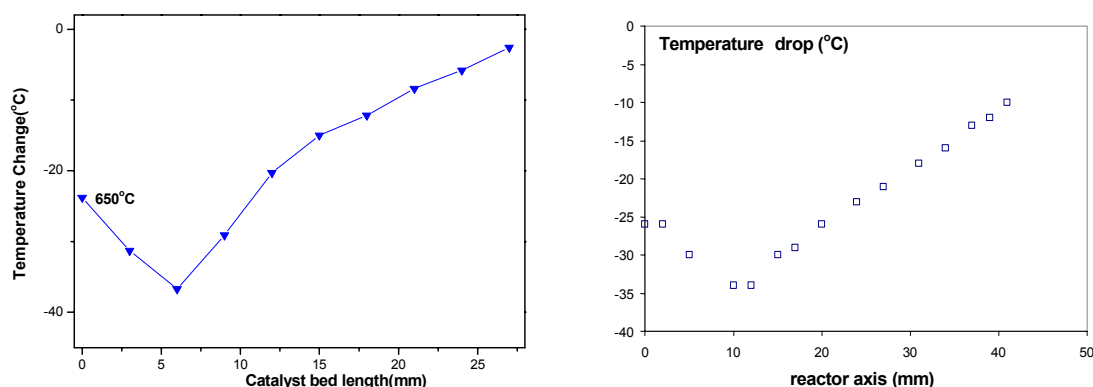


Fig 11 Temperature profile in the fixed bed reactor during ethanol SR at 650°C (left); temperature profile in the micro-structured reactor during methane SR at 850°C (right, unpublished result)

VII.5. Conclusion

It was shown in this chapter that the coating of the selected Ir/Ce400 catalyst under optimized conditions led to a quite stable phase, as attested by long term experiments (till 160h on stream for steam reforming).

Comparing the results obtained both in a fixed bed reactor and in a micro-structured reactor for OSR and SR reactions, a clear benefit was found for the micro-reactor system, essentially assigned to a better heat management, avoiding too abrupt local temperature effects as observed in the fixed bed reactor.

More specifically, a perfectly stable behavior was observed for the case of the OSR reaction in the micro-reactor, after an initial period assigned to ceria sintering.

For the case of SR reaction, the deactivation was much slower and limited for the micro-reactor than for the fixed bed system. Again it was assigned essentially to ceria sintering, but some deactivating carbon deposition (proved for the fixed bed reactor) cannot be discarded for the micro-reactor. Hydrogen productivity over Ir/CeO₂ catalyst in the micro-structured reactor is about 40320 L_{H2}/kg_{cat}/h that is a little higher than the value in the conventional fixed-bed reactor (30160 L_{H2}/kg_{cat}/h). It indicated that the micro-reactor containing 160 platelets could produce enough hydrogen to supply the power for 1kW fuel cell. The quantities of the platelets could be decreased by enlarging the platelets dimension. For example, it only need 16 platelets (100mm x 300mm x 2mm).

Chapter VIII General discussion and conclusion

As mentioned in the introduction section, hydrogen is a clean energy source for an efficient generation of electricity through fuel cell systems. Among the various feedstocks able to produce chemically hydrogen, ethanol is a prominent candidate since containing a large content of hydrogen and being obtained from renewable biomass sources. As such, as a key advantage over fossil fuels, bio-ethanol reforming can be considered as a quasi carbon neutral process towards CO₂ emission.

A number of catalytic systems have already been investigated for hydrogen production by ethanol reforming (partial oxidation, steam reforming or oxidative steam reforming). However, there are still several challenges to overcome to reach a commercial process, which have been discussed in the introduction chapter.

i) For any industrial application, the catalyst deactivation which might be caused by several factors such as coke formation, active phase and/or support sintering, poisoning by products or external agents etc should be resolved.

ii) A compromise has to be found between H₂ yield and CO yield. As a matter of fact, as pointed out by the thermodynamics calculation reported in this work, hydrogen yield increases with reaction temperature, which unfortunately also favors the formation of CO, potential poison for the fuel cell electrodes. The challenge is therefore to maximize hydrogen yield but keeping the CO production as low as possible. Highly active systems able to work at low temperature where the WGS is effective have therefore to be privileged.

iii) Besides the catalyst activity and stability, the mechanism of the ethanol reforming reactions also deserves to be investigated in order to improve catalyst formulations but also optimize operating conditions. In parallel, engineering developments should be carried out for improving heat management of reactions which might be either endothermic or exothermic or both together.

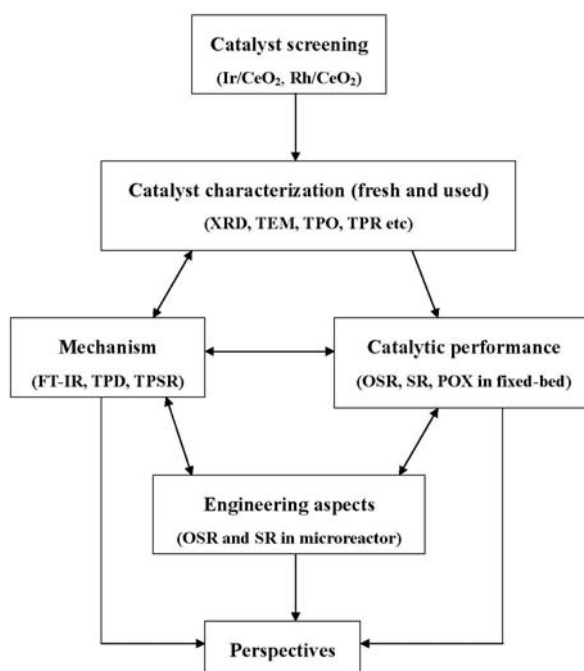
Based on the above challenges and on previous results already obtained in the two laboratories hosting this jointed thesis, we selected performing systems based on ceria as

support and iridium or rhodium as active metals.

From this background revealing numerous and highly interconnected parameters (related to materials structure, operating conditions, engineering aspects, etc), an important aim of the present thesis was to identify and understand key relationships between catalyst structure/composition and catalytic behavior for ethanol reforming.

As reflected by the different chapters on this manuscript, we mainly investigated: i) the catalytic performance for ethanol reforming reactions (POX, SR and OSR) over Ir/CeO₂ and Rh/CeO₂ catalyst in a fixed-bed reactor, including comparison with non noble metal based formulas, ii) the changes in structural characteristics of the reference catalyst with time on stream, iii) the mechanism of adsorption and conversion of ethanol over the reference Ir/CeO₂ catalyst, followed by IR and TPD analyses, iv) the potential interest to process ethanol reforming in micro-structured reactor instead of a fixed bed one.

The following scheme represents the main parts of this work and can be analyzed in term of key relationships between all of the results achieved in the present thesis.



Catalyst composition versus performance and mechanism

By comparing the three OSR, SR and POX reactions for energy efficiency and

hydrogen yield, the oxidative steam reforming of ethanol (OSR) was selected as the best choice for an industrial application, because ensuring a relatively high hydrogen yield, but being close to a thermo-neutral process.

From long term testing, two main features were observed and analyzed for the reference Ir/CeO₂ catalyst:

- Under conditions where ethanol conversion is complete, no significant deactivation was observed, by stating a stable productivity in hydrogen along the run.
- Under conditions where ethanol conversion is only partial (high GHSV), some activity decay was observed which was assigned to a combination of two different phenomena: ceria sintering and coke deposition.

Ceria sintering would essentially proceeds in the initial period while carbon deposition would be a more continuous process, especially under SR conditions.

The main features revealed by the mechanistic study allowed us to explain these aging/stability phenomena:

By following step by step the conversion of ethanol with temperature, the mechanism was shown to depend strongly on the catalyst composition.

Ir/Ce400 and Rh/Ce400 catalysts were compared to evaluate the effect of noble metal nature. For both systems, high activity and stability were found for SR, POX and OSR of ethanol under conditions ensuring full conversion of ethanol (high temperature and low GHSV). The only difference was that rhodium catalyst was found slightly more active for ethanol conversion and therefore producing less CO at lower temperature. The effect of noble metal with the same ceria support was therefore revealed only at low temperature under partial conversion conditions.

When the active phase is deposited on an inert system (like Ni-Cu/SiO₂) or a non redox support like Rh/Al₂O₃, most of the chemical steps involved in the conversion of ethanol to syngas are shown to occur on the metal phase, without a specific role of the support unless to ensure the dispersion of the metallic phase.

For the present case of noble metal (Ir or Rh) supported on ceria, two clearly distinct

types of chemistry were identified:

- ***C₂ chemistry on ceria***: C₂ intermediates are formed and converted according to the sequence: ethanol → ethoxy species → acetaldehyde → acetate species over the ceria surface.

- ***C₁ chemistry at Ir/ceria interface***: C₂ adspecies, possibly migrating along the ceria surface towards Ir particles, are in a second step decomposed into CH_x adspecies (on the metal phase) and carbonate species (on the ceria surface), leading to methane/carbon monoxide and CO₂, respectively.

Thus we can stress the key role of the interface between ceria support and Ir or Rh phase, which determines this transition from C₂ to C₁ chemistry.

A preliminary kinetic analysis of the ethanol SR revealed that the apparent activation energy was about 33kJ/mol and that the reaction rate was of first order with respect to ethanol. In a first approximation, the rather low activation energy, measured in the absence of diffusion limitation, indicates that the activation of ethanol over Ir/CeO₂ is an easy process. In turn, the first order would suggest that there is no surface saturation and that the step converting gaseous ethanol into active adspecies might determine the overall rate of conversion. The C₂ to C₁ steps above mentioned would become rate-determining only for the case of less active Ir(Rh)/ceria interface as discussed in the next paragraph.

From this mechanistic and kinetic view, the above mentioned aging processes can now be understood, first in a simplified way: ceria sintering (either caused by a thermal treatment of the fresh catalysts, or by the reaction itself) strongly affects the state of the Ir(Rh)/ceria interface, which tends to inhibit the ethanol conversion, leading to partial conversion conditions. In turn, partial ethanol conversion (i.e., C₂ products formation like acetaldehyde and ethylene) favors ethylene polymerization and deactivating coke deposition. Thus the two aging phenomena, ceria sintering and coke deposition, are clearly interrelated. The next paragraph aims at a deeper insight of these phenomena.

Catalyst structure versus activity

This investigation was carried out by following the catalytic performance as a function of the initial particle size of ceria (on fresh catalysts) but maintaining the same dispersion of the Ir phase. Similarly, changes in the catalyst structure during time on stream were also carefully analyzed, showing that the Ir (or Rh) dispersion was in all cases maintained constant while the ceria tended to sinter during long term aging periods. For the latter, this sintering would occur rather rapidly, but to a limited extent, especially when starting from initially well dispersed systems, like the Ir/Ce400 reference catalyst.

It was clearly demonstrated that when the ceria is sintered to a certain extent (corresponding to an oxide dispersion below about 2%), even well dispersed metal particles could not anymore ensure the proper interfacial cracking of C_2 intermediates formed from the ethanol activation over ceria. This points out again the key role of ceria not only for activating ethanol and oxidizing it into acetaldehyde, but also for providing to the Ir(Rh)/ceria interface enough OH groups and lattice oxygen to ensure the oxidation of carbonaceous C_1 into CO.

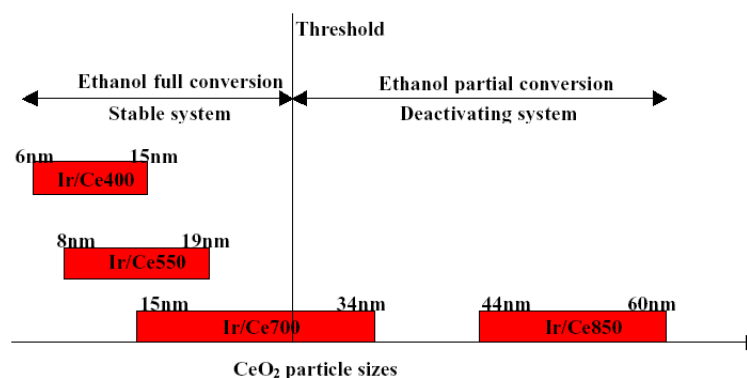
As a consequence, for highly sintered ceria, the formation of deactivating coke, especially under SR conditions, explains the slow activity decline observed for example for the Ir/Ce850 catalyst.

The proper origin of this "threshold" effect for the ceria dispersion is indeed linked to the oxygen transfer ability of the tested systems. For well dispersed systems, the density of structural defects favor both the bulk to surface oxygen diffusion but also the surface transfer of OH groups which are a vector for carbon oxidation, as stated by the mechanistic study. In turn, when the dispersion becomes too low (below 2%), it can be assumed that the density of defects, which are necessary for ensuring oxygen and OH mobility, becomes too low as well. Effectively, it is well recognized that the migration of oxygen is favored by the existence of microdomains in the fluorite structure for which the defects (Frenkel types) form preferential routes for ionic oxygen migration. At too low ceria dispersion, these microdomains are no more interconnected and the oxygen and hydroxyl mobility becomes

strongly inhibited.

To sum up, a clear structure-activity relationship was thus revealed by investigating the influence of the support particle size on catalytic performance for the reference catalyst.

The following scheme tentatively resumes this relationship:



Thus, as can be seen in this scheme, three cases were observed:

i) for ceria highly dispersed systems (Ir/Ce400 and 550 or Rh400), a moderate ceria sintering occurs during long term testing, which keeps however the ceria dispersion in a domain ensuring full conversion of ethanol and therefore a stable behavior,

ii) for ceria less dispersed systems like Ir/Ce700, the catalyst initially converts completely ethanol but as soon as the ceria becomes less dispersed than the threshold level, the conversion decreases and ethylene is produced which leads to coke deposition and progressive conversion decay,

iii) for ceria poorly dispersed support (Ir/Ce850), the catalyst is unable to fully convert ethanol from the beginning of the test and a continuous deactivation is observed all along the testing period.

Another search of relationship was attempted between mechanistic insights catalysts structure and performance improvements provided by engineering aspects.

Engineering aspects versus mechanism and catalyst structures

By comparing the results obtained both in a fixed bed reactor and in a micro-structured reactor for the OSR and SR reactions, a clear benefit was found for the micro-reactor, in term of ethanol conversion and hydrogen yield, measured under high GHSV (short contact

time) i.e., under conditions where the ethanol conversion was kept partial. This effect was essentially assigned to a better heat management, avoiding too abrupt temperature profiles as observed in the fixed bed reactor, and, as a consequence on the catalysts structure, a lower trend to ceria sintering for long term experiments.

As such, a perfectly stable catalytic behavior was observed for the case of the OSR reaction in the micro-structured reactor, after an initial aging period assigned to limited ceria sintering, observed when the fresh catalysts are well dispersed systems (see above case i). For the long term period, an improved heat management (flattened T profiles) limits considerably the ceria sintering and therefore any "structural aging". However, in the case of SR, the regular though limited deposition of coke at partial ethanol conversion (as required for relevant aging analysis) provokes as seen before a slow and continuous conversion decay.

Last but not least, it was shown that under OSR conditions, the microreactor efficiency allows to produce high yields of hydrogen and carbon dioxide (and therefore low yield of carbon monoxide) at relatively low temperature (450°C) at full ethanol conversion, without C₂ side products. Here, the best result was obtained with the Rh/Ce400, allowing to decrease the transition temperature from partial to full ethanol conversion by about 100°C. This important result meets one of the key challenges tackled in this work to produce hydrogen with a minimized carbon monoxide concentration.

Therefore, the present study demonstrated that the micro-structured reactors are a quite relevant alternative to conventional fixed bed reactors, with a controlled and adapted coating procedure leading to performing and stable systems. Again the OSR conditions appear as the best choice for limiting any aging drawbacks (observed for POX due to "structural" sintering and for SR for "poisoning" aging). This unique feature might serve as a strong basis for a further industrial development.

Proposed future work

Despite a much improved overview and understanding of the highly interconnected

parameters controlling the ethanol reforming as shown above, further analyses and feed back towards catalysts formulation and engineering deserve to be proposed as perspective and some of them are currently underway in the two laboratories within the frame of this collaborative program:

i) Further kinetic experiments (extending widely the range of sensitive parameters) are required in order to develop an advanced kinetic model of the ethanol reforming reactions.

ii) From the knowledge gained from the catalysts screening and the key issue of ceria sintering, further improvement of catalyst formulas can be proposed such as combining the Ni/Cu phase, particularly active for WGS equilibrium, but sensitive to deactivation with Rh or Ir phases supported on ceria doped with promoters like Zr and other lanthanides to prevent ceria sintering.

iii) From the engineering and energy efficiency point of view, the work of ethanol reforming in micro-structured reactors has to be continued, by tuning several process parameters such as the design of the micro-channels, the coating thickness, the temperature profiles for ensuring long term stability, by combining endothermic (SR) and exothermic (ethanol combustion) stacks or staged oxygen feeding for OSR and POX systems, also focusing at transient periods (start-up and changes in regime) where only partial conversion will occur.

References

- [1] V. Goltsov, T.N. Veziroglu, L.F. Goltsova. *Int. J. Hydrogen Energy*. 31 (2003) 153.
- [2] M. Ni, M.K.H. Leung, K. Sumathy. *Fuel process Technol.* 87 (2006) 461.
- [3] M. Ni, M.K.H. Leung, K. Sumathy, D.Y.C Leung. *Int. J. Hydrogen Energy*. 31 (2006) 1401.
- [4] M. Ni, M.K.H. Leung, K. Sumathy, D.Y.C Leung. *Renewable Sustainable Energy Rev.* 11 (2007) 401.
- [5] M. Galbe, G.A. Zacchi. *Appl Microbiol Bioethanol*. 59 (2002) 618.
- [6] B.S. Dien, M.A. Cotta, T.W. Jeffries. *Appl Microbiol Biotechnol.* 63 (2003) 258.
- [7] Y. Sun, J.Y Cheng. *Bioresource Technol.* 83 (2002) 1.
- [8] M. Ni, D.Y.C Leung, M.K.H. Leung. *Int. J. Hydrogen Energy*. 32 (2007) 3238.
- [9] E.C. Wanat, K. Venkataramen, L.D. Schmidt. *Appl. Catal. A* 276 (2004) 155.
- [10] A.N. Fatsikostas, D.I. Kondarides, X.E. Verykios. *Catal. Today*. 75 (2003) 145.
- [11] J.R. Salge, G.A. Deluga, L.D. Schmidt. *J. Catal.* 235 (2005) 69.
- [12] S. Cavallaro. *Energy fuels*. 14 (2000) 1195.
- [13] A.M. Silva, A.P.M.G. Barandas, A. Fraga. *Appl. Catal. A* 325 (2007) 193.
- [14] L.V. Mattos, F.B. Noronha, J. Power Sources. 145 (2005) 10.
- [15] D.K Liguras, K. Goundani, X.E. Verykios. *J. Power Sources*. 130 (2004) 30.
- [16] S. Cavallaro, V. Chiodo, S. Freni, N. Mondello, F. Frusteri. *Appl. Catal. A* 249 (2003) 119.
- [17] S. Jankhah, N. Abatzoglou, F. Gitzhofer. *Int. J. Hydrogen Energy*. 33 (2008) 4769.
- [18] P. Tsiakaras, A. Demin, J. Power Sources. 102 (1) (2001) 210.
- [19] F. Aupretre, C. Descorme, D. Duprez. *Catal. Commun.* 3 (2002) 263.
- [20] F. Aupretre, C. Descorme, D. Duprez, D. Casanave, D. Uzio. *J. Catal.* 233 (2005) 464.
- [21] J.P. Breen, R. Burch, H.M. Coleman. *Appl. Catal. B* 39 (2002) 65.
- [22] F. Frusteri, S. Freni, L. Spadaro, V. Chiodo, G. Bonura, S. Donato. *Catal. Commun.*

- 5 (2004) 611.
- [23] D.K. Liguras, D.I. Kondarides, X.E. Verykios. *Appl. Catal. B* 43 (2003) 345.
- [24] A.N. Fatsikostas, D.I. Kondarides, X.E. Verykios. *Catal. Today*. 75 (2002) 145.
- [25] J. Sun, X.P. Qiu, F. Wu, W.T. Zhu. *Int. J. Hydrogen Energy*. 30 (2005) 437.
- [26] J. Comas, F. Marino, M. Laborde, N. Amadeo. *Chem. Eng. J.* 98 (2004) 61.
- [27] Y. Yang, J.X. Ma, F. Wu. *Int. J. Hydrogen Energy*. 31 (2006) 877.
- [28] F. Frusteri, S. Freni, V. Chiodo, L. Spadaro, O. Di Blasi, G. Bonura, S. Cavallaro. *Appl. Catal. A* 270 (2004) 1.
- [29] J. Llorca, N. Homs, P.R. Piscina. *J. Catal.* 227 (2004) 556.
- [30] S. Cavallaro, N. Mondello, S. Freni. *J. Power Sources*. 102 (2001) 198.
- [31] A. Kaddouri, C. Mazzocchia. *Catal. Commun* 5 (2004) 339.
- [32] Y. Okamoto, K. Nagata, T. Adachi, M. Odawara. T. Imanaka. *Appl. Catal.* 73 (1991) 249.
- [33] M.N. Barroso, M.F. Gomez, L.A. Arrua, M.C. Abello. *Appl. Catal. A* 304 (2006) 116.
- [34] F. Marino, G. Baronetti, M. Jobbagy, M. Laborde. *Appl. Catal. A*. 238 (2003) 41.
- [35] F.S. Baltacioglu, A.E. Aksoylu, Z. Onsan. *Catal. Today*. In press.
- [36] L.V. Mattos, F.B. Noronha. *J. Power Sources*. 152 (2005) 50.
- [37] J.R. Salge, G.A. Deluga, L.D. Schmidt. *J. Catal.* 235 (2005) 69.
- [38] D.K. Liguras, K. Goundani, X.E. Verykios. *J. Power Sources*. 130 (2004) 30.
- [39] A.M. Silva, L.V. Mattos, M.A. Fraga, F.B. Noronha. *Catal. Today*. 129 (2007) 297.
- [40] W. Wang, Z. Wang, Y. Ding, J. Xi, G. Lu. *Catal. Lett.* 81 (2002) 63.
- [41] J.R. Salge, G.A. Deluga, L.D. Schmidt. *J. Catal.* 235 (2005) 69.
- [42] L.V. Mattos, F.B. Noronha. *J. Catal.* 233 (2005) 453.
- [43] R.M. Navarro, M.C. Alvarez-Galvan, M. Cruz, F. Rosa, J.L.G. Fierro. *Appl. Catal. B* 55 (2005) 229.
- [44] E.C. Wanat, B. Suman, L.D. Schmidt. *J. Catal.* 235 (2005) 18.
- [45] J. Kugai, V. Subramani, C. Song, M.H. Engelhard, Y.H. Chin. *J. Catal.* 238 (2006)

- 430.
- [46] A. Casanavos, J. Llorca, N. Homs, J.L. Fierro. *J. Mol. Catal. A. Chem.* 250 (2006) 44.
- [47] S. Velu, K. Suzuki, M. Vijayaraj, S. Barman, C.S. Gopinach. *Appl. Catal. B* 55 (2005) 287.
- [48] R.M. Navarro, M.C. Alvarez-Galvan, F. Rosa, J.L.G. Fierro. *Appl. Catal. B* 55 (2005) 229.
- [49] V. Fierro, A. Akdim, H. Provendier, C. Mirodatos. *J. Power Sources*. 145 (2005) 659.
- [50] P. Biswas, D. Kunzru. *Chem. Eng. J.* 136 (2008) 41.
- [51] V. Fierro, O. Akdim, C. Mirodatos. *Green Chem.* 5 (2003) 20.
- [52] V. Fierro, V. Klouz, O. Akdim, C. Mirodatos. *Catal. Today*. 75 (2002) 141.
- [53] S. Freni, G. Maggio, S. Cavallaro. *J. Power Sources*. 62 (2001) 67.
- [54] I. Fishtik, A. Alexander, R. Datta, D. Geana. *Int. J. Hydrogen energy*. 25 (2000) 31.
- [55] T. Ioanides. *J. Power Sources*. 92 (2001) 17.
- [56] J. Xu, X. Zhang, R. Zenobi, J. Yoshinobu, Z. Xu, J.T. Yates Jr. *Surf. Sci.* 256 (1991) 288.
- [57] S.M. Gates, J.N. Russel Jr, J.T. Yates Jr. *Surf. Sci.* 171 (1986) 111.
- [58] J. Rasko, A. Hancz, A. Erdohelyi. *Appl. Catal. A* 269 (2004) 13.
- [59] A.N. Fatsikostas, X.E. Verykios. *J. Catal.* 225 (2004) 439.
- [60] F. Marino, G. Baronetti, M. Jobbagy, M. Loberde. *Appl. Catal. A* 238 (2003) 41.
- [61] M.S. Batista, R.K.S. Santos, E.M. Assaf, J.M. Assaf, E.A. Ticianelli. *J. Power Sources*. 124 (2003) 99.
- [62] J. Sun, X. Qiu, F. Wu, W. Zhu, W. Wang, S. Hao. *Int. J. Hydrogen Energy*. 29 (2004) 1075.
- [63] H. Idriss, K.S. Kim, M.A. Bateau. *J. Catal.* 139 (1993) 119.
- [64] H. Idriss, M.A. Barteau. *Catal. Lett.* 40 (1996) 147.
- [65] P.Y. Sheng, A. Yee, G.A. Bowmaker, H. Idriss. *J. Catal.* 208 (2002) 393.

-
- [66] A. Yee, S.J. Morrison, H. Idriss. *Catal. Today*. 63 (2000) 327.
- [67] P. Biswas, D. Kunzru. *Chem. Eng. J.* 136 (2008) 41.
- [68] J.L. Bi, Y.Y. Hong, C.C. Lee, C.T. Yeh, C.B. Wang. *Catal. Today*. 129 (2007) 322.
- [69] O. Akdim, W. Cai, V. Fierro, H. Provendier, A. van Veen, W. Shen, C. Mirodatos. *Topics in Catalysis*. Doi:10.1007/s11244-008-9122-z.
- [70] J. Sun, D. Luo, P. Xiao, J. Li, S. Yu. *J. Power Sour.* 184 (2008) 385.
- [71] A. Akande, A. Aboudheir, R. Idem, A. Dalai, *Int. J. Hydrogen Energy*. 31(12) (2006) 1707.
- [72] P. Biswas, D. Kunzru. *Chem. Eng. Jour.* 136 (2008) 41.
- [73] R.S. Wegeng, M.K. Drost, C.E. McDonald. U.S. Patent, 5811062, 1997.
- [74] G.A. Deluga, J.R. Salge, L.D. Schmidt, X.E. Verykios. *Science*. 303 (2004) 993.
- [75] J.J. Krummenacher, L.D. Schmidt. *J. Catal.* 222 (2004) 429.
- [76] B.J. Dreyer, I.C. Lee, J.J. Krummenacher, L.D. Schmidt. *Appl. Catal. A* 307 (2006) 184.
- [77] E.C. Wanat, B. Suman, L.D. Schmidt. *J. Catal.* 235 (2005) 18.
- [78] S.T. Kolaczowski. *Catal. today*. 83 (2003) 85.
- [79] J.W. Chen, H. Yang, N. Wang, Z. Ring, T. Dabros. *Appl. Catal. A* 345 (2008) 1.
- [80] A. Casanovas, C. Leitenburg, A. Trovarelli, J. Llorca. *Catal. Today*. 138 (2008) 187.
- [81] P. Reuse, A. Renken, K.H. Santo, O. Gorke, K. Schubert. *Chem. Eng. J.* 101 (2004) 133.
- [82] I. Aartun, T. Gjervan, K. Schubert. *Chem. Eng. J.* 101 (2004) 93.
- [83] A. Rouge, B. Spoetzl, S. Schenk, K. Gebauer, A. Renken. *Chem. Eng. Sci.* 56 (2001) 1419.
- [84] L.F. Brown. *Int. J. Hydrogen Energy*. 26 (2001) 381.
- [85] M.T. Janicke, H. Kestenbaum, U. Hagendorf, F. Schuth, M. Fichtner, K. Schubert. *J. Catal.* 191 (2000) 282.
- [86] E.V. Rebrov, M.H.J.M. de Croon, J.C. Schouten. *Catal. Today*. 69 (2001) 183.
- [87] K. Haas-Santo, O. Gorke, P. Pfeifer, K. Schubert. *Chimia (Aarau)* 56 (2002) 605.

-
- [88] A. Stefanescu, A. C. van Veen, C. Mirodatos, E. Duval-Brunel. *Catal. Today*. 125 (2007) 16.
- [89] N. Dupont, G. Germani, A. C. van Veen, Y. Schuurman, G. Schaeffer, C. Mirodatos. *Int. J. Hydrogen Energy*. 32 (2007) 1443.
- [90] L. Ma, C. Jiang, A.A. Adesina, D.L. Trimm, M.S. Wainwright. *Chem. Eng. J.* 62 (1996) 103.
- [91] I.M. Hsing, R. Srinivasan, M.P. Harold, K.F. Jensen, M.A. Schmidt. *Chem. Eng. Sci.* 55 (2000) 3.
- [92] D. Honiche. *Stud. Surf. Catal* 122 (1999) 47.
- [93] G. Kolb, R. Zapf, V. Hessel, H. Lowe. *Appl. Catal. A* 277 (2004) 155.
- [94] H. Pennemann, V. Hessel, G. Kolb, H. Lowe, R. Zapf. *Chem. Engin. J.* 1355 (2008) S66.
- [95] Y. Men, G. Kolb, R. Zapf, V. Hessel, H. Lowe. *Process safety and environmental protection*. 85 (2007) 413.
- [96] M.T. Janicke, H. Kestenbaum, U. Hagendorf, F. Schuth, M. Fichtner, K. Schubert. *J. Catal.* 191 (2000) 282.
- [97] A. C. van Veen, Y. Schuurman, C. Mirodatos. *Handbook for microprocess engineering*, Vol C. System, "Process & plant engineering", V. Hessel, A. Renken, J. Schouten, Y. Wang and J-I. Yoshida, Wiley VCH, 2008, in press.
- [98] B.C. Zhang, X.L. Tang, Y. Li, W.J. Cai, Y. Xu, W. Shen. *Catal. Commun.* 7 (2006) 367.
- [99] B.C. Zhang, Y. Li, W.J. Cai, Y. Xu, W. Shen. *Int. J. Hydrogen energy*. 33 (2008) 4377.
- [100] B.D. Cullity, *Elements of X-Ray Diffraction*, 2nd ed., Addison–Wesley, Menlo Park, CA, 1978.
- [101] A. Yee, S.J. Morrison, H. Idriss. *J. Catal.* 186 (1999) 279.
- [102] K. Liguras, D.I. Kondrides, X.E. Verykios. *Appl. Catal. B* 43 (2003) 345.
- [103] S. Cavallaro, V. Chiodo, A. Vita, S. Freni. *J. Power Sources*. 94 (2001) 14.

-
- [104] A. Erdohelyi, J. Rasko. *Catal. Today*. 116 (2006) 367.
- [105] A. Trovarelli, *Catal. Rev. Sci. Eng.* 38 (1996) 439.
- [106] F.R. Sarria, J.C. Vargas, A.C. Roger, A. Kiennemann. *Catal. Today*. 133-135 (2008) 149.
- [107] C. Leitenburg, A. Trovarelli. *J. Catal.* 156 (1995) 171.
- [108] V.A. Tsipouriari, A.M. Efstathiou, X.E. Verykios. *J. Catal.* 161 (1996) 31.
- [109] I. Cuauhtemoc, G. Del Angel, G. Torres, V. Bertin. *Catal. Today*. 133-135 (2008) 588.
- [110] T. Miki, T. Ogawa, M. Haneda, N. Kakuta, A. Ueno, S. Tateishi, S.M.S. Matsuura. *J. Phys. Chem.* 94 (1990) 339.
- [111] C. Padeste, N.W. Cant, L. Trimm. *Catal. Lett.* 18 (1993) 305.
- [112] S. Kacimi, Jr. J. Barbier, R. Taha, D. Duprez. *Catal. Lett.* 22 (1993) 343.
- [113] G.S. Zafiris, J. Gorte. *J. Catal.* 143 (1993) 86.
- [114] G.S. Zafiris, J. Gorte. *J. Catal.* 139 (1993) 561.
- [115] S. Imamura, M. Shono, N. Okamoto, R.S. Hamada. *Appl. Catal. A* 142 (1996) 279.
- [116] F. Li, K. Fujimoto. *J. Catal.* 172 (1997) 238.
- [117] A.M. Silva, L.O.O. Costa, A.P.M.G. Barandas, L.E.P. Borges, L.V. Mattos, F.B. Noronha. *Catal. Today*. 133-135 (2008) 755.
- [118] J. Mikulová, J. Barbier Jr, S. Rossignol, D. Mesnard, D. Duprez, C. Kappenstein. *J. Catal.* 251 (2007) 172.
- [119] E.M. Sadovskaya, Y.A. Ivanova, L.G. Pinaeva, G. Grasso, T.G. Kuznetsova, A. van Veen, C. Mirodatos, *J. Phys. Chem. A* 111 (2007) 4498.
- [120] Z.X. Song, W. Liu, H. Nishiguchi, A. Takami, K. Nagaoka, Y. Takita. *Appl. Catal. A* 329 (2007) 86.
- [121] G. Balducci, J. Kaspar, P. Fornasiero, M. Graziani, M. Saiful Islam, J.D. Gale. *J. Phys. Chem. B* 101 (1997) 1750.
- [122] E. Mamontov, T. Egami, R. Brezny, M. Koranne, S. Tyagi. *J. Phys. Chem. B* 104 (2007) 11110.

-
- [123] R. Wang, X. Liu, H. Xu. *Chin. J. Catal.* 28 (2007) 126.
- [124] W. Cai, F. Wang, E. Zhan, A.C. van Veen, C. Mirodatos, W. Shen. *J. Catal.* 257 (2008) 96.
- [125] W. Cai, B. Zhang, Y. Li, Y. Xu, W. Shen. *Catal. Commun.* 8 (2007) 1588.
- [126] N. Laosiripojana, S. Assabumrungrat. *Appl. Catal. B* 66 (2006) 29.
- [127] T. Nishiguchi, T. Matsumoto, H. Kanai, K. Utani, Y. Matsumura, W.J. Shen, S. Imamura. *Appl. Catal. A* 279 (2005) 273.
- [128] M.A. Goula, S.K. Kontou, P.E. Tsiakaras. *Appl. Catal. B* 49 (2004) 135.
- [129] J. Llorca, P.R. Piscina, J. Dalmon, J. Sales, N. Homs. *Appl. Catal. B* 43 (2003) 355.
- [130] J.C. Vargas, S. Libs, A.C. Roger, A. Kiennemann. *Catal. Today*. 107-108 (2005) 417.
- [131] A.M. Silva, A.P.M.G. Barandas, L.O.O. Costa, L.E.P. Borges, L.V. Mattos, F.B. Noronha. *Catal. Today*. 129 (2007) 297.
- [132] F. Zhou, X. Zhao, H. Xu, C. Yuan, J. Phys.Chem.C 111 (2007) 1651.
- [133] S.M. Stagg-Williams, F.B. Noronha, G. Fendley, D.E. Resasco. *J. Catal.* 194 (2000) 240.
- [134] S. Royer, D. Duprez, S. Kaliaguine. *Catal. Today*. 112 (2006) 99.
- [135] F. Dong, A. Suda, T. Tanabe, Y. Nagai, H. Sobukawa, H. Shinjoh, M. Sugiura, C. Descorme, D. Duprez. *Catal. Today*. 90 (2004) 223.
- [136] C. Descorme, Y. Madier, D. Duprez. *J. Catal.* 196 (2000) 167.
- [137] J.R. Rostrup-Nielsen, *Phys. Chem. Chem. Phys.* 3 (2001) 283.
- [138] A. Haryanto, S. Fernando, N. Murali, S. Adhikari. *Energy Fuels*. 19 (2005) 2098.
- [139] P.D. Vaidya, A.E. Rodrigues. *Chem. Eng. J.* 117 (2006) 39.
- [140] A. Yee, S.J. Morrison, H. Idriss. *J. Catal.* 191 (2000) 30.
- [141] G. Jacobs, R.A. Keogh, B.H. Davis. *J. Catal.* 245 (2007) 326.
- [142] O. Akdim, PhD thesis, Lyon1 University, # 298-2004.
- [143] R. Pestman, R. M. Koster, A. van Duijne, J. A. Z. Pieterse, V. Ponc. *J. Catal.* 168 (1997) 265.
- [144] J. Kaspar, P. Fornasiero, M. Graziani. *Catal. Today* 50 (1999) 285.

-
- [145] M.H. Yao, R.J. Baird, F.W. Kunz, T.E. Hoost. *J. Catal.* 166 (1997) 67.
- [146] P.D. Vaida, A.E. Rodrigues. *Ind. Eng. Chem. Res.* 45 (2006) 6614.
- [147] D.A. Morgenstern, J.P. Fornango. *Energy Fuels.* 19 (2005) 1708.
- [148] N. Homs, J. Llorca, P.R. Piscina. *Catal. Today.* 116 (2006) 361.
- [149] H.V. Fajardo, L.F.D. Probst. *Appl. Catal. B* 66 (2006) 29.
- [150] J.P. Breen, R. Burch, H.M. Coleman. *Appl. Catal. B* 39 (2002) 65.
- [151] G. Chen, S. Li, H. Li, F. Jiao, Q. Yuan. *Catal. Today* 125 (2007) 97.
- [152] M.J. Stutz, D. Poulikakos. *Chem. Eng. Sci.* 60 (2005) 6983.
- [153] M. Levent, D.J. Gunn, M. Bousiffi. *Int. J. Hydrogen. Energy.* 28 (2003) 945.
- [154] G. Chen, S. Li, Q. Yuan. *Catal. Today.* 120 (2007) 63.
- [155] R.S. Howell, M.K. Hoatalis. *J. Electrochem. Soc.* 149 (2002) 143.
- [156] A. Stefanescu, A.C. van Veen, C. Mirodatos, J.C. Beziat, E. Duval-Brunel. *Catal. Today.* 125 (2007) 16.
- [157] M.S. Lim, M.R. Kim, J. Noh, S.I. Woo. *J. Power Sources.* 140 (2005) 66.
- [158] J.Y. Won, H.K. Jun, M.K. Jeon, S.I. Woo. *Catal. Today.* 111 (2006) 158.
- [159] T. Conant, A. Karim, S. Rogers, S. Samms, G. Randolph, A. Datye. *Chem. Eng. Sci.* 61 (2006) 5678.
- [160] D.R. Sahoo, S. Vajpai, S. Patel, K.K. Pant. *Chem. Eng. J.* 125 (2007) 139.
- [161] M. Benito, J.L. Sanz, R. Isabel, R. Padilla, R. Arjona, L. Daza. *J. Power Sources.* 151 (2005) 11.
- [162] N. Dupont, G. Germani, A.C. van Veen, Y. Schuurman, G. Schäfer, C. Mirodatos. *Int. J. Hydrogen Energy.* 32 (2007) 1443.
- [163] I. Dincer. *Energy Sources.* 20 (1998) 427.
- [164] S. Duim. *Int. J. Hydrogen Energy.* 27 (2002) 235.
- [165] M. Ni, D.Y.C. Leung, M.K.H. Leung, K. Sumathy. *Fuel. Process. Technol.* 87 (2006) 461.
- [166] M. Noelia Barroso, M.F. Gomez, L.A. Arrua, M.C. Abello. *Appl. Catal. A* 304 (2006) 116.

-
- [167] T. Montini, L. de Rogatis, V. Gombac, M. Graziani. *Appl. Catal. B* 71 (2007) 125.

List of Publications

I **Weijie Cai**, Baocai zhang, Yongli, Yide Xu, Wenjie Shen. Hydrogen production by oxidative steam reforming of ethanol over an Ir/CeO₂ catalyst.

Catalysis communications 8 (2007) 1588-1594.

II **Weijie Cai**, Fagen Wang, Ensheng Zhan, A.C. Van Veen, C. Mirodatos, Wenjie Shen. Hydrogen production from ethanol over Ir/CeO₂ catalysts: A comparative study of steam reforming, partial oxidation and oxidative steam reforming.

Journal of catalysis. 257 (2008) 96-107.

III **Weijie Cai**, Fagen Wang, A.C. Van Veen, H. Provendier, C. Mirodatos, Wenjie Shen. Autothermal reforming of ethanol for hydrogen production over an Rh/CeO₂ catalyst.

Catalysis Today. 138 (2008) 152-156.

IV **Weijie Cai**, Fagen Wang, Wenjie Shen. The preparation of Ir/CeO₂ catalyst and its application in hydrogen production from ethanol.

China patent. Application number: 200710012341.0

V **Weijie Cai**, Fagen Wang, Wenjie Shen. Autothermal reforming of ethanol for hydrogen production over Co/CeO₂ catalyst.

Journal of molecular catalysis (china). In press.

VI **Weijie Cai**, Baocai Zhang, Qiying Liu, Yide Xu, Wenjie Shen. Hydrogen production from ethanol over Ir/CeO₂ catalysts: Reaction pathway and stability.

Oral, EUROPACAT VIII, Turku, Finland, 2007.8

VII Baocai Zhang, Xiaolan Tang, Yong Li, **Weijie Cai**, Yide Xu, Wenjie Shen. Steam reforming of bioethanol for the production hydrogen over ceria-supported Co, Ir and Ni catalysts.

Catalysis communications. 7 (2006) 367-372.

VIII Baocai Zhang, **Weijie Cai**, Yong Li, Yide Xu, Wenjie Shen. Hydrogen production by steam reforming of ethanol over an Ir/CeO₂ catalyst: reaction mechanism and stability of the catalyst.

International Journal of Hydrogen Energy. 33 (2008) 4377-4386.

IX Junlong Liu, Ensheng Zhan, **Weijie Cai**, Juan Li, Wenjie Shen. Methanol selective oxidation to methyl formate over ReO_x/CeO₂ catalysts.

Catalysis letters. 120 (2008) 3-4.

X Ourdia Akdim, **Weijie Cai**, Vanessa Fierro, Hélène Provendier, Andre van Veen, Wenjie Shen, Claude Mirodatos. Oxidative steam reforming of ethanol over Ni-Cu/SiO₂ and Rh/Al₂O₃: effect of metal and support on reaction mechanism.

Topics in Catalysis. Doi:10.1007/s11244-008-9122-z.

Acknowledgement

I am grateful to all the people who made possible the success of this scientific project and who gave me three wonderful and unforgettable years. This work has been accomplished from September 2006 to October 2008 in the French and Chinese collaborating laboratories of IRCELYON (Villeurbanne, France) and Dalian institute of chemical physics, Chinese Academy of Science.

My gratitude goes first to my supervisors. Without their constant and illuminating instruction, this thesis could not reach its present form.

Mr Claude. Mirodatos, Directeur de Recherches au CNRS, and Mr Andre. Van Veen, Madame Helene Provendier welcomed me warmly into the laboratory and supported me so much in all my stay in France. I was blessed in the three years, with their guidance, encouragement, unreserved help, hospitality, motivation, enthusiasm, immense knowledge, invaluable technique and editorial advice, which really supported me through my whole PhD studies. Not only in science but also in life experience, their cordial help started from the first day of this thesis and never stopped until the end of this thesis.

Mr. Wenjie Shen, professor, Director of catalytic reaction chemistry group, Dalian institute of chemical physics, Chinese Academy of Science, who led me into the world of catalysis chemistry, gave me the first view of the research and introduced me to the concept and method about how to make a research. “ Extensive reading, intensive thinking, smart design, skilled experimental techniques and scientific insight” what he taught me are always echoed in my mind. His guide, his broad-mindedness and his human and professional qualities have been of fundamental help for my whole thesis, even for my whole life.

I gratefully thank Prof. D. Duprez from Université de Poitiers, Prof J.G. Wang from Institute of Coal Chemistry (CAS), Prof P. Miele from Université Claude Bernard-Lyon I for accepting to refer and judge this manuscript as members of my PhD jury.

I must also express my deepest gratitude and thanks to my colleagues who were in DICP or Engineering and process intensification group at IRCELYON in France during my

stay. They gave me a lot of instructions and technique support during my experiments.

I also wish to express my appreciation to all the facilities in the IRCELYON, Claude Bernard University in France and in DICP in china.

I gratefully acknowledge the French government. Without their financial support provided for my PhD studies, I could not achieve this work.

Titre:

‘Production d'hydrogène par reformage de l'éthanol sur catalyseurs à base d'iridium et rhodium supportés sur cérine’

Résumé:

L'objectif principal de ce travail était l'étude de systèmes catalytiques stables, actifs et sélectifs pour les réactions de vapo-reformage, oxyvaporeformage et oxydation partielle de l'éthanol en vue de produire de l'hydrogène avec une concentration réduite de monoxyde de carbone. Deux formulations principales, Ir/CeO₂ et Rh/CeO₂, ont été sélectionnées pour étudier le mécanisme des réactions de surface de l'éthanol adsorbé par FT-IR et TPD et pour être testées en micro-réacteur structuré. Il a été montré que la cérine joue un rôle déterminant quant à la dispersion de la phase active en évitant son frittage lors de la réaction et quant à l'inhibition du cokage du fait de ses propriétés rédox. Par ailleurs, la dispersion de ce support qui peut décroître lors de tests de longue durée détermine le niveau de conversion de l'éthanol et le vieillissement du catalyseur. Les principales étapes élémentaires du mécanisme réactionnel ont été identifiées, liées à la formation de produits intermédiaires dans les régimes transitoires et/ou lorsque la conversion de l'éthanol reste partielle (à basse température, faibles temps de contact). Pour les trois réactions étudiées, les excellentes performances obtenues en réacteur microstructuré proviennent essentiellement d'une meilleure gestion des effets thermiques, ce qui ouvre de réelles perspectives d'application industrielle.

Mots clefs.

Hydrogène, reformage de l'éthanol, catalyseurs Ir/CeO₂ et Rh/CeO₂, mécanisme réactionnel, réacteurs micro-structurés.

Title:

‘Hydrogen production from ethanol over ceria supported iridium and rhodium catalysts’

Abstract.

The main objective of the thesis was to investigate the catalytic performance of stable, active and selective catalytic systems for ethanol steam reforming, ethanol partial oxidation and the combined auto-thermal reforming of ethanol. Two main formulations Ir/CeO₂ and Rh/CeO₂ were selected to i) investigate surface reaction of adsorbed ethanol via FT-IR and TPD techniques to investigate reaction mechanism; ii) check the ethanol reforming reaction in fixed-bed and micro-structured reactor. Ceria support was found to prevent the highly dispersed active metal particles from sintering and to inhibit coke formation through strong metal-support interactions and redox property. In addition, ceria dispersion was shown to monitor the extent of ethanol conversion and therefore the aging properties of the catalytic systems. It was also possible to identify key elementary steps in reaction mechanism, revealing intermediate products, characteristic of transient, low temperature and short contact time regimes. For the three reactions, excellent performances were obtained with the micro-structured reactor, essentially due to a better heat management, offering real perspectives for an industrial development.

Key words:

Hydrogen, ethanol reforming, Ir/CeO₂ and Rh/CeO₂ catalysts, reaction mechanism, micro-structured reactors.